Extrusion Pulping of Natural Fibres

Determination, Implementation and Verification of Constitutive Equations required for Modelling

Annita P.H. Westenbroek

Cover Design: Patrick van Gerner

EXTRUSION PULPING OF NATURAL FIBRES

DETERMINATION, IMPLEMENTATION AND VERIFICATION OF CONSTITUTIVE EQUATIONS REQUIRED FOR MODELLING

PROEFSCHRIFT

ter verkrijging van

de graad van doctor aan de Universiteit Twente,

op gezag van de rector magnificus,

prof. dr. F.A. van Vught,

volgens besluit van het College voor Promoties

in het openbaar te verdedigen

op vrijdag 10 maart 2000 te 16.45 uur.

door

Anna Petronella Helena Westenbroek

geboren op 6 mei 1972

te Steggerda

Dit proefschrift is goedgekeurd door de promotor

Prof. dr. ir. K.R. Westerterp

en de assistent-promotor

Prof. dr. G. Weickert

Aan mijn ouders

Aan Mark

Contents

Chapter 4. Drainage through swollen hemp bast fibres during compression

Chapter 5. Flowability of hemp bast fibres at high consistency

Chapter 6. Extrusion pulping; relations between process conditions and pulp quality

Chapter 1

General Introduction

1.1 Introduction

During recent decades the pulp and paper industry has been criticised for its negative impact on the natural environment [1,2]. Measures taken to tackle these problems include increased recycling of paper, more sustainable management of tree plantations and forests and a shift towards less harmful pulp and paper technologies. A come back for non-wood fibres as the raw material of paper may further contribute to the solution of some of these problems. Because of the increased interest for the application of non-wood fibres in the pulp and paper industry, the demand for bleached non-wood pulp has been increased [3-5]. Chemical pulping was traditionally used for bast fibres like hemp, flax, seedflax, jute, kenaf and ramie for papermaking purposes. Such processing yields a very high quality pulp with exceptional properties. Because of the high cost of such pulps, applications have been limited to specialities including teabag and filter papers, cigarette and similar papers, technical papers and specialty printing and writing papers.

In a comparison between chemical and mechanical pulping of bast fibres, van Roekel [4] concluded that extrusion pulping is a technically and economically viable process for the chemi-mechanical pulping of non-wood fibres. Chemi-mechanical pulping provides a much higher yield (typically 80 %) and a much lower use of chemicals. Moreover, extrusion pulping also allows cutting to a desired fibre length, so subsequently the pulps can be handled by bulk papermaking systems. Mechanical pulps, however, possess lower strengths than chemical pulps, and some lignin is still maintained in the fibre. In comparison to alkaline peroxide bleached mechanical softwood pulp and a softwood kraft pulp, extruded fibres appeared to show a higher tear strength, a lower tensile strength and a lower dewatering rate [4].

During extrusion pulping fibres are shortened, fibre bundles, consisting of elementary fibres are defibrated and elementary fibres are fibrillated. The extent of this processing as well as the amount of energy consumed during processing is thought to be greatly affected by chemical treatment, screw configuration, screw rotation speed and throughput. As different fibre applications require different fibre properties, it would be useful to have a model describing the relations between fibre properties, process conditions and screw configuration. This model could be used to adjust process parameters to product quality requirements, with minimum energy and chemicals consumption and to develop new applications.

1

The aim of the research described in this thesis was to elucidate the mechanism behind extrusion pulping in order to be able to develop a model that describes the relation between process conditions, screw configuration, energy consumption and product quality. This encloses the development of a geometry model and the determination of the constitutive equations for those rheological properties that are critical for the extrusion pulping process.

1.2 Extrusion Pulping

Extrusion pulping is a mechanical or chemimechanical pulping method in which fibres are processed by means of compression and shear forces. The basic principles of this pulping method have been developed over the last 25 years, with successful results on pilot and industrial applications of annual plants like cotton, hemp and flax [6-12]. The original BiVis (French for twin screw) process [13-16] was designed with two pulping extruders in series, the first for impregnation and partial cutting, the second for bleaching and additional cutting. The extrusion process evaluated in this study was derived from the BiVis process, but uses only one extruder and screw elements are especially developed for this purpose. This extrusion pulping process, for which a patent is pending, can be used for producing several paper qualities from wood and non-wood fibres [3-5].
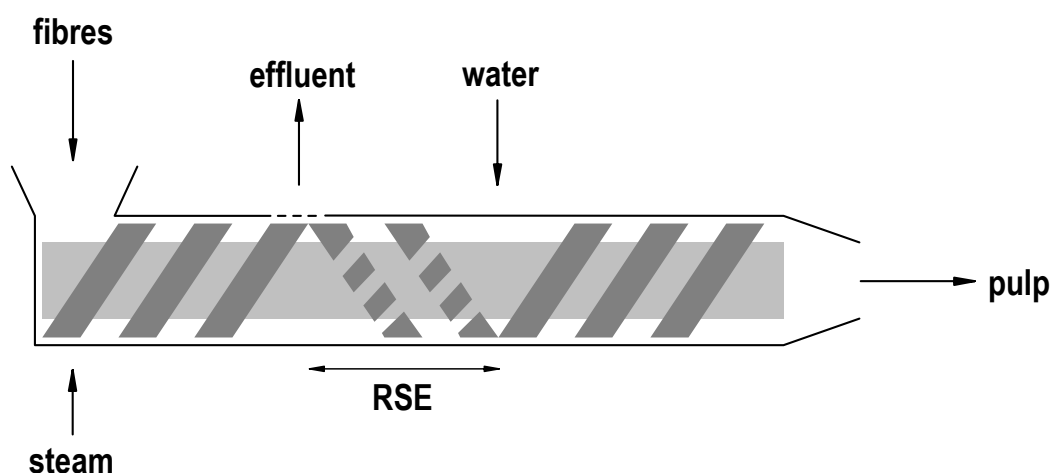
Figure 1.1. *Side view diagram of the extruder.*

Extrusion pulping is based on the use of a corotating twin screw extruder as the main pulping device. Figure 1.1 shows the basic operating principle of a pulping extruder. The pulping extruder consists of an eight-shaped barrel with two corotating intermeshing screws inside [13-16]. Fibrous material is fed into the barrel by transport screws. The main screw element used in extrusion pulping processes is the reversed screw element (RSE) (Fig. 1.2). This is an element with threads, whose pitch is opposite to the transport screws. This results in accumulation and compression of the fibres in the space between the transport screws and the RSE's. The high compression and shear forces cause defibration, fibrillation and shortening of the fibres. Excess water pressed out of the fibre mass is extracted through barrel filters placed upstream from the RSE. The pressure drop created in passing a RSE heats the pulp mass and provides rapid impregnation of liquids which can be supplied through an injection port downstream from the RSE. Machined slots are regularly distributed in the threads of the RSE, through

which the fibres can eventually pass forward. This combination of transport screw, RSE, filter and injection port can be repeated along the barrel. One combination of subsequent transport screw, RSE and transport screw is shown in Figure 1.3. The geometry parameters of the intermeshing screws of the twin-screw extruder are defined in Appendix A.

Figure 1.2. *Reversed Screw Element*

Figure 1.3. *Subsequent intermeshing transport screws, RSE's and transport screws.*

Usually higher temperatures and impregnation are applied in extrusion pulping. At higher temperatures lignin softens and technical fibres are easily defibrated into elementary fibres. Sodium hydroxide partly decomposes the lignin, which also facilitates defibration.

In order to elucidate the mechanism behind extrusion pulping a high speed film has been made through a plexiglass barrel element while a plug of black fibres was added to the extruder to observe mixing. The plexiglass element was placed right above the compression chamber. The film showed that fibres moved in plug flow. Plugs of fibres are pushed forward by the flights of the screws. Without RSE's there is no axial dispersion: no residence time distribution takes place. The axial velocity, v, of the plugs of fibres in the transport screws depends on the screw speed, W, and the pitch of the transport screw, p:

$$v = pW \qquad\qquad [1.1]$$

At the RSE no forward transportation is possible, resulting in an accumulation of fibres in the space formed by the first screw chamber of the RSE and the last chamber of the transport screw. This space, which is locked by the flights of the intermeshing second screw, decreases when the screws turn. Fibres present in the space are compressed, not able to flow anywhere. The film shows that at a sudden instance the fibre mass breaks and shears into small pieces and plugs of fibres are transported via the slots in the RSE in the direction of the outlet of the extruder. Smaller plugs of fibres flow via the spaces between the screws and the barrel and between the two screws towards other screw chambers. Subsequently, a new compression chamber is formed of the screw chambers of RSE and transport screw, which is filled with fibres still present if the RSE and new fibres provided by the transport screw. From these observations it is concluded that the fibre mass retains certain strength. The shear stresses in the fibre mass increase with increasing compression and when they exceed a certain value fibres start to shear along each other and plugs of fibres are broken. It is suggested that these high compression and shear forces cause cutting, fibrillation and defibration of the fibres. The extent of processing depends on both process conditions (temperature, throughput, screw speed, impregnation) and screw configuration.

Screw configuration

The characteristic dimensions of the flights and channels of intermeshing trapezoidal transport screws and RSE's are outlined in Appendix A. The RSE-configuration can further be varied with:
- Width of slots in RSE flights;
- Amount of slots in RSE flights;
- Direction of slots in RSE flights;
- Position of slots in RSE flights;
- Tangential position of RSE with respect to the transport screw.

The width of the slots and the amount of slots in the RSE appear to have a pronounced effect on the extent of shortening and the specific energy consumption, P. A smaller slot width results in a higher energy consumption and more cutting (Fig. 1.4 and 1.5) [17]. The direction of the slots in the RSE can be axially or helicoidally. Experiments with softwood fibres revealed that the relation between energy consumption and extent of cutting is similar for helicoidal and axial RSE slots. However, an RSE with axial slots causes more cutting and a higher energy consumption than an RSE with helicoidal slots with the same width.

The screws of the Clextral BC45 extruder are mounted on the axis by 13 splines. This means that screw elements can be places in 13 different ways with respect to their adjacent screws. This position is called the tangential position. It has been observed that the tangential position of the RSE with respect to the transport screw affects the specific power consumption, while the extent of cutting is not significantly affected (Fig. 1.6 and 1.7) [17].
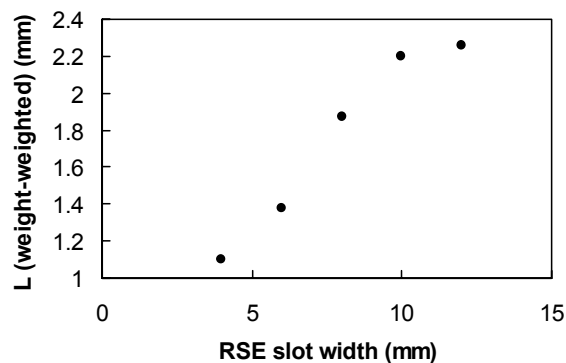
Figure 1.4: *Weight-weighted fibre length versus RSE slot width, extrusion of softwood fibres, tangential position = 0*
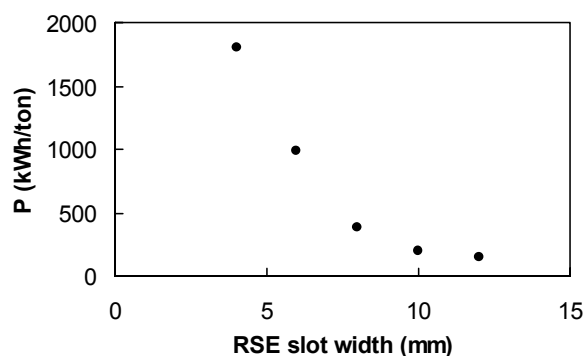
Figure 1.5: *Specific power consumption versus versus RSE slot width, extrusion of softwood fibres, tangential position = 0*
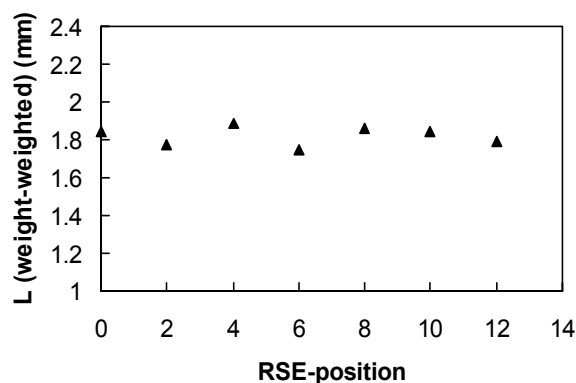
Figure 1.6: *Weight-weighted fibre length versus tangential position of the RSE with respect to the transport screw, extrusion of softwood fibres, slot width = 8 mm.*
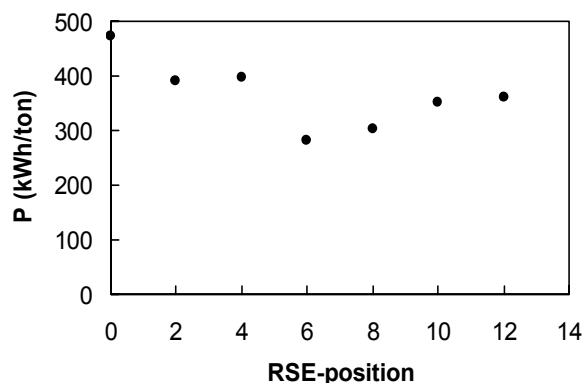
Figure 1.7: *Specific power consumption versus tangential position of the RSE with respect to the transport screw, extrusion of softwood fibres, slot width = 8 mm.*

The mechanism behind twin screw extrusion has been thoroughly examined for food and polymer processing [18-24]. Research is based on modelling flow, mixing, temperature and residence time distribution. Axial dispersion is described by the presence of different kinds of leak flows between the screw chambers caused by pressure gradients [23]. Tayeb et al. [21,22] and Vergnes et al. [25,26] developed a mathematical model for the flow of molten starch through the RSE of a twin-screw extruder. In this model the material displays Newtonian or Power Law behaviour and can flow through the slots, through the screw channels and through the intermeshing zone between the two screws. They showed that a higher throughput or a higher screw speed results in a shorter mean residence time and a narrower residence time distribution and that it is possible to obtain different product qualities by varying the geometry or the process conditions. Janssen [18] and Martelli [19] used Newtonian liquid rheology, while Yacu [20] and van Zuilichem [23] used the power law model for their modelling of food processing by means of the twin-screw extrusion. In their modelling of flow, residence time distributions and viscous dissipation in an RSE Tayeb et al. [21,22] use a Newtonian rheology and Vergnes et al. [25,26] use the power law model.

As fibres do not show liquid rheology, modelling by means of leak flows cannot be applied to extrusion pulping. Fibres move in plug flow in the transport screws and mixing between the screw chambers does not occur.

5

1.3 Characteristics of non-wood fibres

Our attention was mainly focused on non-wood bast fibres, because of the excellent ability of extrusion pulping to process very long cellulosic fibres and fibre bundles (of up to 1.5 m) to a pulp with a controlled fibre length and narrow fibre length distribution. Non-wood fibres, including hemp and flax, are suitable as raw materials for paper [3-5], as reinforcement in recycled paper and board [27], as replacement of synthetic fibres in nonwovens [28] or as reinforcement for composites [29-33].

Hemp (*Cannabis sativa* L.) is an annual fibre crop and one of the oldest crops known to man. It has been cultivated since ancient times for the provision of fibre for many practical purposes. It is a fast growing crop and is cultivated in many countries throughout the world. Hemp consists of two very different types of fibres, bast and woody core fibres [34]. Bast fibre bundles are located in the outer layer of the stem. Each fibre bundle is composed of overlapping bast fibres [35] and a cross section consists of ten to forty elementary fibres (Fig. 1.7A and B).
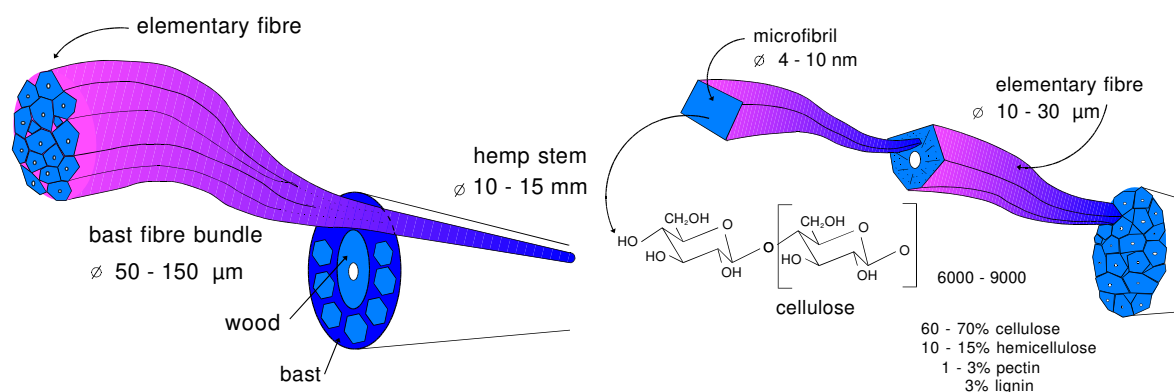
***Figure 1.7 (A+B)**: Schematic reproduction of a hemp stem*

The length of the elementary fibres varies between 5 and 55 mm and the thickness is on average 20μm. Hemp bast fibres consist of 60-70 % highly crystalline cellulose and other components such as hemicellulose (10-15 %), lignin (3 %), pectin(1-3 %), mineral matter, fats and waxes [36]. The woody core fibres are thin walled (wall thickness on average 2 μm) and short (0.55 mm) and have a chemical composition which resembles hard wood; approximately 40 % cellulose, 20 % hemicellulose and 20% lignin [37].

Because of differences in both morphology and chemical composition, wood fibres, for example for spruce and aspen, and bast fibres from hemp and flax have different papermaking abilities. Average values for morphological properties and chemical composition have been summarised for spruce, aspen, flax bast and hemp bast fibres (Table 1).

Table 1.1. Morphology and chemical composition of selected wood and non-wood fibres [35,36,38-48]

	Length (mm)	Diameter (μm)	Aspect ratio	Wall fraction (%)	Cellulose (%)	Hemi-cellulose (%)	Pectin (%)	Lignin (%)
Spruce	3.5	36	100	33	43	29		27
Aspen	1.0	21	50	40	53	31		16
Hemp bast	20	20	1000	50-80	60-70	10-15	1-3	4
Flax bast	28	21	1350	> 90	70-80	12-18	1-3	3

1.4 Modelling extrusion pulping

1.4.1 Introduction

The aim of the research described in this thesis was to elucidate the mechanism behind extrusion pulping in order to be able to develop a model that describes the relation between process conditions, screw configuration, energy consumption and product quality. With this model extrusion pulping could be optimised to obtain controlled product quality and more efficient energy consumption. This encloses the development of a geometry model and the determination of the constitutive equations for those rheological properties that are critical for the extrusion pulping process.

As described in paragraph 1.2 it is observed that fibre processing only takes place in the so-called compression chamber. This chamber consists of the last screw chamber of the transport screw before the RSE and the first screw chamber of the RSE, and is locked by the flights of the intermeshing screws. The extent of processing depends on the compression and shear forces in this space. Modelling should therefore be confined to this space. As the geometry of this space is rather complicated, it is suggested to start with a simplified model, which only describes the volume decrease versus time to be able to calculate compression forces. The volume of the compression chamber depends on the pitch of both transport screws and RSE and on the tangential position of the RSE with respect to the transport screw. The development of the model describing the volume decrease of the compression chamber during extrusion is outlined in Appendix A. Relations have been developed for both the RSE chamber and the transport screw chamber which depend on the screw dimensions of both screws. The total volume of the compression chamber is achieved by simple addition of both models. The effect of tangential rotation of the RSE with respect to the transport screw can be observed by applying an extra initial angle to the model of one of the screws (Fig. 1.8).

The volume decrease versus time can be obtained by multiplying the relation between volume decrease and screw angle with the screw speed. The amount of fibres during each compression in the compression chamber depends on the filling degree of the extruder, which is defined as the ratio between throughput and screw speed.
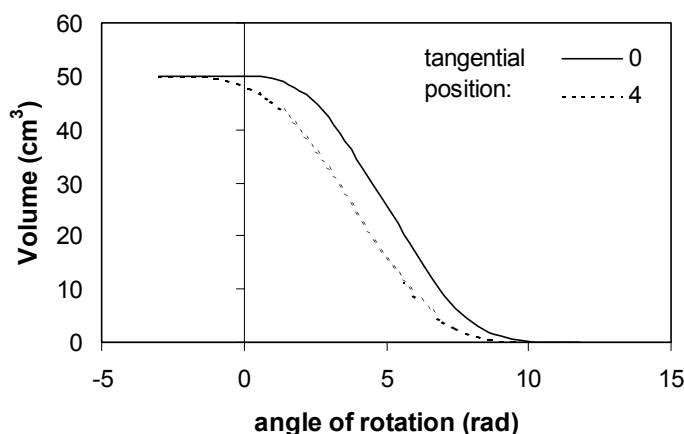
Figure 1.8. *Volume of the compression chamber versus the angle of rotation.*

1.4.2 Constitutive equations

A good description of the extrusion pulping mechanism and energy consumption requires the rheological model of fibres, which is characterised by the constitutive equations. Although fibres possess a wide range of rheologic properties, only those properties need to be taken into account that are critical for the extrusion pulping process. Fibres appear to be processed when pressurised, suggesting that processing is related to the friction between the fibres. The presence of water might play an important role in this mechanism, as water impedes the fibres in approaching each other too near and it decreases the friction between fibres. During compression water is squeezed out of the pulp, facilitating the fibres to reach each other.

A suspension of cylindrical fibres having a length l and a diameter d is non-dilute, when a fibre cannot rotate freely without encountering other fibres: at concentrations higher than $1/l^3$. If spacing between fibres becomes of order d (at a concentration of $1/dl^2$), the fibre motion is so restricted that the suspension ceases to be a fluid [49]. Below this concentration the system behaves as a viscoelastic liquid [50] and above this concentration it behaves as an elastic solid material [49]. The orientation distribution of the rods in the 'solid' elastic material is not random anymore, when the concentration approaches $1/d^2l$. In case of fibres with an l/d ratio of 1000, a random suspension with a volume fraction above 0.1 % has to be regarded as a solid material. When fibres are laying parallel to each other, this boundary lays higher. Bast fibre pulps with a consistency of at least 10% in the extruder should according to the above-mentioned theory always be regarded as a solid material.

It is generally believed that, at medium and high consistencies and with long fibres, the network is so strong that fibres move in plug flow. Moreover, the networks won't break uniformly in the model viscometers developed for liquids. In this case the plug of material slips along the wall and the determined stress will be the wall shear stress, which is the stress at the wall needed before the plug starts to move [51,52]. This wall shear stress is based on the friction between the fibre mass and the wall and depends both on the roughness of the wall and the kind of fibre.

Above a critical concentration the network strength exhibited by the fibre suspensions arises from frictional forces resulting from elastic fibre bending. Normal forces are imposed on the contact points between the fibres. Lord [53] divides the field of fibre friction into three categories: 1. friction between two single fibres; 2. friction between a single fibre and a fibre assembly, and 3. friction between fibre assemblies. The first and second category have been studied extensively on cotton and several synthetic fibres [53-58]. Less work has been carried out on the frictional forces between fibre assemblies [53,59,60]. Lord [53] notes that the pattern of fibres parallel to the shear plane strongly influences the frictional behaviour, but the exact effect of orientation is still unknown and the effect of fibres perpendicular to the shear plane has never been investigated. Moreover, it has been mentioned that macroscopic forces on a fibrous system are transmitted by the fibres in a complicated way [56], but none of the authors mentions a method to calculate pressures on the fibres at different locations in a fibrous system. Moreover, at higher normal forces the required shear forces exceed the fibre tensile strength, so that shearing will lead to breaking of the fibre instead of a moving along the surrounding fibres. At this point it appeared necessary to investigate the rheology of high consistency pulp. The ability to extend low and medium consistency pulp models to higher consistencies is investigated and discussed in the following section.

Fibre suspensions

The evaluation on pulp or suspension viscosity is mostly carried out by experiments on model apparatus and data are filled in model equations [52,61,62]. Hydrodynamical theories which predict the Newtonian viscosity for dilute suspensions have been developed by Burgers [63] for cylindrical rods. This theory can be expressed as follows:

$$\eta_r = 1 + \alpha_0 C \qquad\qquad [1.2]$$

The dimensionless factor α_0 is determined by the shape, dimensions and orientations of the suspended fibres. Experimental investigations on the viscosity of a non-dilute suspension of fibres in a Newtonian fluid have been reported among others by Blakeney [64], Rosinger et al. [65] and Maschmeyer and Hill [66]. The experimental results indicate that a fibre suspension displays non-Newtonian behaviour, which can be time-dependent and can have a power law and yield stress region. Moreover, each author suspects that the fibre orientation induced by the flow geometry strongly influences the shearing properties of the suspension and Blakeney [64] observed that a very slight fibre curvature has a significant effect on the viscosity. Blakeney extended Burgers' equation to account for fibre-fibre interactions as follows:

$$\eta_r = 1 + k_1 C + k_2 C^2 \qquad\qquad [1.3]$$

Maschmeyer and Hill [66] observed that both the quantitative and qualitative aspects of fibre suspension rheology depend strongly on fibre length. Utracki and Fisa [67] summarise relationships between the rheology of composites and the volume fraction of fibres. All relationships are in principle developed as a correction on the non-filled liquid viscosity for the presence of fibres. Utracki and Fisa note that polydispersity, particle shape and structure formation may significantly complicate the analysis of the viscosity versus volume fraction dependence. Vaxman et al. [68-70] and Vincent and Agassant [71] studied fibre orientation in suspensions. Vincent and Agassant [71] showed that the orientation of fibres is different in different types of steady flow. Often orientation in the flow direction is observed, which

increases with shear rate and fibre length [69-71]. Vaxman et al. also observed fibre breakage at high shear rates.

Rheological behaviour and fibre orientation during the flow of fibre suspensions involve complex interactions between the dynamics of fibre orientation development and the flow field. Further non-linearity's are brought into the system by multi-particle interactions, comparable physical dimensions of the flow field and the fibres and the flexibility of the fibres. Fundamental studies performed on the flow behaviour of fibre suspensions mostly involve only one or two of the above mentioned complex interactions. Batchelor [72,73] developed a general fundamental constitutive equation for suspensions of particles of any shape in Newtonian liquids at arbitrary concentrations. However, he only considered the dependence of the bulk stress on the instantaneous configuration of the particles; 'history' effects are set aside. Application of Batchelor's general result to non-dilute suspensions is difficult according to Dinh and Amstrong [74], because calculation of the macroscopically observable stress requires knowledge of the details of the local velocity field around every particle. Dinh and Amstrong [74] developed a single particle model for semi-concentrated suspensions of long fibres by beginning with Batchelor's [72] general result. Dinh and Amstrong use an 'effective' medium as approximation for the fibre suspension surrounding the test particle. Further they assume the particle in a homogeneous flow field and they introduce a distribution function to account for the probability that the test fibre selected has a specific location and orientation at time t. The constitutive equations of Dinh and Amstrong [74] are not able to predict the change of orientation of the fibres caused by shear stress.

Cintra and Tucker [75] report that in recent years a rapid progress has started in the ability to model the orientational structure in fibre-reinforced composites. Cintra and Tucker developed a family of orthotropic closure approximations for modelling of flow-induced fibre orientation in short rigid fibre-reinforced composites. These closures approximate the fourth-order moment tensor for fibre orientation in terms of the second-order moment tensor. The equations developed by Cintra and Tucker [75] are complicated and are only valid for dilute suspensions and perfectly rigid rods.

It revealed that both empirical [63-67] and fundamental models [72-75] for suspensions and composites are based on the pure liquid viscosity corrected for the presence of fibres. The high consistencies, which are encountered during extrusion, are beyond the validity range of these models and use of an extension of those models still assumes liquid flow properties. Furthermore, the fundamental models are based on rigid rods, do not include fibre friction and model equations are too complicated to lead to mathematically solvable systems when applied to complicated flow regimes. Extension to flexible fibres, fibre friction and high consistencies will make the models even more complicated.

According the concentration regimes for fibre suspensions, at high consistencies like encountered during extrusion fibre masses should be regarded as solids. The properties of solids and liquids differ so much that the mechanisms of flow of these phases are quite dissimilar. First of all, solids can transfer shear stresses under static conditions, they have a static angle of friction greater than zero, whereas liquids do not [76]. This is why solids form piles whereas liquids form level surfaces. Secondly many solids, when consolidated, possess cohesive strength and retain a shape under load [76]. Thirdly, the shear stresses, which occur in a slowly deforming bulk solid, can usually be considered independent of the rate of shear and dependent on the mean pressure acting within the solid. The situation is reversed in a

liquid; the shear stresses are dependent on the rate of shear and independent of the mean pressure [76].

Therefore, in order to obtain the right model to describe the flow of high consistency fibre masses, the fundamentals behind solid flow have been studied for its applicability to fibres at high consistency. The rheology of granular materials has been evaluated on the basis of interparticle friction. Both granular material and high consistency fibre masses consist of macroscopic particles interacting with each other according to classical mechanics. Moreover, like fibres, granular materials can contain liquids.

Granular Materials

The classical theory of the dynamics of granular materials contains the assumption that stress in the solid phase is not influenced by any property of the interstitial fluid [77,78], while a sizable fraction of this literature refers to dry granular flow, where there is no interstitial fluid at all [79]. Broersma [80] pays attention to granular materials containing fluids. He refers to the removal of vegetable oils from beans, nuts and seeds by mechanical means like a press or a screw extruder. Due to the granular character of the material, surface stresses will retain oil in the seed mass, even under pressure, where no further deformation happens. Broersma [80] describes the theory of Gans [81] who developed a model for the removal oil from seeds.

Gans [81] considers a seed mass as consisting of a compressible solid part, which may show pure elastic and pure viscous behaviour (according to Gans to describe as a Maxwell body) and an incompressible fluid part, oil, which shows viscous behaviour according to Newton's law. During the processing the elastic solid part is compressed and producing oil and the incompressible oil leaves the seed mass. In the seed mass the flux of oil depends on the radius and length of the capillaries, on the pressure drop over the length of the capillaries and on the viscosity of the oil. The consistency of the seed mass is thus of primary importance for the oil output. With respect to this seed mass consistency Gans uses Darcy's law. Gans applies Newton's fluid friction law to the seed mass, as a "quasi fluid", but comments that if Coulomb's friction law for moving solid bodies would apply, than any shear stress between moving seed mass planes would equal the pressure on that plane times a friction coefficient.

Flow of liquid out of a compressible porous solid is also observed in juice expression from fruit or vegetable pulp. The description of those processes is mainly based on the flow of liquid out of a solid-liquid mixture, but it describes also the pressurising of a solid-liquid system. The expression process is used for example to recover meat juices from meats, to expel whey from cheese curds, to dewater moist processing wastes, or to recover sugar juices from sugar cane, etc. Singh and Kulshreshtha [82], for example, developed a mathematical model to describe the juice expression process from a saturated bed of a solid-liquid system, and confirmed their model with experiments with carrots. The model was based on a fundamental mass balance and on Terzaghi's [83] theory of one-dimensional soil consolidations. The model developed by Singh and Kulshreshtha comprises relationships to describe the flow of juice through a porous bed, the mass balance for the juice, the distribution of solid and liquid pressure in the cake and the dependence of the porosity on the solid pressure.

The yield or shear strength should be considered in discussing the flow-no flow criteria of a solid [76]. An unconsolidated solid has no yield strength, but, when pressures arise under the weight of the superimposed mass, particles are brought closer together causing the

11

material to consolidate and gain strength. The higher the pressure the greater the consolidation and the strength of the material. The shear strength of a material is the maximum shear stress on a surface in the material before the material ruptures. The wall shear strength is the stress needed at the wall before a plug of particles starts to move in the apparatus.

Being composed of natural fibres, which do not interact mechanically as do metallic atoms, a unique value of the shear strength cannot be given. Coulomb [84] provided the first comprehensive description of shear strength for soil. He stated that the limit of shear resistance is composed of two components, namely cohesion and friction. Cohesion is that part of resistance that can be measured by the direct rupture of two parts of a body in tension. Cohesion does not depend on perpendicular pressure on the rupture surface [85]. Friction, on the other hand, is a process wherein shear resistance depends upon the perpendicular pressure on the sliding surface. The shear resistance of many materials is proportional to normal pressure on a particular plane within a material. Coulomb's law can be expressed as follows:

$$\tau = c + \sigma_n \tan \phi \qquad\qquad [1.4]$$

The tangent of the angle of internal friction, $\tan \phi$, is the coefficient of friction commonly used when computing the sliding resistance of one material body over another. In this application, the coefficient is that of frictional strength on an internal surface, and is the constant of proportional increase in shear strength with increasing normal pressure on the surface. The term c, normally denoted as the cohesional strength of a material, describes the presence of any kind of structural strength.

1.4.3 The model

Constitutive equations

The system consists of two phases; a solid hydrophilic fibre network and a liquid phase. Forces acting on the fibre network compress the solid matrix. This requires relationships between the stress on the solid matrix and the volumetric strain. The liquid phase is expressed from the solid matrix by hydraulic forces. The speed of liquid expression depends on the permeability of the matrix and the hydraulic pressure gradient. Modelling the drainage behaviour requires knowledge of the flow paths of the liquid. Because liquid encounters a higher flow resistance in the fibre cell wall compared to between the fibres, it is necessary to know how much liquid is located in the interstices between the fibres and how much is located in the porous structure of the fibre wall. This requires a relation describing the dependence of volumetric swelling of the fibres on the stress on the solid matrix. Local stress forces in the solid matrix can be calculated using the stress-strain relationship and Poisson's ratio for the fibre network for the transfer of stresses. To be able to use the solid flow model in the development of an extrusion pulping model for natural fibres the shear strength parameters of fibres should be known.

With knowledge of the relations described above the compression and shear forces in the wet fibre mass can be modelled during compression for different process conditions and screw configurations. To be able to relate process conditions to product quality, relations between the compressive and shear forces and the fibre properties are required. These should be obtained by implementation of experimental results into the model.

Summarised we need the following constitutive equations for fibres to be able to build the extrusion pulping model:
-   compressibility of the fibre mass
-   swelling of the fibres
-   drainage through the fibre mass, permeability of the fibre mass
-   shear strength of the fibre mass

These constitutive equations have been experimentally determined for hemp bast fibres and are described in this work.

The equations for extrusion pulping model

The total stress on the fibres is the sum of the hydraulic pressure and the pressure on the solid matrix:

$$\sigma_{tot} = \sigma_s + \sigma_l \qquad [1.5]$$

There is no gradient in total stress:

$$\overline{\nabla}\sigma_{tot} = 0 \qquad [1.6]$$

$$\rightarrow \overline{\nabla}\sigma_s = -\overline{\nabla}\sigma_l \qquad [1.7]$$

The conservation of mass leads to

$$\frac{1}{V_t}\frac{\partial V_t}{\partial t} = -\left(\overline{\nabla}\cdot\overline{q}\right) \qquad [1.8]$$

The relation between the overall stress on the solid and the volumetric strain is required to describe the compression mechanism:

$$\sigma_s = \sigma_s\left(\frac{V_s}{V_t}\right) \qquad [1.9]$$

Fluid flow through the porous fibrous medium is described with Darcy's law:

$$\overline{q} = K(\varepsilon)\overline{\nabla}\sigma_l = -K(\varepsilon)\overline{\nabla}\sigma_s \qquad [1.10]$$

The relation between the permeability, K, and the porosity, ε, needs to be determined.
Liquid is held both by the fibre cell wall, causing a volumetric swelling of the fibres, and in the interstices between the fibres. This requires a relation between the extent of swelling and the stress on the solid matrix, $X(\sigma_s)$. The distribution of the liquid is described with the following additional equations:

$$V_l = V_{l,bf} + V_{l,a} \qquad [1.11]$$

$$V_f = V_{l,a} + V_s = X(\sigma_s)V_s \qquad [1.12]$$

13

$$V_t = V_{l,bf} + V_f \qquad\qquad\qquad [1.13]$$

The porosity is the ratio between the volume of liquid between the fibres and the total volume of the volume element:

$$\varepsilon = \frac{V_{lbf}}{V_t} = \frac{V_{lbf}}{V_l + V_s} \qquad\qquad\qquad [1.14]$$

The relation between the shear strength and the normal stress on a plane is described with Coulomb's law (no cohesional forces):

$$\tau = \sigma_s \tan\phi\left(\frac{V_l}{V_t}\right) \qquad\qquad\qquad [1.15]$$

As the speed of the piston, u(t), determines total volume decrease the following boundary condition applies:

$$\frac{dV}{dt} = u(t)A = \int_V \frac{\partial V_t}{\partial t} dV \qquad\qquad\qquad [1.16]$$

Schematic diagram of model

The schematic diagram in Figure 1.9 shows how the different geometric and constitutive relations can be combined into a model for calculation of the compression and shear forces in the 'compression chamber' of the extruder for different process conditions.

1.5 Outline of this study

The aim of the research described in this thesis was to elucidate the mechanisms behind extrusion pulping in order to develop a model that describes the relation between process conditions, screw configuration and product quality. This encloses the determination of the constitutive equations for those rheological properties that are critical for the extrusion pulping process.

Chapter 2 discusses the behaviour of hemp bast fibres under compression. Compression and relaxation behaviour of hemp bast fibres have been studied under different conditions. The influence of strain rate, pre-treatment, temperature and maximum stress has been studied. The effect of repeated compression on the fibres is discussed as well.

The swelling of hemp bast fibres under pressure is described in Chapter 3. Experiments are performed at different pressures with fibres soaked in water or in 0.2 M NaOH. The extent of swelling and the distribution of liquid between the fibres and the space between the fibres are related to the pressure.

Shear stress

$$\tau = \sigma_s \tan \phi \left(\frac{V_l}{V_t} \right)$$

Volume decrease

$$\Delta V_t$$

Solid stress

$$\sigma_s \left(\frac{V_s}{V_t} \right)$$

Fibre swelling

$$X(\sigma_s)$$

Porosity

$$\varepsilon = 1 - \frac{XV_s}{V_t}$$

Total stress

$$\sigma_t = \sigma_l + \sigma_s$$

Liquid pressure

$$\overline{q} = K(\varepsilon)\overline{\nabla}\sigma_l$$

$$\overline{q} = \frac{\partial V_t}{\partial t}$$

Permeability

$$K(\varepsilon)$$
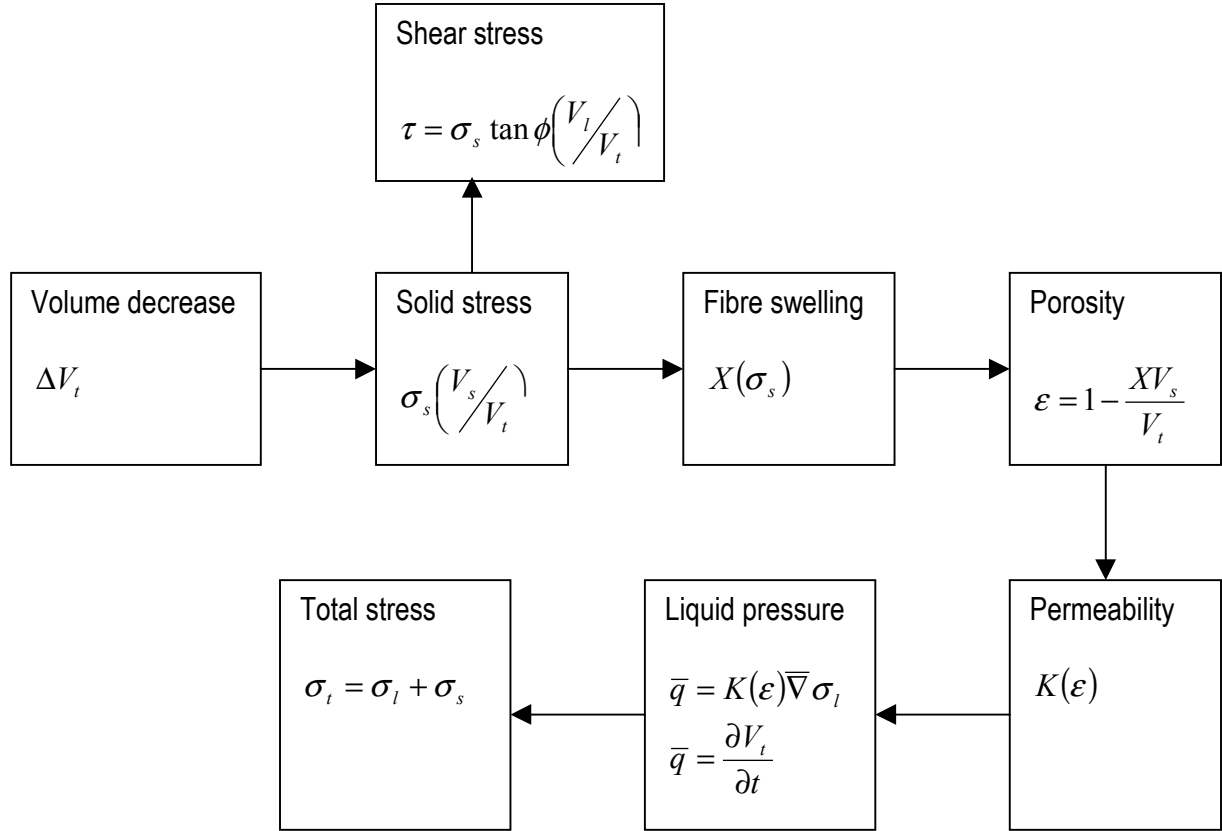
Figure 1.9. Schematic diagram of the model

The drainage through hemp bast fibre pulp has been studied for fibres in water and different concentrations of sodium hydroxide. These results are given in Chapter 4. The experimental results are fitted to three flow models based on different principles; a decreasing permeability model, the Kozeny-Carman model, and the Kozeny-Carman model in combination with a swelling model.

The shear strength of hemp bast fibres under pressure has been analysed for different pretreatments and moisture contents. The results are summarised in Chapter 5.

In order to gain insight in the mechanisms underlying extrusion pulping, the behaviour of hemp fibres during extrusion has been observed and extrusion experiments have been performed while varying different parameters and studying energy consumption and differences in the extrusion product. Results and insight gained from these experiments are described in Chapter 6.

1.6 Nomenclature

A	cross-sectional area	m^2
C	volume concentration of fibres	%
c	cohesional strength	Pa
d	fibre diameter	m
K	permeability	$m^4 N^{-1} s^{-1}$
l	fibre length	m
P	specific energy consumption	$kWh \cdot ton^{-1}$
p	screw pitch	m
q	flux	$m \cdot s^{-1}$
t	time	s
$\tan \phi$	internal friction coefficient	-
$\tan \delta$	internal friction coefficient	-
u	speed of piston	$m \cdot s^{-1}$
V	volume	m^3
v	axial velocity	$m \cdot s^{-1}$
W	screw speed	s^{-1}
X	factor describing volumetric swelling	-
α_0	dimensionless factor	-
ε	porosity	-
η_r	the relative viscosity = η / η_0	-
σ	stress	Pa
τ	shear stress	Pa
ϕ	angle of internal friction	-

Subscripts

a	adsorbed
bf	between the fibres
f	fibre
l	liquid
n	normal
s	solid
tot	total
t	total of volume element
w	wall

1.7 References

1. Postel, S. and Ryan, J.C. (1991): In "State of the world 1991" WW Norton & Company, New York, p. 75-92.
2. McDougall, F.J., Morrison, I.M., Stewart, D., Weyers, J.D.B. and Hillman, J.R. (1993): Plant fibres: botany, chemistry and processing for industrial use, J. Sci. Food Agric. 62, 1-20.
3. van Roekel, G.J., Lips, S.J.J., Op den Kamp, R.G.M. and Baron, G. (1995): Extrusion pulping of true hemp bast fibre (*Cannabis sativa* L.), Tappi Conference, Chigago, USA, p. 477-485.
4. van Roekel, G.J. (1995): Chemimechanical pulping of fibre hemp, Bioresource Hemp, Frankfurt a/M, Germany.
5. van Roekel, G.J. (1996): Bulk papermaking applications for bast fibre crops using extrusion pulping, PIRA International, Peterborough, England, p. paper 26, 29 pp.
6. Kurdin, J.A. and Bohn, W.L. (1984): Mechanical pulping by extrusion, Tappi Pulping Conference, San Fransisco CA, USA, p. 265-274.
7. Kurdin, J.A. (1985): New developments in mechanical pulping, South. Pulp Paper, 45-51.
8. de Choudens, C., Angelier, R. and Combette, P. (1984): Pâtes mécaniques de résineux pâtes chimicomécaniques de feuillues, Revue A.T.I.P 38: 8, 405-416.
9. de Choudens, C., Angelier, R. and Lombardo, G. (1987): Pâtes chimico-mécaniques blanchies obtenues par le procédé "BiVis", Revue A.T.I.P 41: 2, 63-68.
10. de Choudens, C. and Angelier, R. (1990): Les Pâtes chimico-thermo-mécaniques blanchies obtenues par le procédé BiVis, Revue A.T.I.P. 44: 3, 137-146.
11. Babé, F. (1995): Fabriquer la pâte à partir de sorgho: opération réussie, Papier, Carton & Cellulose 44: 5-6, 24-25.
12. N'Diaye, S., Rigal, L., Larocque, P. and Vidal, P.F. (1996): Extraction of hemicelluloses from polar, *Populus tremuloides*, using an extruder-type twin-screw reactor: a feasibility study, Bioresource Techn. 57, 61-67.
13. Creusot-Loire (1977): Procédé et machine de fabrication de pâte à papier, France, Patent 75 23911.
14. Creusot-Loire (1980): Procédé et machine de fabrication de pâte à papier, France, Patent 78 26865.
15. de Choudens, C. and Bourne, C. (1979): Procédé pour la fabrication de pâtes papetières mécano-chimiques à haut rendement, France, Patent 77 21024.
16. de Choudens, C., Angelier, R., Combette, P. and Lesas, C. (1989): Procédé de fabrication de pâtes chimicomécaniques ou chimicothermo-mécaniques blanchies, Patent 87 11082.
17. Westenbroek, A.P.H. and van Roekel, G.J. (1996): Internal report.
18. Janssen, L.P.B.M. (1978): "Twin screw extrusion". Elsevier Scientific Publishing Company, Amsterdam.
19. Martelli, F.G. (1983): "Twin screw extruders: A basic understanding". Van Nostrand, Reinhold, New York.
20. Yacu, W.A. (1985): Modeling a twin-screw co-rotating extruder, J. Food Eng. 8: 1, 1-21.
21. Tayeb, J. and Della Valle, G. (1988): Theoretical computation of the isothermal flow through the reverse screw element of a twin Screw extrusion cooker, J. Food Sci. 53: 2, 616-625.

22. Tayeb, J., Della Valle, G., Barrès, C. and Vergnes, B. (1992): In "Food extrusion science and technology", J. L. Kokini, C. Ho and M. V. Karwe, ed., Marcel Dekker Inc., New York, p. 41-70.

23. van Zuilichem, D.J. (1992): Extrusion cooking; Craft or Science?, Thesis, Agricultural University, Wageningen.

24. Jager, T. (1992): Residence time distribution in twin-screw extruders, Thesis, Agricultural University, Wageningen.

25. Vergnes, B., Barrès, C. and Tayeb, J. (1992): Computation of residence time and energy distributions in the reverse screw element of a twin-screw extrusion cooker, J. Food Eng. 16, 215-237.

26. Vergnes, B. (1996): Analysis and modelling of the twin-screw extrusion process, Clextral, Firminy, France, p. 60-67.

27. Seth, R.S. (1996): Optimizing reinforcement pulps by fracture toughness, Tappi J. 79: 1, 170-178.

28. de Jong, E., van Roekel, G.J., Snijder, M.H.B. and Zhang, Y. (1999): Towards industrial applications of bast fibre pulps; their potential as a nonwood source is discussed, Pulp Paper Canada 100: 9, T270-T273.

29. Snijder, M.H.B., Wissing, E. and Modder, J.F. (1997): Polyolefins and engineering plastics reinforced with annual plant fibers, 4th Int. Conf. Woodfiber-plastic Composites, Madison (Wisconsin), USA, p. 181-191.

30. Herrera-Franco, P.J. and Aguilar-Vega, M. (1997): Effect of fiber treatment on the mechanical properties of LDPE-henequen cellulosic fiber composites, J. Appl. Pol. Sci. 65: 1, 197-207.

31. Heijenrath, R. and Peijs, T. (1996): Natural-fibre-mat-reinforced thermoplastic composites based on flax fibres and polypropylene, Adv. Pol. Let. 5: 3, 71-75.

32. Mieck, K.-P., Nechwatal, A. and Knobelsdorf, C. (1995): Faser-Matrix-Haftung in Kunststoffverbunden aus thermoplastischer Matrix und Flachs, 2a, Angew. Makromol. Chem. 225, 37-49.

33. Sanadi, A.R., Caulfield, D.F., Jacobson, R.E. and Rowell, R.M. (1995): Renewable agricultural fibers as reinforcing fillers in plastics: mechanical properties of kenaf fiber - polypropylene composites, Ind. Eng. Chem. Res. 34, 1889-1896.

34. Harsveld van der Veen, J.E. (1995): The effect of age on quality of hemp bast fibres as raw material for pulp and papermaking, Biorohstoff Hanf.

35. Matthews, J.M. (1947): "Textile fibres, their physical, microscopical and chemical properties". John Wiley & Sons, New York.

36. Kirby, R.H. (1963): "Vegetable fibres, botany, cultivation and utilization". Interscience Publishers Inc., New York.

37. van der Werf, H.G.M., Harsveld van der Veen, J.E., Bouma, A.T.M. and ten Cate, M. (1994): Quality of hemp (*Cannabis Sativa* L.) stems as a raw material for paper, Ind. Crops Prod. 2, 219-227.

38. Dence, C.W. and Reeve, D.W. (1996): "Pulp Bleaching- Principles and Practice". Tappi Press, Atlanta.

39. Catling, D. and Grayson, J. (1982): "Identification of vegetable fibres". Chapman and Hall, London.

40. Fengel, D. and Wegener, G. (1984): "Wood; Chemistry, Ultrastructure, Reactions". Walter de Gruyter, Berlin.

41. Gilmour, S.C. (1955): "Paper: Its making, merchanting and usage : the paper merchant's textbook". National Assn. of Paper Merchants, London.

42. Batra, S.K. (1989): In "Handbook of Fibre Science and Technology", M. Lewin and E. M. Pierce, ed., Marcel Dekker Inc., New York, p. 727-807.

43. Kocurek, M.J., Hamilton, F. and Leopold, B. (1987): "Pulp and paper manufacture, Volume 3: Secondary fibres and non-wood pulping". Joint Textbook Committee of the Paper Industry, Canada.

44. Rance, H.F. (1980): "The raw materials and processing of papermaking". Elsevier Scientific Publishing Company, Amsterdam.

45. Rydholm, S.A. (1965): "Pulping Processes". John Wiley and Sons, Inc., New York.

46. Smook, G.A. (1982): "Handbook for pulp and paper technologists". Tappi, Atlanta.

47. Hägglund, E. (1951): "Chemistry of Wood". Academic Press Inc., Publishers, New York.

48. Ranalli, P. (1998): In "Advances in hemp research", P. Ranalli, ed., Food Products Press, An Imprint of The Haworth Press, Inc., New York, p. 61-84.

49. Doi, M. and Kuzuu, N.Y. (1980): Nonlinear elasticity of rodlike macromolecules in condensed state, Polym. Sci.: Polym. Phys. Ed. 18, 409-419.

50. Doi, M. and Edwards, S.F. (1978): Dynamics of rod-like macromolecules in concentrated solution. Part I, J. Chem. Soc., Faraday Trans. 2 74: 3, 560-570.

51. Singh, K.M. and Stenuf, T.J. (1986): Determination of wall shear stress of medium and high consistency pulps, Tappi Engineering Conference, Book 2, Atlanta, USA, p. 589-591.

52. Longdill, G.R. and Duffy, G.D. (1988): The shear behavior of medium concentration wood pulp suspensions, Appita 41: 6, 456-461.

53. Lord, E. (1955): Frictional forces between fringes of fibres, J. Textile Inst. 46, P41-P58.

54. El Mogahzy, Y.E. and Gupta, B.S. (1993): Friction in fibrous materials. Part II: Experimental study of the effects of structural and morphological factors, Textile Res. J. 63: 4, 219-230.

55. de Jong, H.G. (1993): Yarn-to-yarn friction in relation to some properties of fiber materials, Textile Res. J. 63: 1, 14-18.

56. Andersson, S.R. and Rasmuson, A. (1997): Dry and wet friction of single pulp and synthetic fibres, J. Pulp Paper Sci. 23: 1, J5-J11.

57. Postle, L.J. and Ingham, J. (1952): The relation between external pressure and inter-fibre forces in untwisted slivers, J. Text. Inst. 43, T87-T90.

58. Cox, D.R. (1952): The relation between external pressure and inter-fibre forces in untwisted slivers, J. Text. Inst. 43, T87-T90.

59. Martindale, J.G. (1947): An instrument for the measurement of the forces operating between fibres during drafting, J. Text. Inst. 38, T151-T166.

60. Morrow, J.A. (1931): The frictional properties of cotton materials, J. Text. Inst. 22, T425-T440.

61. Chase, W.C., Donatelli, A.A. and Walkinshaw, J.W. (1989): Effects of freeness and consistency on the viscosity of hardwood and softwood pulp suspensions, Tappi J. 72: 5, 199-204.

62. Crowell, E.P. (1976): Interlaboratory evaluation of pulp viscosity measurements, Tappi J. 59: 4, 142-145.

63. Burgers, J.M. (1938): In "Second report on viscosity and plasticity" Nordemann, New York, p. 113-184.

64. Blakeney, W.R. (1966): The viscosity of suspensions of straight rigid rods, J. Colloid Interface Sci. 22, 324-330.

65. Rosinger, E.L.J., Woodhams, T. and Chaffrey, C.E. (1974): Shear flow behavior of complex asbestos fibril dispersions, Trans Soc. Rheol. 18: 3, 453-466.

66. Maschmeyer, R.O. and Hill, C.T. (1977): Rheology of concentrated suspensions of fibers in tube flow II; An exploratory study, Trans. Soc. Rheol. 21: 2, 183-194.

67.   Utracki, L.A. and Fisa, B. (1982): Rheology of fiber- or flake-filled plastics, Polymer Composites 3: 4, 193-211.

68.   Vaxman, A., Narkis, M., Siegmann, A. and Kenig, S. (1989, I): Short-fiber reinforced thermoplastics I, Rheological properties of glass-reinforced Noryl, Polymer Composites 10: 2, 78-83.

69.   Vaxman, A., Narkis, M., Siegmann, A. and Kenig, S. (1989, II): Short-fiber reinforced thermoplastics II, Interrelation between fiber orientation and rheological properties of glass-reinforced Noryl, Polymer Composites 10: 2, 84-91.

70.   Vaxman, A., Narkis, M., Siegmann, A. and Kenig, S. (1989, III): Short-fiber reinforced thermoplastics III, Effect of fiber length on rheological properties and fiber orientation, Polymer Composites 10: 6, 454-462.

71.   Vincent, M. and Agassant, J.F. (1984): In "Interrelations between processing structure and properties of polymeric materials", J. C. Seferis and P. S. Theocaris, ed., Elsevier Science Publ. BV, Amsterdam, p. 241-248.

72.   Batchelor, G.K. (1970): The stress system in a suspension of force-free particles, J. Fluid Mech. 41: 3, 545-570.

73.   Batchelor, G.K. (1971): The stress generated in a non-dilute suspension of elongated particles by pure straining motion, J. Fluid Mech. 46: 4, 813-829.

74.   Dinh, S.M. and Amstrong, R.C. (1984): A rheological equation of state for semiconcentrated fiber suspensions, J. Rheology 28: 3, 207-227.

75.   Cintra, J.S., Jr. and Tucker III, C.L. (1995): Orthotropic closure approximations for flow-induced fiber orientation, J. Rheology 39: 6, 1095-1122.

76.   Jenike, A.W. (1967): "Storage and flow of solids". University of Utah, Utah.

77.   Jenkins, J.T. and Savage, S.B. (1983): A theory of the rapid flow of identical, smooth, nearly elastic spherical particles, J. Fluid Mech. 130, 187-202.

78.   Haff, P.K. (1983): Grain flow as a fluid-mechanical phenomenon, J. Fluid Mech. 134, 401-430.

79.   Jackson, R. (1986): Some features of the flow of granular materials and aerated granular materials, J. Rheology 30, 907-930.

80.   Broersma, G. (1972): "Behaviour of granular materials". Stam Technical Publications, Culemborg.

81.   Gans, H.P.H. (1948): Bijdrage tot het verkrijgen van inzicht in hetgeen zich in een wringer afspeelt (Contribution to the understanding of the extruding process in a mechanical extraction apparatus), Thesis, University of Technology, Delft.

82.   Singh, S. and Kulshreshtha, M. (1996): Mathematical modelling of juice expression from carrots under uniaxial compression, J. Food Eng. 27, 323-336.

83.   Terzaghi, K. (1943): "Theoretical soil mechanics". John Wiley, New York.

84.   Coulomb, C.A. (1776): Essai sur une application des règles des maximis et minimis à quelques problèmes de statique relatifs à l'architecture., Academie royale des Sciences: Mémoires de Mathématique et de Physique, presentés à l'Academie royale des Sciences, par divers savants, et lus dans les Assemblées 7, 343-382.

85.   McKyes, E. (1989): "Agricultural engineering soil mechanics". Elsevier, Amsterdam.

Chapter 2

Compressibility of hemp bast fibres [*]

Summary

A force-based characterisation of the extrusion pulping process is necessary to be able to predict the effects of extrusion on fibres. To determine which forces are beneficial and which only cause energy consumption, the nature and the origin of the forces have to be known. This paper discusses the behaviour of hemp bast fibres under compression to better understand the underlying mechanisms involved in the application of energy to the fibres. Untreated, water soaked and NaOH-soaked hemp bast fibres were subjected to varying loads and loading rates and the resulting stress-density and relaxation curves were studied.

The stress-density relationship of hemp bast fibres was described with the compressibility equation. The coefficient of the compressibility equation decreased with temperature and moisture content. Fibres became more flexible and fibre bending became more important in the mechanism of fibre compression. The higher flexibility resulted in a lower stress over the whole density range. The compressibility equation also applied to the stress-density curve during compression of soaked fibres at low densities. However, at higher density the stress increased faster, because of flow resistance caused by the dense fibre mat. The flow limitation was advanced at higher strain rates and enhanced at higher sodium hydroxide concentrations.

Relaxation was described with a generalised Maxwell model. The extent of relaxation slightly decreased with increasing maximum stress, increased with strain rate and increased with moisture content. Soaked fibres showed a much higher relaxation, which, however, was mostly caused by the high maximum stress because of the flow resistance at higher densities. When regarding the solid stress instead of the total stress, relaxation appeared to be lower. Mechanical pulping processes should therefore be operated at such low strain rates, that the stress observed only depends on the density obtained and not on the flow resistance.

During repeated compression both maximum stress and the extent of relaxation decreased with the number of repetitions and the total plastic strain increased until a point was reached at which no further changes were observed. However, the total plastic strain showed a higher dependence on the maximum stress during repeated compression than on the number of compressions. Repeated compression of wet fibres resulted in the formation of a compact fibre mat with a high flow resistance causing high stress peaks.

2.1 Introduction

Non-wood fibres, including hemp and flax, are suitable as raw materials for paper [1-3], as reinforcement in recycled paper and board [4], as replacement of synthetic fibres in nonwovens [5] or as reinforcement for composites [6-9]. Bast fibre bundles are located in the outer layer of the stem. Each hemp fibre bundle is composed of overlapping bast fibres [10] and a cross section consists of ten to forty elementary hemp fibres, 'glued' together with pectin and/or lignin (Fig. 2.1). The length of the elementary hemp fibres varies between 5 and 55 mm and the thickness is about 20 μm. In comparison with wood, hemp bast fibres have a thick cell wall and a small lumen. Hemp bast fibres consist of 60-70 % highly crystalline cellulose. Other components include hemicellulose (10-15 %), lignin (3 %), pectin (1-3 %), mineral matter, fats and waxes [5,11].
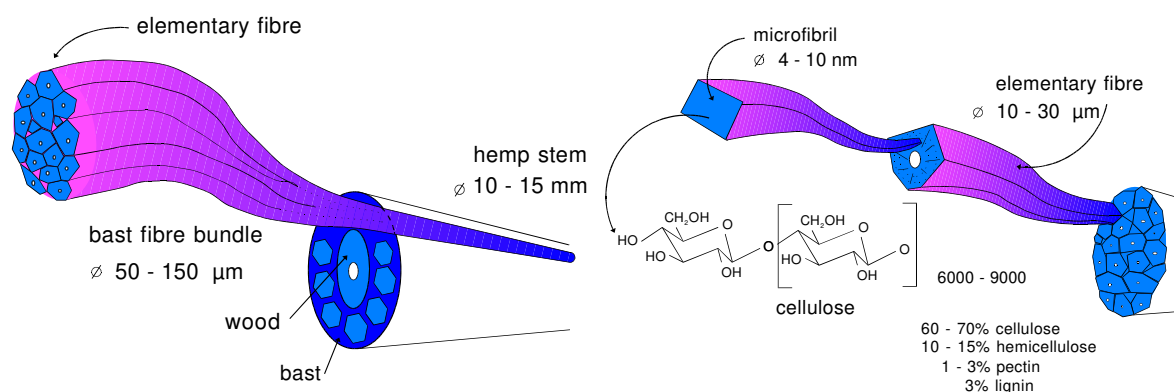
Figure 2.1 (A+B): *Schematic reproduction of a hemp stem*

Extrusion pulping is a chemi-mechanical pulping method, which is especially useful in processing long non-wood fibres, including hemp and flax. These long fibres can be fed unshortened to the pulping process. In the extruder the fibres are shortened and the fibre bundles, consisting of elementary fibres, are defibrated and elementary fibres are fibrillated, which is achieved by repeated compression and shear forces in the extruder [1,3].

The repeated compression and relaxation of fibres results in a mechanical disruption of the bonds holding together the lamella between the elementary fibres, while the shear forces help to fibrillate the fibres [12-14]. Van Roekel et al [1] evaluated results obtained from hemp extrusion pulping trials with softwood market pulps. It was concluded that extrusion pulping is an economically, technically and environmentally viable alternative to the traditional chemical pulping technology for non-wood fibres.

Both pulp quality and energy requirement are greatly affected by the configuration of the extruder screws, the screw rotation speed and the throughput [1,15]. The process can be better controlled if the relations between the product properties, extruder configuration and extrusion conditions are known. Our ultimate goal is to establish an extrusion-pulping model, which will predict the choice of process parameters required for a specific fibre length, fibre length distribution and degree of defibration and fibrillation. With this model the process can be controlled, the energy consumption can be minimised and scale-up rules and new applications can be developed.

This modelling requires information about the fundamentals of energy absorption by the fibres during deformations as well as the resulting changes in the mechanical properties of the fibres. The analysis should be focused on the effect of the different mechanisms behind compression of the fibre network [16-18]. Pulp fibres can consume energy in numerous ways and the method of energy application will have a substantial influence on the final pulp properties [18]. Hence, a better understanding of the forces exerted on fibres as they pass through the extruder may offer greater insight in controlling the process and making it more efficient. To determine which forces in extrusion are beneficial and which only consume energy, one must first know what the forces are and where they come from.

The mechanical loading of the extruder can be classified into three principal cyclic-type force actions: shear, compression and tension. To obtain a qualitative understanding of the extrusion process, attention needs to be given to the effects these forces have on single fibre morphology and stiffness. Compression of a fibre mass may result in slippage of the fibres, fibre bending and compression of the fibre wall [18,19]. Differences in morphology and chemical composition may cause significant differences in compression behaviour between wood and non-wood fibres.

As extrusion is often performed with pre-treated fibres it is important to examine the influence of soaking liquids on the behaviour of fibres during compression. Sodium hydroxide is often used to decompose the lignin in and between the fibres to facilitate defibration. Use of sodium hydroxide results in more swollen fibres and an easy slippage of elementary fibres along each other. In this paper the compressibility and relaxation of dry hemp bast fibres and hemp bast fibres soaked in water and sodium hydroxide solutions have been studied at different temperatures and strain rates. The effect of moisture content of the dry fibres has been studied as well. The effect of repeated compression on the stress-density relationship, relaxation and the resulting plastic strain has been examined. The results were compared to results obtained with wood fibres and the mechanism of compression has been analysed.

2.2 Materials and Methods

Hemp (Cannabis sativa L., Felina 34) bast fibre bundles were removed from the hemp stem by scutching and hackling. These bundles were cut to lengths of 5 ± 3 mm for easier handling. For each experiment 1.0 gram of dry fibres was used. The dry hemp fibres had a dry matter content of 91%. For experiments with pre-treated fibres the fibres were soaked for at least 4 hours in 16 ml of water, 0.2 M NaOH-solution or 1.0 M NaOH at 20°C before each experiment. After soaking the water or NaOH solution was drained from the fibres. The drained fibres were used for the experiments (typical dry matter content of about 30 %). Compression experiments were also carried out with fibres dried in an oven before analysis. The dry matter content of these fibres during compression was about 98 %.

2.2.1 Apparatus
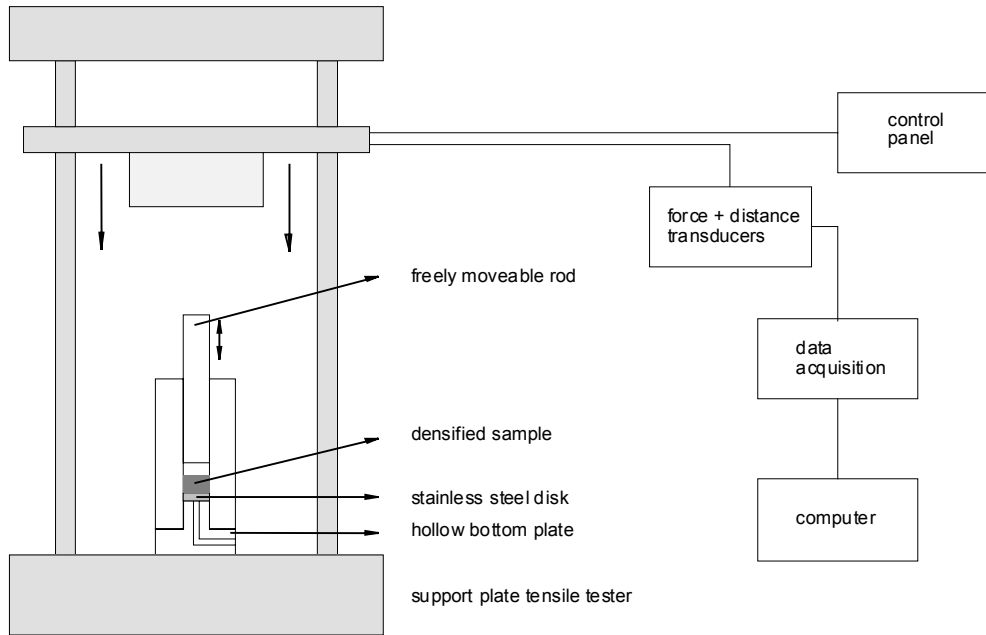
Figure 2.2: *The compression cell*

A Zwick 1445 tensile tester was used in combination with a compression cell, as drawn schematically in Figure 2.2. The compression cell contained a cylinder with a diameter of 13 mm, which was locked at the bottom by a stainless steel disk. The fibres were put in the cylinder and compressed by means of a freely movable rod placed in the cylinder. The force required to move the rod was negligible compared to the force required for compression of the fibre network. In the case of saturated fibres, a stainless steel filter replaced the stainless steel disk. Liquid pressed out of the pad flowed via the filter through a small tunnel in the bottom plate to the outside of the cell. The resistance of the filter to water flow was negligible. Compression at constant speed was accomplished by placing the compression cell in the tensile tester and choosing a compression test program with constant speed in the control system of the tensile tester. The compression speed of the used tensile tester was adjustable up to 400 mm/min. By on-line data-acquisition the force required to obtain the compression was recorded.

2.2.2 Method

The strain of the fibre network is defined as the relative volume decrease:

$$\varepsilon = \frac{\Delta V}{V_0} \tag{2.1}$$

V_0 is the volume of dry fibre network (91 % d.m.) at zero strain. The point of zero strain was set at a density of 0.25 g/cm^3 (dry matter content: 91 %), so that $V_0 = 4$ cm^3 for 1.0 gram of dry fibres (91 % d.m.). This corresponded to an initial thickness of 3 cm for the fibre network.

During extrusion the strain rate on the fibre network can be varied between 0.1 s^{-1} (low screw speed, high filling degree) and 30 s^{-1} (high screw speed, low filling degree), but is normally varied between 0.4 and 5 s^{-1}. However, with the used tensile tester strain rates to a maximum of 0.22 s^{-1} can be obtained, which is below the normal range used during extrusion. As recent extrusion experiments have shown that at low speeds fibres are more processed [15], the influence of strain rates was studied here at a lower range of strain rates, 0.006 – 0.22 s^{-1}.

Experiments at higher temperature were performed by heating the fibres and the compression cell by means of a water bath, which was set at the desired temperature. Depending on the screw speed during extrusion the fibres are allowed to relax for 0.2 to 10 seconds. The relaxation behaviour was therefore studied up to 10 seconds after the maximum stress. During repeated compression the material was allowed to relax for 10 seconds and then compressed again to the same strain. During repeated compression with pre-treated fibres some water or sodium hydroxide was added after each compression.

The stress development during the experiments was recorded by online data-acquisition and was combined with the simultaneous strain and density course in a Labview program.

2.3 Results and Discussion

2.3.1 Stress-density relationship during compression

The average stress-density history of the fibres must be known for a good description of the energy consumption in a mechanical pulping process [16]. Many studies have shown that the bulk density of a thick mat compressed under a static pressure obeys the compressibility equation [18-23]:

$$\rho = M \, \sigma^N \qquad\qquad [2.2]$$

for a wide range of natural and synthetic fibres, where M and N are empirical constants for a given fibre type. The empirical compressibility equation combines the several complicated mechanisms during compression into a manageable formula. The existence of a physical meaning of the constants M and N depends on the underlying mechanisms. Rewriting yields:

$$\sigma = \left(\frac{\rho}{M}\right)^{\frac{1}{N}} \qquad\qquad [2.3]$$

Taking the logarithm of each side results in:

$$\log \sigma = \frac{1}{N} \log \rho - \frac{1}{N} \log M \qquad\qquad [2.4]$$

If the compressibility equation applies, a plot of the logarithm of the stress against the logarithm of the density results in a straight line with slope 1/N and intercept 1/N log M.
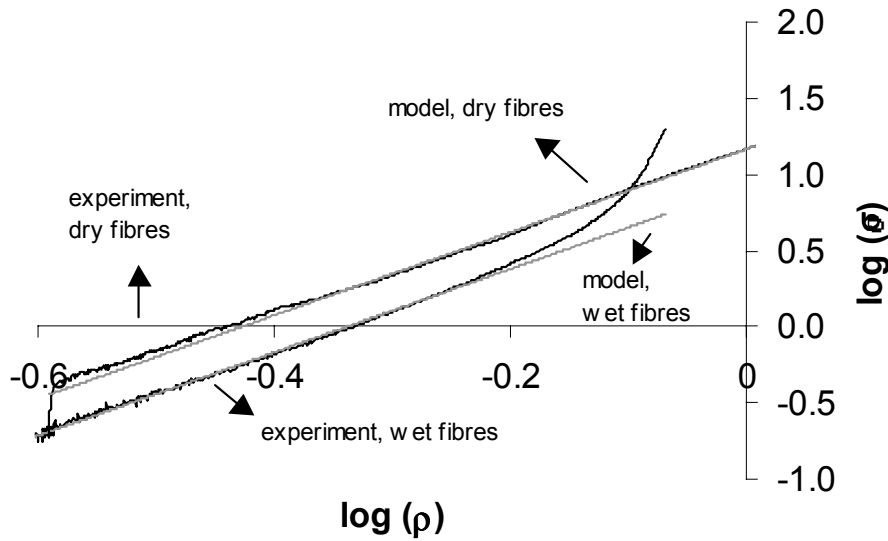
Figure 2.3. *Logarithmic stress density curve for dry (91 % d.m.) and wet fibres modelled with the compressibility equation, 20 °C, 0.028 s^{-1}*

In Figure 2.3 the logarithmic value of the stress is drawn against the logarithm of the density for one of the dry hemp fibre compression experiments (dry matter content 91 %) at a strain rate of 0.028 s^{-1} and a temperature of 20 °C. The compressibility equation seems to apply for most of the curve. Linear regression yields the following values for the parameters of the compressibility equation, at 20°C, at a strain rate 0.028 s^{-1}.

N = 0.37 ± 0.01

M = 0.40 ± 0.01 g.cm^{-3} MPa$^{-0.37}$

It is important to know the underlying mechanisms causing the compressibility equation to be valid, because the applicability of the compressibility equation alone does not directly elucidate the mechanisms causing the force-deformation relation to be of this form. Jones [19] divided the single fibre deformation by fibre mat compression into three categories of fibre behaviour; fibre bending, fibre compression, and fibre slippage at points of fibre-to-fibre contact. Since the load supported by each contact will depend upon the total number and distribution of contact points, the importance of compression of fibres at points of contact will be closely interrelated to both fibre bending and slippage behaviour. As hemp bast fibres contain a negligible lumen, it is assumed that fibre compression is negligible compared to fibre bending and fibre slippage.

Senger [18] assumed that compression of a wood fibre floc results in only fibre bending and fibre compression. He developed the following relation between the total normal force resulting from fibre bending and the decrease in thickness, when considering incompressible fibres:

$$\sigma = C_1 \left(\frac{1}{\theta^3} - \frac{1}{\theta_i^3} \right) \qquad\qquad [2.5]$$

in which C_1 is a parameter depending on pulp properties including fibre length, coarseness, stiffness and floc grammage. Stiffer fibres result in a higher value for C_1. θ is the resulting

26

thickness of the fibre floc and θ_i is the initial thickness. This equation implies a third order relationship between stress and density at higher densities.
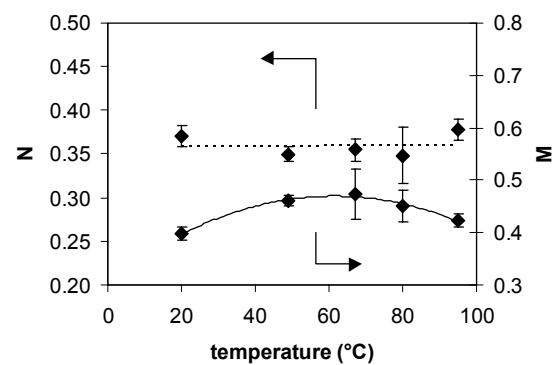
The exponent of the compressibility equation for dry hemp bast fibres at 20 °C was found to be 0.37. This suggested that the mechanism of compression of hemp bast fibres was somewhat different compared to the compression of wood fibres studied by Senger [18]. Apparently, fibre bending is not the only mechanism in hemp fibre compression resistance. This difference between hemp and wood fibres might be explained by their difference in composition and morphology. As compression of the cell wall is more difficult, fibre slippage as suggested by Jones [19] might become more important during fibre mass compression. The lower order stress-density relationship for hemp bast fibres might thus be caused by the occurrence of fibre slippage, which is not included in Senger's model [18].

The compression experiments were repeated at different strain rates (at 20°C) and at different temperatures (at a constant strain rate of 0.028 s^{-1}). The strain rate appeared to have no significant influence on the slope of the stress-density curve, while M slightly increased with strain rate (Fig. 2.4A). Also the temperature had little influence on the slope, but M clearly showed a dependence on temperature (Fig. 2.4B). At low temperatures M increased with temperature. An increase in temperature increases the mobility of the polymeric chains and thus increases the flexibility of the wood fibres [14,24,25]. At higher temperatures M decreases with temperature. According to Senger's model [18] M increases when fibres become more flexible. Dry hemp bast fibres appeared to become more flexible at higher temperature and, to a lesser extent, at higher strain rate (Fig. 2.4A and B). The decrease in M with temperature at higher temperatures was probably caused by a decrease in moisture content that coincided with the temperature increase. At lower moisture content the fibre flexibility decreased, causing a decrease in M (Fig. 2.6B).

Apparently, the mechanism behind the dry hemp fibre compression did not change with strain rate or temperature as the exponent of the compressibility equation did not change with both parameters.
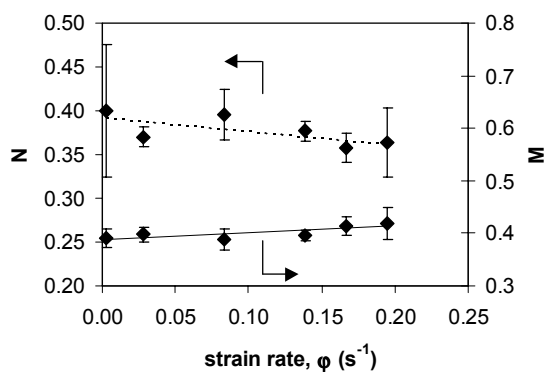

Figure 2.4A. *Influence of strain rate on the para-meters of the compressibility equation, dry fibres (91 % d.m.), 20 °C*

Figure 2.4B. *Influence of temperature on the parameters of the compressibility equation, dry fibres (91 % d.m.) 0.028 s^{-1}*
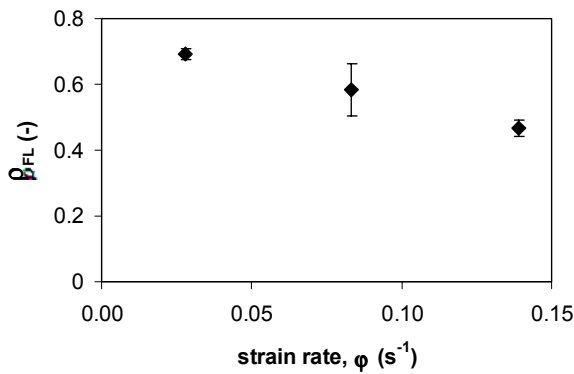
Figure 2.5A. *Influence of strain rate on the density, ρ_{FL}, at which the stress starts to deviate more than 5 % from the stress calculated with the compressibility equation, fibres in water, 20 °C*
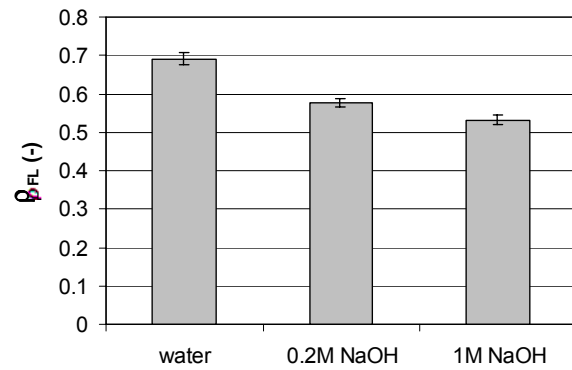
Figure 2.5B. *Influence of different pretreatments on the strain, ρ_{FL}, at which the stress starts to deviate more than 5 % from the stress calculated with the compressibility equation, 20 °C, 0.028 s^{-1}*
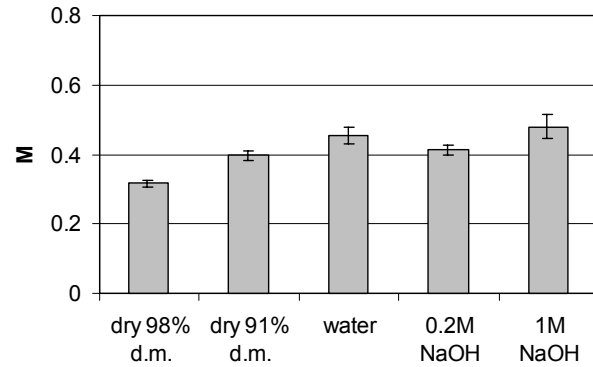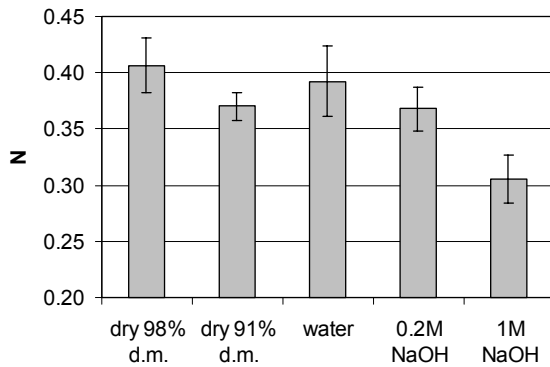
Figure 2.6A + B. *Influence of different pretreatments on the parameters of the compressibility equation, 20 °C, 0.028 s^{-1}*

The first part of the logarithmic stress-density curve during compression of water and sodium hydroxide soaked fibres was straight and could be described with the compressibility equation. However, at higher densities the curve deviated from a straight line and the stress sharply increased (Fig. 2.3). This was caused by flow limitation. At higher density the fibre mass became more compact and showed a higher resistance to liquid flow. When the flow resistance becomes higher than the resistance for fibre compression the total stress becomes controlled by the liquid flow instead of by density. This flow resistance becomes even more important at higher strain rates or when fibres are more swollen by sodium hydroxide (Fig. 2.5A and B) [13]. When the curve starts to deviate from the compressibility curve the compression behaviour is determined by both compression of the network and the drainage mechanism and has to be described with both the compressibility equation and a drainage model.

The exponent of the compressibility equation for water soaked fibres was comparable to dry fibres (Fig. 2.6A). However, the exponent decreased significantly with increasing sodium hydroxide concentration. Use of a 1 M sodium hydroxide concentration resulted in a third order relationship. Decomposition of the lignin increases the extent of swelling and flexibility of the fibres. Swelling of the fibres increases the cell wall volume and the cell wall becomes

more compressible and a higher flexibility results in an easier bending. This results in a shift to a compression mechanism in which compression of the fibre wall and bending of the fibres become more important than fibre slippage [24-27]. The exponent might be higher for water soaked fibres compared to dry fibres because of slippage of fibres along each other which is facilitated by the presence of water [20,21].

For dry fibres the exponent significantly decreased with moisture content (Fig. 2.6A). Lower moisture content results in stiffer fibres, which are less easy to bend. This makes fibre slippage even more important than fibre bending in the compression of hemp bast fibres. The flexibility of the fibres increased with higher moisture content, which resulted in a higher M (Fig. 2.6B). Addition of sodium hydroxide decreases fibre coarseness. According to Senger's model M decreases with decreasing fibre coarseness. However, a higher concentration of sodium hydroxide increases fibre flexibility, resulting in an increase of M.

Compression experiments with water soaked fibres were repeated at different temperatures and at different strain rates. The strain rate had little influence on the exponent of the compressibility equation. In contrast to dry fibres M slightly decreased with increasing strain rate for water soaked fibres (Fig. 2.7A). As at higher strain rates the effect of flow limitation will be more pronounced, it is advisable to study the drainage behaviour of the fibres instead of studying the compression behaviour at higher strain rates.

The exponent N decreased with temperature (Fig. 2.7B) while M increased with temperature (Fig. 2.7B). Higher temperature results in more flexible fibres. The bending mechanism becomes more important at higher temperature, because more flexible fibres are easier to bend. This results in a higher exponent of the compressibility equation.
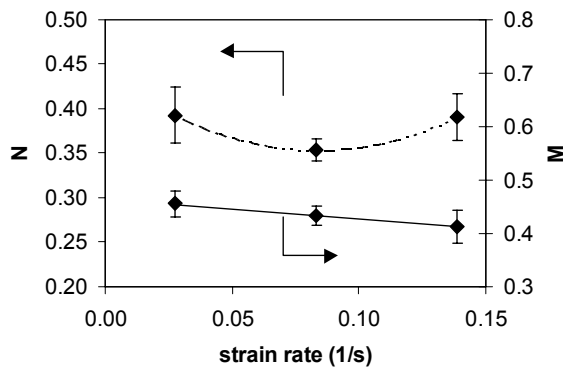
Figure 2.7A. *Influence of strain rate on the parameters of the compressibility equation, fibres in water, 20 °C*
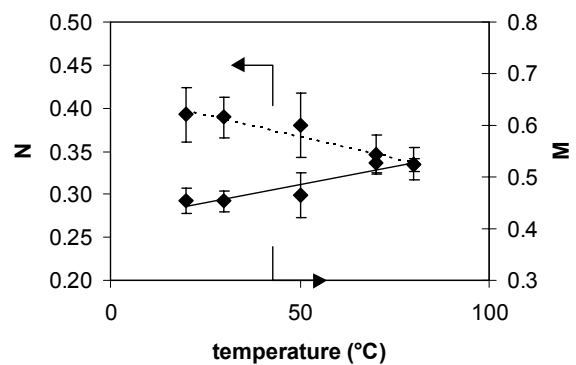
Figure 2.7B. *Influence of temperature on the parameters of the compressibility equation, fibres in water, 0.028 s^{-1}*

2.3.2 Relaxation

The viscoelastic behaviour of wood fibres seems to be time-dependent of stress and strain [13,23,25,28,29]. This results in a dependency on strain rate and loading time. The behaviour of wood chips and fibres has been shown to depend on the time required to complete a mechanical test [13,22,23,28].

The relaxation of hemp bast fibres was recorded after compression at different conditions. Several empirical models have been developed to describe viscoelastic behaviour of materials, including the Maxwell model, consisting of a spring and dashpot in series, generally used to describe relaxation, and the Voigt model, a spring and dashpot in parallel, generally used to describe creep [28,30]. Our relaxation curve of dry hemp bast fibres (91 % d.m.) was fitted with the Maxwell model for compression [30]:

$$\sigma = \left(\frac{\rho}{M}\right)^{\frac{1}{N}} \bullet \left(1 - B\left(1 - e^{-t/\tau}\right)\right) \qquad [2.6]$$

in which B is a parameter describing the maximum relaxation that can be obtained. In this model t=0 is the time at which relaxation starts. For our experiments it was assumed that relaxation began when the stress was removed. The maximum stress at this point was calculated with the compressibility equation. In order to obtain the value for B hemp fibres were allowed to relax for 10 minutes after a compression at a strain rate of 0.028 /sec at 20°C. The ultimate stress after relaxation for 10 minutes appeared to be 57.1 % of the maximum stress. This resulted in a value for B of 0.43 at a strain rate of 0.028 /sec, a maximum stress of 9.2 MPa and at 20°C.

The relaxation time can be calculated by fitting Eq. [2.6] to the relaxation curves. Rewriting Eq. [2.6] yields:

$$\ln\left(1 - \frac{1}{B}\left(1 - \sigma\left(\frac{\rho}{M}\right)^{-\frac{1}{N}}\right)\right) = -\frac{t}{\tau} \qquad [2.7]$$

Modelling was carried out with the relaxation curve of the experiment mentioned above, obtained with a compression rate of 0.028/sec and a maximum stress of 9.2 MPa at a temperature of 20°C. The curve obtained when plotting the left hand term of Eq. [2.7] against t (Fig. 2.8A) is not straight, which means that the stress-relaxation cannot be expressed by a single exponential term. This can be solved by using the generalised Maxwell model, consisting of n Maxwell elements in parallel [30]:

$$\sigma = \left(\frac{\rho}{M}\right)^{\frac{1}{N}} \bullet \left(1 - B\left(1 - b_1 e^{-t/\tau_1} - b_2 e^{-t/\tau_2} - \ldots - b_n e^{-t/\tau_n}\right)\right) \qquad [2.8]$$
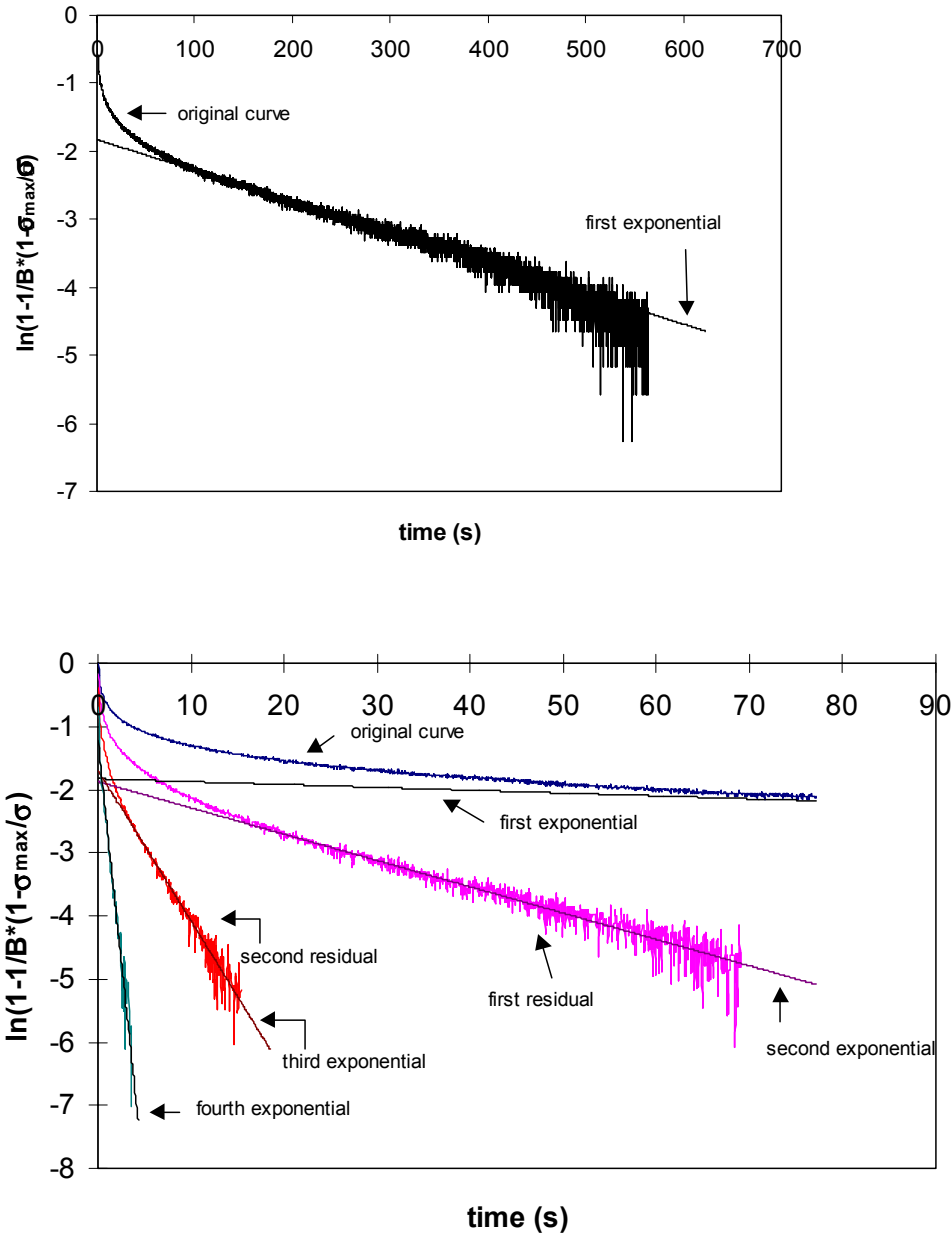
Figure 2.8A + B. *Modelling relaxation*

The necessary multi-term expression is obtained by the successive residual method [28,30,31] (Fig. 2.8B):

$$\sigma = \left(\frac{\rho}{M}\right)^{\frac{1}{N}} \bullet (1 - 0.43\,(1\ -\ 0.20\,e^{-t/221}\ -\ 0.19\,e^{-t/24}\ -\ 0.23\,e^{-t/4.2} - 0.37e^{-t/0.72}\,)) \qquad [2.9]$$

The multi-term equation used to fit the relaxation curve suggests that there are more relaxation processes occurring simultaneously. All deformation mechanisms taking place during compression of the fibre network will relax with their own specific relaxation times. Relaxation of the deformation of the cell wall will probably exhibit the shortest relaxation

31

time, slower relaxation will occur as bent fibres will partly stretch back and slippage will eventually take place as a result of relaxation of the other mechanisms.

The shape of the relaxation curve is assumed to be similar for all samples. The differences in extent of relaxation will depend on the extent at which the above-mentioned mechanisms of relaxation occur. Differences in relaxation of hemp bast fibres at different conditions have been analysed by recording the percentage of stress relaxation, R, after the maximum stress has been obtained. The stress after 10 seconds of relaxation, $\sigma_r(10)$ was compared with the maximum stress the sample experienced for all experiments performed at different strain rates:

$$R_{10} = \frac{\sigma_{max} - \sigma_r(10)}{\sigma_{max}} = \frac{\left(\frac{\rho}{M}\right)^{\frac{1}{N}} - \sigma_r(10)}{\left(\frac{\rho}{M}\right)^{\frac{1}{N}}} \qquad [2.10]$$

It can be concluded that the extent of relaxation strongly decreases when the dry fibres have a higher dry matter content and slightly decreases with maximum stress (Fig. 2.9A). The extent of relaxation was not much influenced by temperature (data not shown).

In contrary to what was observed during compression the strain rate seemed to have a significant influence on the extent of relaxation (Fig. 2.9B). At low strain rates the extent of relaxation strongly increased with strain rate, but at higher rates the extent of relaxation reached a maximum of about 36 %. At lower strain rates the material may have already experienced some relaxation during slow compression. The flat curve at higher strain rates suggests that there is no need to research the effect of higher strain rates.

The model predicts an extent of relaxation after 10 seconds of 29 % for experiments carried out at a strain rate of 0.028 s^{-1} and a temperature of 20 °C. Observed is an average extent of relaxation of 31 %. It is assumed that influences of strain rate on the extent of relaxation can be approximated by adjusting the value of parameter B in the model.
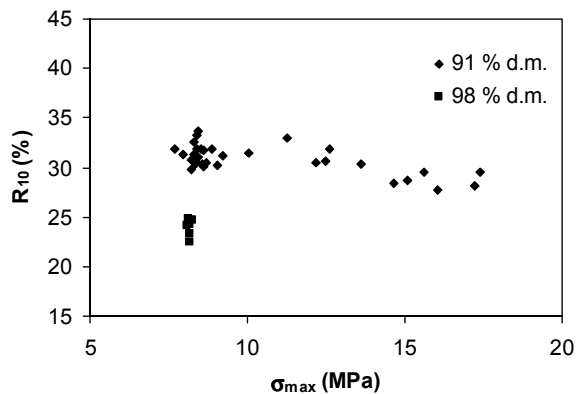
Figure 2.9A. *Stress relaxation of dry fibres versus maximum stress after compression, different moisture contents, 20 °C, 0.028 s⁻¹*
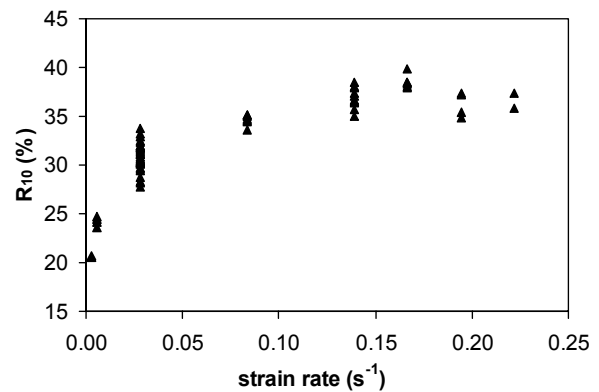
Figure 2.9B. *Stress relaxation of dry fibres versus strain rate, σₘₐₓ: 6.7-9.7 MPa, 20 °C, 0.028 s⁻¹*
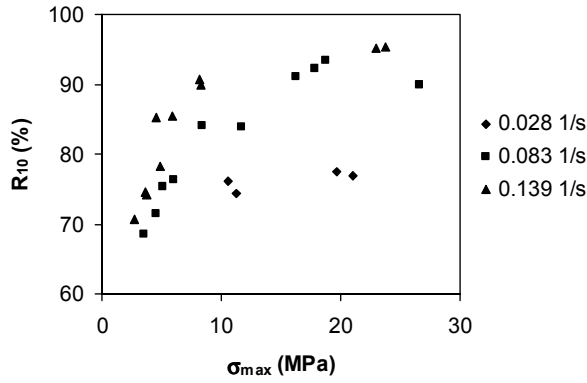
Figure 2.10A. Stress relaxation of fibres in water versus maximum stress at different strain rates, 20 °C
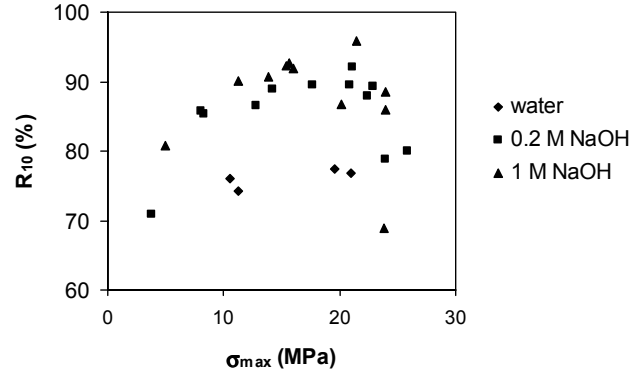
Figure 2.10B. Stress relaxation of fibres in different liquids versus maximum stress, 20 °C, 0.028 s⁻¹

This yields the following relation for relaxation valid for strain rates higher than 0.15 s⁻¹:

$$\sigma = \left(\frac{\rho}{M}\right)^{\frac{1}{N}} \cdot (1 - 0.43 \cdot \frac{0.36}{0.29} \cdot (1 - 0.20e^{-t/221} - 0.19e^{-t/24} - 0.23e^{-t/4.2} - 0.37e^{-t/0.72})) \qquad [2.11]$$

The maximum stress obtained in compression of soaked fibres not only depends on the ultimate density achieved, but is influenced also by the flow resistance during compression. As the extra stress caused by flow limitation exhibits immediate total relaxation when the compression force is removed, the observed relaxation after 10 seconds was much higher and increased with the stress increase caused by flow limitation (Fig. 2.10A). A higher strain rate and use of sodium hydroxide enhanced flow limitation (Fig. 2.10B). Temperature did not have any influence on this relaxation behaviour (data not shown).

As the maximum stress obtained was mostly influenced by flow resistance it is better to compare the stress after 10 seconds with the maximum stress that would be obtained in the absence of flow resistance. This stress was determined by calculating the stress at the maximum density with use of a straight line through the curve at low density (see Fig. 2.3). The relaxation at 10 seconds was recalculated with these values for the maximum stress. Like with dry fibres the extent of relaxation now showed a decrease with the maximum stress obtained (data not shown).

2.3.3 Deformation cycling

As during extrusion fibres are subjected to constant deformation cycling, it is important to study the effects of repeated compression and relaxation on the fibre morphology and the energy consumption. The dry hemp bast fibres were subjected to repeated compression at different strain rates. Figure 2.11 shows the difference in stress course between first and second loading for dry fibres (91% d.m.) at a strain rate of 0.028/sec and 20 °C. Due to permanent deformation during the first loading, stress increase was retarded during the second compression. The maximum stress obtained was lower during the second compression. The plastic strain indicated that some irreversible changes had taken place in the fibre network, when it was compressed. During the first compression the number of contacts increased because of fibre bending. Furthermore unrecoverable fibre slippage and repositioning are important contributors to fibre bed deformation [19,20].

33
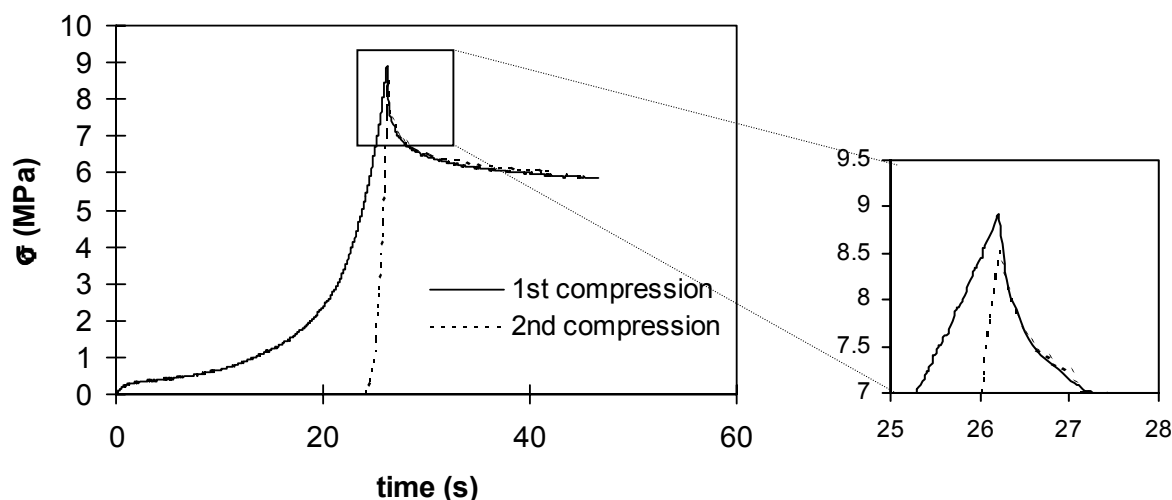
Figure 2.11. *Stress course during first and second compression (Enlarged maxima included), dry fibres (91 % d.m.), 20 °C, 0.028 s^{-1}*

During repeated compression both maximum stress and the extent of relaxation decreased and the total plastic strain increased (Fig. 2.12). The amount of non-recoverable deformation per cycle decreased until a point was reached at which no more non-recoverable deformation was observed with repeated cycling. The decrease in non-recoverable deformation implies that the energy absorbed decreases with cycling. This is also observed with wood and wood fibres [19,21,28]. At this point the material is called mechanically conditioned. Repeated compression to higher stresses resulted in similar curves. However, the extent of relaxation was lower and the observed plastic strain higher. The dependency of the plastic strain on the maximum stress was much stronger than the dependency on the amount of compressions.

The experiments were repeated at higher strain rates and with water and sodium hydroxide soaked fibres. The strain rate appeared to have no significant influence on repeated compression of dry fibres. Repeated compression with water or sodium hydroxide soaked fibres yielded very high stress peaks. As the fibre mass became more dense with each
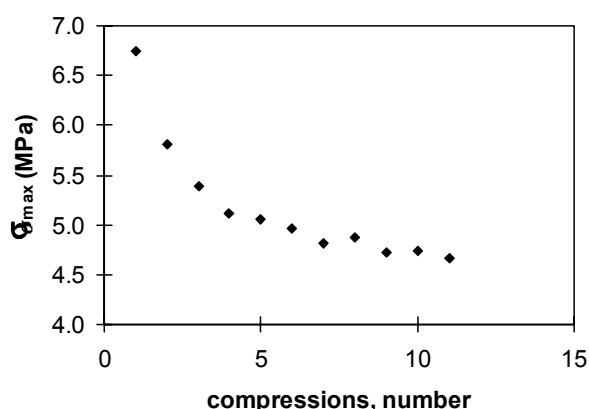
Figure 2.12A. *Maximum stress during repeated compression, dry fibres (91% d.m.), 20 °C, 0.028 s^{-1}*
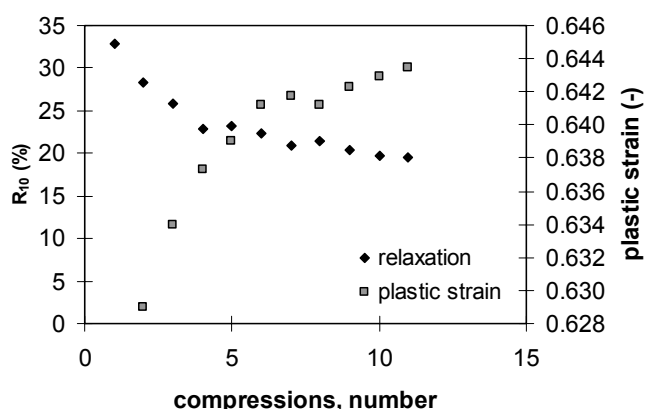
Figure 2.12B. *Extent of relaxation after 10 seconds and the resulting plastic strain during repeated compression, dry fibres (91% d.m.), 20 °C, 0.028 s^{-1}*

compression the flow resistance became higher with each compression. This resulted in stress peaks which became higher with each compression. Repeated compression at higher strain rate enhanced this phenomenon.

At higher strain rates the stress became controlled by flow resistance at lower densities. The power consumption during compression of the fibre mass became much higher and only a small part of it was consumed by deformation of the fibres. It can thus be concluded that extrusion should be operated at such low strain rates, that the stress observed only depends on the density obtained and not on flow resistance. At higher strain rates a great part of the energy consumed will be dissipated because of flow resistance.

2.4 Conclusions

The stress-density relationship for dry hemp bast fibres can be described with the compressibility equation. The mechanism of compression of hemp fibres depends on the compression conditions. Fibres become more flexible at higher temperatures and higher moisture content. This also causes fibre bending to become more important during compression, which results in a higher exponent of the compressibility equation. Soaking of fibres results in a sharp stress increase at higher densities caused by flow resistance of the dense fibre mass. Flow limitation is advanced at higher strain rates and enhanced at higher sodium hydroxide concentrations. At lower density the compressibility equation is also applicable to the curves for wet fibres. The exponent of this equation decreases with increasing concentration of sodium hydroxide and with increasing temperature, because of a higher flexibility causing bending to become more important during compression.

Relaxation of dry fibres is modelled with the generalised Maxwell model. The extent of relaxation slightly decreases with the maximum stress, increases with the strain rate during compression and decreases with dry matter content. The observed relaxation after compression of soaked fibres is much higher, caused by an extra high maximum stress because of flow resistance appeared during compression. However, the stress of the solid phase is much lower and shows a lower relaxation which decreases with the maximum solid stress.

Compression of hemp fibres results in a deformation of which a significant part is non-recoverable. When compression is repeated on dry fibres the total non-recoverable deformation increases and the stress exerted by the fibres decreases until a point is reached at which no more non-recoverable deformation occurs. Repeated cycling results in decreasing energy dissipation per cycle.

Repeated compression of wet fibres results in an increasing density of the fibre mass, causing an increasing flow resistance. This phenomenon causes high peak stresses followed by strong relaxation. As at this point the duration of drainage is much higher than the duration of compression of the solid matrix, the resulting curve is mainly indicative of the drainage process. The stress peaks become even higher when repeated compression is performed at higher strain rates. It can be concluded that processes, in which fibres are repeatedly compressed, should operate at such strain rates, that the stress observed only depends on the density obtained and not on flow resistance.

Acknowledgements

The author gratefully acknowledges the discussions with E. de Jong of the Department of Fibre and Paper Technology of ATO.

2.5 Nomenclature

B	parameter describing the maximum obtainable relaxation	-
b_n	constant in generalized Maxwell model	-
M	coefficient in compressibility equation	$g.cm^{-3}.Pa^{-N}$
N	exponent in compressibility equation	-
R_{10}	percentage of stress relaxation after 10 seconds	%
T	temperature	°C
t	time	s
V_0	volume at zero strain	m^3
ΔV	volume change	m^3
ε	strain	-
θ	thickness of a fibre floc	m
θ_i	initial thickness of a fibre floc	m
ρ	density	$g.cm^{-3}$
ρ_{FL}	density at which flow limitation starts	-
ρ_0	density at zero strain	$g.cm^{-3}$
σ	stress	MPa
σ_{max}	maximum stress	MPa
$\sigma_r(10)$	stress after 10 seconds of relaxation	MPa
τ	relaxation time	s
φ	strain rate	s^{-1}

2.6 References

1. van Roekel, G.J., Lips, S.J.J., Op den Kamp, R.G.M. and Baron, G. (1995): Extrusion pulping of true hemp bast fibre (*Cannabis sativa* L.), Tappi Conference, Chigago, USA, p. 477-485.
2. van Roekel, G.J. (1995): Chemimechanical pulping of fibre hemp, Bioresource Hemp, Frankfurt a/M, Germany.
3. van Roekel, G.J. (1996): Bulk papermaking applications for bast fibre crops using extrusion pulping, PIRA International, Peterborough, England, p. paper 26, 29 pp.
4. Seth, R.S. (1996): Optimizing reinforcement pulps by fracture toughness, Tappi J. 79: 1, 170-178.
5. de Jong, E., van Roekel, G.J., Snijder, M.H.B. and Zhang, Y. (1999): Towards industrial applications of bast fibre pulps; their potential as a nonwood source is discussed, Pulp Paper Canada 100: 9, T270-T273.
6. Herrera-Franco, P.J. and Aguilar-Vega, M. (1997): Effect of fiber treatment on the mechanical properties of LDPE-henequen cellulosic fiber composites, J. Appl. Pol. Sci. 65: 1, 197-207.

7. Mieck, K.-P., Nechwatal, A. and Knobelsdorf, C. (1995): Faser-Matrix-Haftung in Kunststoffverbunden aus thermoplastischer Matrix und Flachs, 2a, Angew. Makromol. Chem. 225, 37-49.

8. Sanadi, A.R., Caulfield, D.F., Jacobson, R.E. and Rowell, R.M. (1995): Renewable agricultural fibers as reinforcing fillers in plastics: mechanical properties of kenaf fiber - polypropylene composites, Ind. Eng. Chem. Res. 34, 1889-1896.

9. Snijder, M.H.B., Wissing, E. and Modder, J.F. (1997): Polyolefins and engineering plastics reinforced with annual plant fibers, 4th Int. Conf. Woodfiber-plastic Composites, Madison (Wisconsin), USA, p. 181-191.

10. Matthews, J.M. (1947): "Textile fibres, their physical, microscopical and chemical properties". John Wiley & Sons, New York.

11. Kirby, R.H. (1963): "Vegetable fibres, botany, cultivation and utilization". Interscience Publishers Inc., New York.

12. Rance, H.F. (1980): "The raw materials and processing of papermaking". Elsevier Scientific Publishing Company, Amsterdam.

13. Uhmeier, A. and Salmén, L. (1996): Influence of strain rate and temperature on the radial compression behavior of wet spruce, J. Eng. Mat. Technol. 118: 3, 289-294.

14. Dumail, J.F. and Salmén, L. (1997): Compression behaviour of saturated wood perpendicular to grain under large deformations, Holzforschung 51: 4, 296-302.

15. Westenbroek, A.P.H., van Roekel, G.J., de Jong, E., Weickert, G. and Westerterp, K.R. (1999): Extrusion pulping; relation between process conditions and product properties, in preparation.

16. Page, D.H. (1989): The beating of chemical pulps - The action and the effects, Fundamentals of Papermaking, Cambridge, Fundamental Research Committee, British Paper and Board Makers' Association, p. 1-38.

17. Giertz, H.W. (1964): A new way to look at the beating process, Norsk Slogindustri 18: 7, 239-248.

18. Senger, J.J. (1998): The forces on pulp fibres during refining, M. A. Sc. Thesis, Department of Mechanical Engineering, University of British Columbia, Vancouver, Canada.

19. Jones, R.L. (1963): The effect of fiber structural properties on compression response of fiber beds, Tappi 46: 1, 20-27.

20. Han, S.T. (1969): Compressibility and permeability of fibre mats, Pulp Paper Mag. Can. 70: 2, 65-77.

21. Wilder, H.D. (1960): The compression creep properties of wet pulp mats, Tappi 43: 8, 715-720.

22. Miles, K.B. and May, W.D. (1990): The flow of pulp in chip refiners, J. Pulp Paper Sci. 16: 2, J63-J71.

23. Miles, K.B. and May, W.D. (1993): Predicting the performance of a chip refiner; a constitutive approach, J. Pulp Paper Sci. 19: 6, J268-J274.

24. Stone, J.E. and Scallan, A.M. (1965): A study of cell wall structure by nitrogen adsorption, Pulp Paper Mag. Can. 8, T407-T414.

25. Salmén, N.L. (1984): Mechanical properties of wood fibres and paper, STFI-meddelande serie D nr 199.

26. Bendzalova, M. and Pekarovicova, A. (1996): Accessibility of swollen cellulosic fibres, Cellulose Chem. Technol. 30: 1-2, 19-32.

27. Kunesh, R.H. (1967): Strength and elastic properties of wood in transverse compression, Forest Prod. J. 18, 65-72.

28. Bodig, J. and Jayne, B.A. (1982): "Mechanics of wood and wood composites". Van Nostrond Reinhold Company, New York.

29. Sayegh, N.N. and Gonzalez, T.O. (1995): Compressibility of fibre mats during drainage, J. Pulp Paper Sci. 21: 7, J255-J261.
30. Mohsenin, N.N. (1986): "Physical properties of plant and animal materials". Gordon and Breach Science Publishers, New York.
31. Sitkei, G. (1986): "Mechanics of agricultural materials". Elsevier, Amsterdam.

Chapter 3

# Swelling of hemp bast fibres under pressure

Summary

In developing a rheology model for non-wood fibres, drainage behaviour appeared to be an important factor in describing the flow and frictional behaviour of pulp in machinery in which fibres are processed by means of repeated compression and shear. In modelling the drainage behaviour, knowledge of the distribution of the liquid in the fibre cell wall and the spaces between the fibres during compression is required. Although extensive research has been carried out on atmospheric swelling of several cellulosic fibres, swelling under pressure has hardly been studied.

Therefore the volumetric swelling of hemp bast fibres has been investigated in water and NaOH-solution under pressures up to 100 bar. The measured total volume of the hemp-liquid system appeared to be lower than the solid volume plus the volume of absorbed liquid. The observed volume contraction was attributed to a pressure-dependent decrease in specific volume of the liquid in the fibre. Pressure forces water molecules to migrate to places between the molecules of the cell wall components, which are not accessible under atmospheric pressure. It is shown that removal of lignin by NaOH-treatment results in more places per gram of dry fibre becoming available at higher pressures, from which it was concluded that mainly cellulose was responsible for the observed contraction at higher pressures.

The swollen cell wall becomes more flexible by the removal of lignin, which results in a higher volumetric swelling under pressure compared to untreated fibres. Fibres swollen by water are shown to fill 59 % of the total space at atmospheric pressure, which increases to 79 % at 100 bar. Fibres swollen by a NaOH-solution fill 75 % of the total space at atmospheric pressure, which increases to 84 % at 100 bar.

3.1 Introduction

Non-wood fibres, including hemp and flax, are suitable as raw materials for paper [1-3], as reinforcement in recycled paper and board [4], as replacement of synthetic fibres in nonwovens [5] or as reinforcement for composites [6-10]. Bast fibre bundles are located in the outer layer of the stem. Each fibre bundle is composed of overlapping bast fibres [11] and a cross section consists of ten to forty elementary fibres (Fig. 3.1). The length of the elementary fibres varies between 5 and 55 mm and the thickness is about 20 µm. Hemp bast
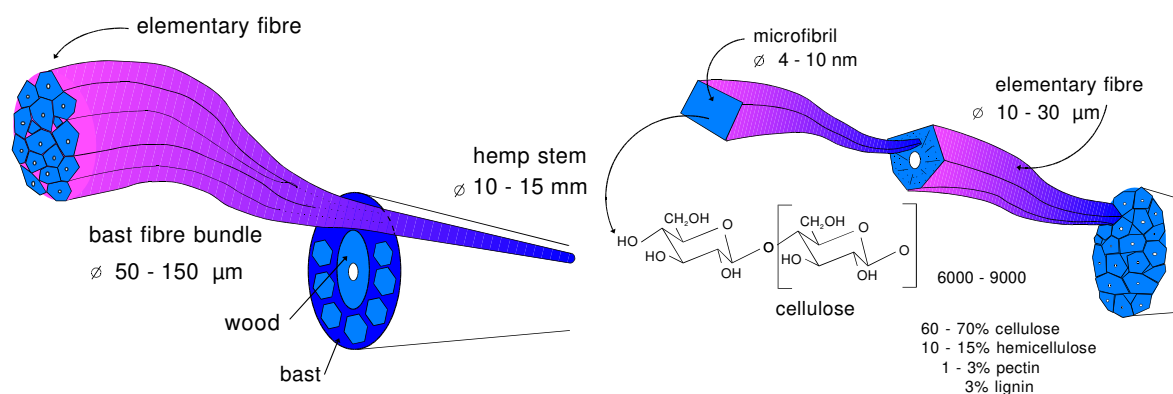
Figure 3.1 A and B. *Schematic reproduction of a hemp stem*

fibres consist of 60-70 % highly crystalline cellulose and other components such as hemicellulose (10-15 %), lignin (3 %), pectin(1-3 %), mineral matter, fats and waxes [12]. Because of their long length, bast fibres are more difficult to process than short wood fibres. Mechanical pulping by extrusion shows advantages compared to refining, because long bast fibre bundles can be fed unshortened to the pulping process. In the extruder the fibres are shortened and the fibres bundles, consisting of elementary fibres glued together with lignin and/or pectin, are defibrated [1,3] and elementary fibres are fibrillated. This is achieved by repeated compression and shear forces in the extruder.

The repeated compression and relaxation of fibres results in a mechanical disruption of the bonds holding together the lamella between the elementary fibres, while the shear forces help to fibrillate the fibres [13,14]. Van Roekel et al. [1] evaluated results obtained from hemp extrusion pulping trials with softwood market pulps. The yield proved to be high and the energy consumption was as low as half of that for mechanical softwood pulps. It was concluded that extrusion pulping is an economically, technically and environmentally viable alternative to the traditional chemical pulping technology for non-wood fibres.

Both pulp quality and energy requirement are greatly affected by the configuration of the extruder screws, the screw rotation speed and the throughput [1]. The process can be better controlled if the relation between the product properties and the extruder configuration and extrusion conditions can be formulated. Our ultimate goal is to establish an extrusion pulping model which will predict the choice of process parameters required for a specific fibre length, fibre length distribution and degree of defibration and fibrillation. With this model the process can be better controlled and new applications and scale-up rules may be developed.

This modelling process requires information about the fundamentals of deformation and consolidation behaviour of fibres. Such information is not only useful for describing the extrusion pulping process but for all mechanical processes, including refining, in which pulps are subjected to compression and shear forces, and are based on the same deformation and consolidation principles. Mechanical properties, including internal friction, and flow behaviour of pulps are influenced by the presence of liquids [15]. During extrusion the fibre mass is compressed and liquid expressed [1]. The extent of liquid expression depends on the screw speed and configuration, but also on pulp and fibre properties like swelling, fines content and degree of fibrillation. The fines content and degree of fibrillation are dependent

on the amount of mechanical action of the extruder screws and some measure of their combined presence can be obtained by measuring the dewatering rate.

Modelling the drainage behaviour requires knowledge of the flow paths of the liquid [16-23]. Because liquid encounters a higher flow resistance in the fibre cell wall compared to between the fibres, it is necessary to know how much liquid is located in the interstices between the fibres and how much is located in the porous structure of the fibre wall. This means that the volume fraction occupied by swollen fibres has to be known. Important for the calculation of this fraction is the volumetric swelling of the fibres at different pressures and after different pretreatments. This paper discusses the effects of pressure on the volumetric swelling behaviour of hemp bast fibres in pure water and in dilute NaOH-solution.

3.1.1 Swelling

Hemp fibres store liquid in two ways, by molecular and by capillary adsorption. There is an essential difference between the two storage modes. Starting from completely dry material liquid is bound first by molecular adsorption and then by capillary adsorption only after a certain moisture content has been achieved [24]. At consistencies met during extrusion, fibre cell walls are fully saturated and liquid is also held by interstices between the fibres.

The swelling ability of non-wood fibres is restricted by stiff, cross-linked lignin present in the fibre walls [25]. According to Salmén [26] lignin is rigid at room temperature. In order for the fibres to swell, the lignin has to be softened or removed by chemical treatment [27-29]. If the lignin is softened the fibre walls can swell under the action of the electrostatic forces between the carboxylic acid groups [30]. Ottestam [25] observed more swelling at higher temperatures and at a higher alkalinity. These conditions also facilitate separation of the fibre bundles into elementary fibres.

The swelling behaviour of mechanical and chemical wood fibres has been investigated extensively. However, only a few studies have focused on other cellulose fibres including cotton [31], sugar cane bagasse [29], ramie [32], hemp woody core [33], and viscose rayon [34]. Swelling has generally been measured by the fibre saturation point (FSP), which is defined as the amount of liquid contained within a saturated cell wall. There are different ways to measure this FSP. In the porous plate technique [35] wet fibres, from which part of the liquid is removed by applying a known vapour pressure for a few days, are weighed wet and dry. The non-solvent water technique [35] is based on a concentration difference after immersing wet fibres in a solution of polymer molecules large enough for not filling the fibre pores. The solute exclusion technique [33,36-39] is based on the same principle, but uses differently sized polymers for determination of the pore size distribution. Other methods are based on the extrapolation to zero moisture content of the relations between physical properties and moisture content [40]. The easiest method for determining the FSP is by correlations with the measurement of the water retention value under specific circumstances [25,29,31,36,38,41-43]. Analyses of the methods shows that the FSP can be strongly influenced by the method used [40,44].

The value obtained with these methods is the weight of liquid per dry weight of fibre. For drainage modelling the volumetric swelling is more important than swelling based on mass. The determination of the volumetric swelling from the FSP requires the specific volume of the liquid in the fibres. Volumetric swelling has been investigated before, but not often in combination with weight increase. A few researchers assume that in the wet state, fibre walls

are swollen above their dry volume by an amount equal to the volume of liquid they contain [35,36,42]. Several other authors, however, mention a contraction of the total volume of the fibre-liquid system at low moisture contents [45-51]. This means that the volume of dry fibres plus that of the liquid taken up is more than the volume of the resulting swollen fibres. Alince [45] measured a contraction of up to 4 % at moisture contents higher than 14% at atmospheric pressure. Valko [51] mentions that the amount of fluid displaced by a gram of fibres depends on the nature of the fluid. This dependence may be caused by the differences in the ease with which various liquids penetrate the capillaries or the differences in the volume contraction under the influence of the mutual attraction forces of the swelling liquid and the swelling medium. Valko calculates that the density of absorbed water in cellulose appears to be 5 to 7 % higher than that of free water under atmospheric pressure. Filby and Maas [46] report that the volume of the cellulose-water system is smaller than given by the components cellulose and condensed water only at moisture contents lower than 8 %. Stamm [50] reports a contraction of maximal 0.035 cm^3/g dry material under atmospheric pressure. Seifert [49] reports a volume contraction between wood and water, up to 15 % moisture content at atmospheric pressure. He reports densities of 1.48, 1.95 and 1.55 g/cm^3 for the water absorbed on cellulose, hemicellulose and lignin respectively. The density of the absorbed water decreases with moisture content down to unity at a moisture content of 15 %. However the mechanism behind contraction is not clear. Valko [51] poses that submolecular or supermolecular interstices disappear or are reduced when water is taken up, where the former is correctly denoted as contraction. Weltzien [52] mentions the possibility that certain spaces within the fibres may be reached by water after swelling though they may be barred to helium gas in the dry state. Hermans [48] writes that sorption is associated with a process of molecular dispersion (quite comparable to the solution of one substance in another) rather than with surface adsorption of supramolecular particles, so there is no more reason to speak of internal surface action as there is in the case of an ordinary mixture of two fluids, or a solution of a solid in a fluid.

The influence of stress on the moisture content of fibres has been studied in accordance with the change in sorption isotherm of dry natural fibres in air, which has been reported to be stress dependent [53-59]. This mechanosorptive phenomenon results in a change in equilibrium moisture content of the fibres. Under application of tensile stress the equilibrium moisture content increases, but compressive stress results in a decrease. Most research mentioned on swelling has been carried out to obtain the atmospheric swelling. Higher pressures are used in the porous plate method (up to 10 bar), but this method is designed to determine the atmospheric swelling [35,60]. Laivins and Scallan [61] studied the effect of pressing on the fibre saturation point, determined by adding a polymer solution to the wet pulp, with the polymer having a molecular diameter greater than the largest pore openings in the fibre wall. They find that at pressures higher than 15 MPa hardly any of the liquid is located between the fibres. In their calculations Laivins and Scallan assume parallel flow of liquid from the fibre cell wall and from the spaces between the fibres. In practice liquid from the fibres will flow into the spaces between the fibres and mix with the liquid in these spaces before leaving the pulp pad. Calculation with some combination of flow in series and in parallel, however, would certainly influence their results. Their results therefore seem questionable.

Our research has been focused on determining the extent of volumetric swelling under pressures up to 100 bar after different pretreatments, by weighing as well as measuring volumes of wet fibres under pressure.

3.1.2 Calculations on fibre swelling

At the beginning of drainage the pressure is mainly supported by liquid phase. By pressure gradients liquid is gradually expressed and the pressure shifts to the solid phase. As the pressure in the solid phase determines the extent of volumetric swelling, swelling can only be determined in relation to pressure, when equilibrium has been reached and the applied pressure is totally supported by the solid phase. In our experiments fibres are compressed and allowed to drain till equilibrium has been reached. The experiments are set up assuming contraction will take place at higher pressures and the volumetric swelling of the fibre, ΔV_f, is not equal but directly proportional to the absorbed volume, $V_{l,a}$. The proportionality constant, Q, is the ratio between the density of free liquid, ρ_l, and the density of liquid in the fibre cell wall, ρ_{fl}, and can be defined in two ways:

$$Q = \frac{\text{volumetric swelling}}{\text{absorbed volume}} = \frac{\Delta V_f}{V_{l,a}} = \frac{\rho_l}{\rho_{fl}} \qquad [3.1]$$

The total volume of liquid which can be absorbed by the fibres, $V_{l,a}$, is directly proportional to the total dry fibre volume, $V_{s,t}$, and will depend on pressure:

$$V_{l,a} = k(P)V_{s,t} \qquad [3.2]$$

Liquid is present in two phases, absorbed by the fibres, $V_{l,a}$, and as free water between the fibres, $V_{l,bf}$:

$$V_{l,t} = V_{l,a} + V_{l,bf} \qquad [3.3]$$

The total liquid volume, $V_{l,t}$, assuming no contraction can be calculated from the measured total mass, M_t, dry matter content, x, and the known density of the free liquid, ρ_{fl}:

$$V_{l,t} = \frac{M_t(1-x)}{\rho_{fl}} \qquad [3.4]$$

Combination of Eq. 3.1 to 3.3 yields the following relation for the total measured volume of the fibre-liquid-system, V_t:

$$V_t = V_{s,t} + \Delta V_f + V_{l,bf} = [1+(Q-1)k(P)]V_{s,t} + V_{l,t} \qquad [3.5]$$

This yields the following relation for Q:

$$Q = \frac{1}{k(P)}\left(\frac{V_t - V_{l,t}}{V_{s,t}} - 1\right) + 1 \qquad [3.6]$$

Q can be calculated for each experiment if the dependency k(P) is known. This pressure dependency will be approximated by a fit through the experimental curve of the ratio between total liquid volume and total solids volume against pressure. The value of this ratio is higher than the ratio between absorbed water and total solids volume but the shape of the curve,

especially at higher pressures, is assumed to be similar. The resulting equation will be adjusted to the absorbed water content by using the fibre saturation point at atmospheric pressure.

The volumetric swelling per unit volume of dry fibre is given by:

$$\frac{\Delta V_f}{V_{s,t}} = Qk(P) \tag{3.7}$$

The extent of contraction [62], C, can be calculated with the following equation:

$$C = \frac{V_{t,c} - V_t}{V_{t,c}} \cdot 100\% = \frac{(1-Q)k(P)V_{s,t}}{V_{s,t} + V_{l,t}} \cdot 100\% \tag{3.8}$$

in which $V_{t,c}$ is the calculated volume, the sum of dry fibre volume and liquid volume if no contraction would occur:

$$V_{t,c} = V_{s,t} + V_{l,t} = V_{s,t} + V_{l,a} + V_{l,bf} \tag{3.9}$$

For drainage modelling the distribution of the liquid over the two phases is required. The fraction of volume occupied by swollen cell wall is now given by:

$$\phi_{\text{swollen fibre}} = \frac{V_{s,t} + \Delta V_f}{V_t} = \left(1 - \phi_{l,bf}\right) \tag{3.10}$$

3.2 Materials and Methods

Hemp (*Cannabis sativa L.,* Felina 34) bast fibres were cut to lengths between 3-8 mm. For each experiment 0.5 gram of fibres were soaked for at least 4 hours in 16 ml of tap water or 0.2 M NaOH-solution in water at 20ºC. The fibres were put in vacuum before the liquid was added for soaking, to avoid any entrapped air.

3.2.1 Apparatus

A Zwick 1445 tensile tester was used in combination with a compression cell as drawn schematically in Figure 3.2. The compression cell contains a cylinder with a diameter of 1.3 cm, which is sealed at the bottom by a stainless steel disk. The fibres are put in the cylinder and are compressed by means of the pressure head of the tensile tester, which acts on the freely movable rod placed in the cylinder. The liquid pressed out of the pad flows via the edges of the disk through a small tunnel in the bottom plate to the outside of the swell-o-meter. By on-line data-acquisition the force required to obtain the compression is recorded.

3.2.2 Method

The material is compressed slowly to a certain volume to avoid peak pressure and is allowed to relax until the change of pressure during a 10 minute interval is less than 0.5 bar (1.5 to 10 hours). During this relaxation the liquid is allowed to drain. When the applied pressure does
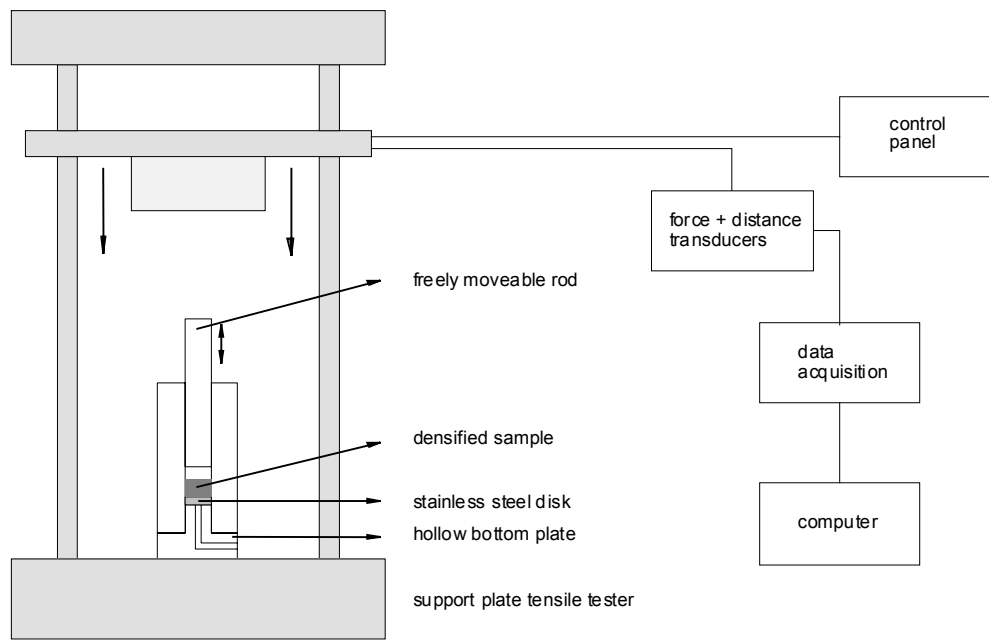
Figure 3.2: *The compression cell*

not change anymore, it is assumed that the hydraulic pressure in the fibre pad has become zero and the applied pressure is totally acting on the solid matrix. The liquid in the bottom plate tunnel is extracted by inserting small hydrophilic tissues in the bottom hole. All water is removed from the bottom hole, when inserted tissues are removed dry. The pad of fibres is removed by removing the bottom and the stainless steel disk. The pad is weighed and the dry matter content of the fibres is determined. The density of the hemp bast fibres was measured by Helium displacement using a Micromeritics AccuPyc 1330.

3.3 Results

The objective of the performed experiments was to obtain values for the extent of volumetric swelling of hemp bast fibres under pressure, in water and in NaOH solution. The time required for relaxation was higher with increasing stress.

The results from compression tests performed with the swell-o-meter on the Zwick tensile tester (Table 3.1 and 3.2) show that the total volume measured is lower than the sum of the calculated liquid and solid volumes for pressures higher than 6 bar. This suggests a value for Q lower than 1. The obtained dry matter content increases with applied pressure (Fig. 3.3), and reaches a dry matter content of 65 % for water soaked fibres at 62 bar and 60 % for fibres soaked in 0.2 M NaOH at about 52 bar. Fitting the curve relating the ratio between the total

45

Table 3.1. Results of compression tests, fibres in water

Pressure P (bar)	Total mass M_t (g)	Total volume V_t (measured) (cm³)	Dry matter content, d.m. (%)	Solid volume V_s (calculated) (cm³)	Liquid volume, V_l (calculated) (cm³)	Total volume V_t (calculated) (cm³)
4.2	2.51	2.31	37.6	0.63	1.57	2.20
15.0	2.17	1.76	52.5	0.76	1.03	1.79
27.5	1.73	1.32	61.1	0.71	0.67	1.38
43.8	2.69	2.04	60.7	1.09	1.06	2.15
61.7	2.19	1.60	65.3	0.95	0.76	1.71

Table 3.2. Results of compression tests, fibres in 0.2 M NaOH

Pressure P (bar)	Total mass M_t (g)	Total volume V_t (measured) (cm³)	Dry matter content, d.m. (%)	Solid volume V_s (calculated) (cm³)	Liquid volume, V_l (calculated) (cm³)	Total volume V_t (calculated) (cm³)
5.4	3.76	3.31	39.1	0.98	2.29	3.27
15.7	3.18	2.56	50.0	1.06	1.59	2.65
27.2	3.21	2.45	57.1	1.22	1.37	2.59
34.7	3.03	2.33	56.6	1.14	1.31	2.45
51.8	2.40	1.81	60.0	0.96	0.96	1.92

liquid volume and the total solids volume to the applied pressure (Fig. 3.4) results in the following equations:

$$\frac{V_{l,t}}{V_{s,t}} = \frac{70+P}{18+2.6P} \quad \text{water} \tag{3.11a+b}$$

$$\frac{V_{l,t}}{V_{s,t}} = \frac{25+P}{7.5+1.3P} \quad \text{0.2 M NaOH}$$

As the shape of the curves of the relative absorbed volume and the relative total liquid volume is assumed to be similar, Eq. 3.11 will be used to develop a relation for k(P). Just using Eq. 3.11 implies an equality between the absorbed volume and the total liquid volume, so no liquid would be present between the fibres. To retain a similar shape only the numerator will be adjusted. The fibre saturation point of the hemp bast fibres under atmospheric conditions was determined by the water retention value (under conditions determined by Scallan and Carles [38]) to be 1.26 g/g for water soaked fibres, which is 1.89 cm³/cm³ ($\rho_s = 1.5$ g/cm³, $\rho_l = 1.0$ g/cm³). The fibres soaked in 0.2 M NaOH show a FSP of 1.5 g/g, which is 2.25 cm³/cm³ ($\rho_s = 1.5$ g/cm³, $\rho_l = 1.0$ g/cm³).

For $V_{l,a}/V_{s,t}$ (water) to be 1.89 at atmospheric pressure, the numerator of Eq. 3.11a should be multiplied by 0.486 to obtain k(P). For $V_{l,a}/V_{s,t}$ (0.2 M NaOH) to be 2.25 at atmospheric pressure, Eq. 3.11b should be multiplied by 0.675:

$$k(P) = \frac{34 + 0.49P}{18 + 2.6P} \quad \text{water}$$

$$k(P) = \frac{17 + 0.68P}{7.5 + 1.3P} \quad \text{0.2 M NaOH} \tag{3.12}$$

With use of Eq. 3.6 and 3.12 Q is calculated for each experiment (Table 3.3 and 3.4). Although Q values higher than 1 are obtained at low pressures, Q is assumed to have a maximum equal to one. Higher Q values are obtained because at low pressures swollen fibres and water do not fully fill the compression chamber. Contraction will take place at pressures higher than a certain critical pressure at which water molecules start to penetrate the cellulose structure. Q seems to reach a minimum at higher pressures (Fig. 3.5). The curves are fitted with the following equations:

Figure 3.3. *Dry matter content versus applied pressure*

$$\text{if } P < P_{krit}: \quad Q = 1 \qquad \text{water}$$

$$\text{if } P > P_{krit} \quad Q = \frac{50 + (P - P_{crit})}{50 + 1.9(P - P_{crit})}$$

$$\text{if } P < P_{krit}: \quad Q = 1 \qquad \text{0.2 M NaOH} \tag{3.13}$$

$$\text{if } P > P_{krit} \quad Q = \frac{10 + (P - P_{crit})}{10 + 1.25(P - P_{crit})}$$
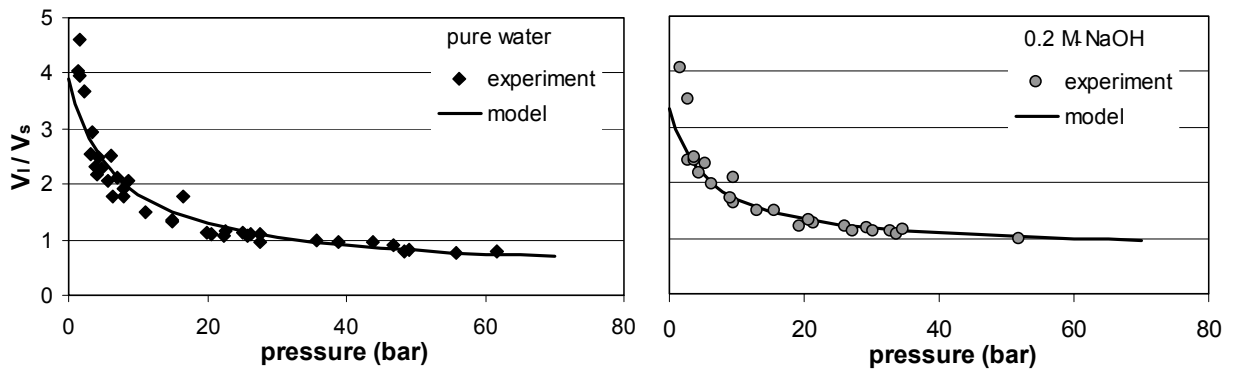
Figure 3.4. *Fit of experimental results of the ratio between liquid and solid volume versus applied pressure*

47

Table 3.3. *Ratio of specific volumes and contraction results, fibres in water*

Pressure, P (bar)	Q (-)	C (%)
4.2	1.14	-5.2
15.0	0.95	1.6
27.5	0.85	4.0
43.8	0.76	5.2
61.8	0.68	6.4

Table 3.4. *Ratio of specific volumes and contraction results, fibres in 0.2 M NaOH*

Pressure, P (bar)	Q (-)	C (%)
5.4	1.03	-1.2
15.7	0.91	3.5
27.2	0.86	5.4
34.7	0.85	5.3
51.8	0.83	5.9
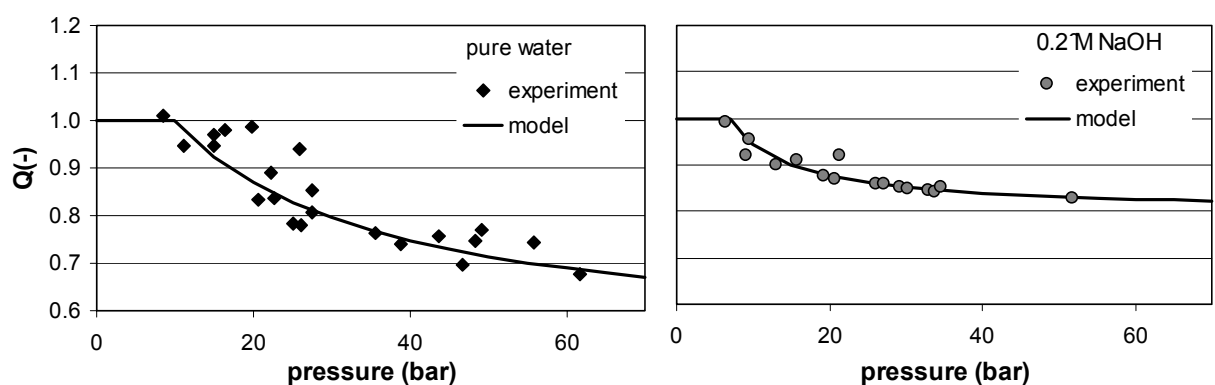
Figure 3.5. *Ratio between the specific volumes of absorbed and free liquid versus applied pressure*
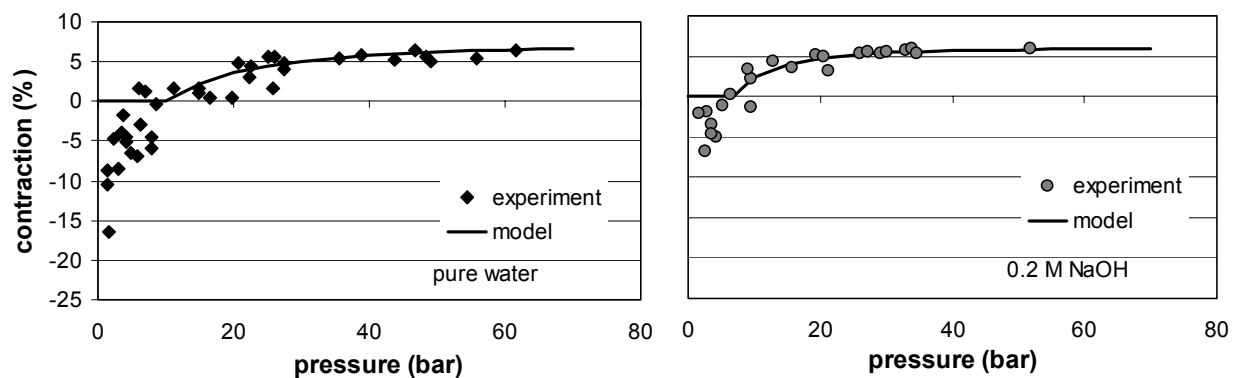
Figure 3.6. *Contraction versus pressure*
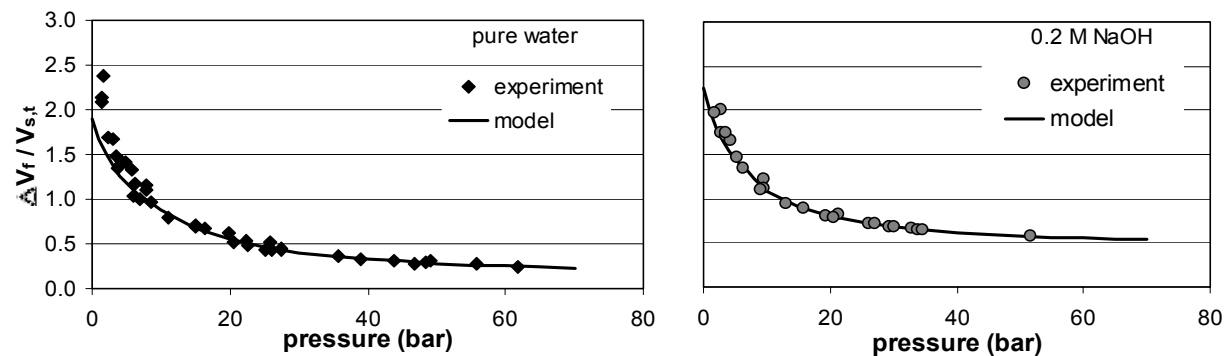
Figure 3.7. *Volumetric swelling versus applied pressure*

48
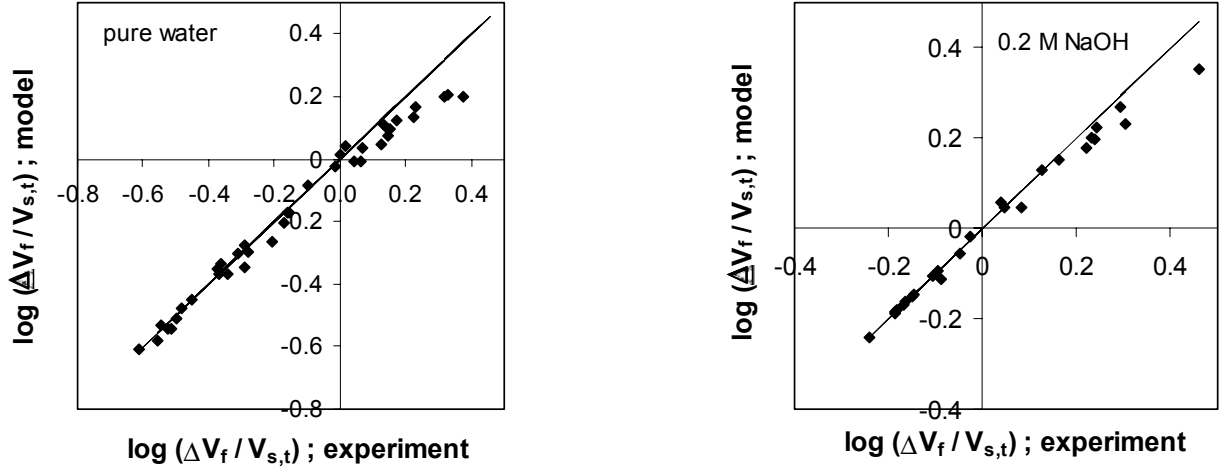
Figure 3.8. *Parity plots for volumetric swelling. A: fibres in water B: fibres in 0.2 M NaOH*

According to relations provided by Alince [45] contraction percentages are calculated (Table 3.3 and 3.4). The contraction increases with pressure (Fig. 3.6), and reaches a maximum at high pressures. If the model would be extendable to pressures higher than 100 bar, the contraction degree of the fibre-water system would according to the developed model not exceed 6.5 % The contraction of the fibres in a 0.2 M NaOH solution would not exceed 6 %.

The model for volumetric swelling per unit volume of dry fibre is now given by:

$$\text{if } P < P_{krit}: \quad \frac{\Delta V_f}{V_{s,t}} = \frac{34 + 0.49P}{18 + 2.6P}$$

$$\text{if } P > P_{krit}: \quad \frac{\Delta V_f}{V_{s,t}} = \left(\frac{34 + 0.49P}{18 + 2.6P}\right) \cdot \left(\frac{50 + (P - P_{crit})}{50 + 1.9(P - P_{crit})}\right) \quad \text{water}$$

$$\text{if } P < P_{krit}: \quad \frac{\Delta V_f}{V_{s,t}} = \frac{17 + 0.68P}{7.5 + 1.3P} \quad \text{0.2 M NaOH}$$

$$\text{if } P > P_{krit}: \quad \frac{\Delta V_f}{V_{s,t}} = \left(\frac{17 + 0.68P}{7.5 + 1.3P}\right) \cdot \left(\frac{10 + (P - P_{crit})}{10 + 1.25(P - P_{crit})}\right)$$

[3.14]

These equations are valid for pressures up to 60 bar. The resulting curves are drawn in Figure 3.7. The parity plots (Fig. 3.8) show that the best agreement of the model with the experimental values is observed at low values of volumetric swelling, thus at high pressures. At low pressures the model is less accurate.

From Eq. 3.14 we can calculate a minimum volumetric swelling in water of 0.19 cm^3/cm^3 at 100 bar. The FSP at this point, calculated from the absorbed amount of water, is 0.13 g/g. The volumetric swelling of hemp bast fibres in 0.2 M NaOH is 0.50 cm^3/cm^3 at 100 bar, corresponding with a FSP of 0.33 g/g. If the model would be extendable to higher pressures, the volumetric swelling would reach a minimum of 0.10 cm^3/cm^3 in water and 0.40 cm^3/cm^3 in 0.2 M NaOH at infinite pressure.

49
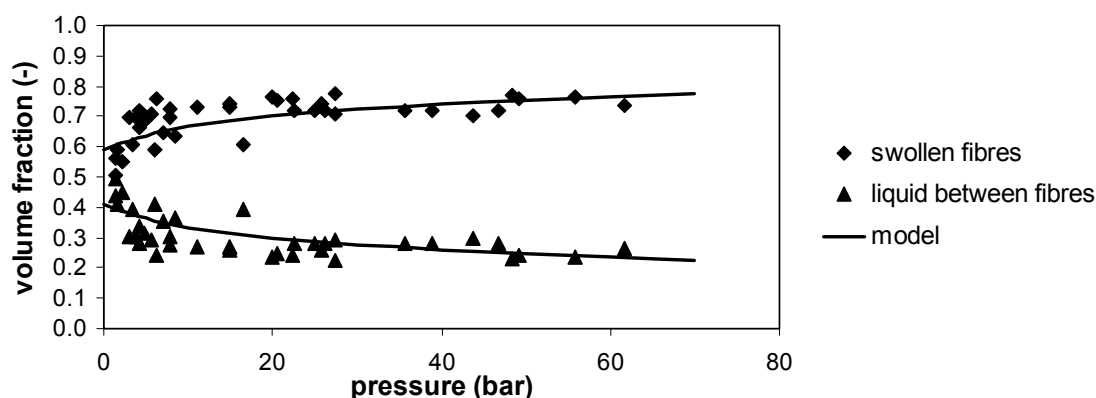
Figure 3.9. *Volume fraction swollen fibre versus applied pressure, fibres in water*

For drainage modelling the distribution of the liquid over the two phases is required. Model calculations show a volume fraction of swollen fibres in water increasing slowly from 0.59 at atmospheric pressure to 0.79 at 100 bar (Fig. 3.9). The volume fraction of swollen fibres in a NaOH-solution increases from 0.75 at atmospheric pressure to 0.84 at 100 bar.

3.4 Discussion

From the experimental results it follows that contraction increases with pressure and reaches a maximum of 6.5 %. The highest contraction observed by other authors is only 4% [45] at low moisture contents. However, a direct comparison of the contraction phenomenon observed by other authors is not possible, as previous studies on contraction were performed under atmospheric pressure and contraction was not observed at moisture contents as high as those of the experiments of this paper.

There are two possible hypotheses for the high contraction extent; the solids density could be higher than previously reported (because of the higher pressures used in this study) or the liquid in the cell wall could have a lower specific volume when pressurised. The required solids density for an equality of the measured and the calculated volume, assuming a constant liquid density in the cell wall of 1 g/cm^3, should be approximately 1.7 g/cm^3 (Fig. 3.10). This high value for the density of cell wall components has not been reported before. As a solid density is hardly influenced by pressure, we may assume that the measured values for this density are valid under high pressure and a more logical explanation of the observed contraction should therefore be a lower specific volume of liquid in the cell wall, because of the high pressures applied. Calculations show that the

Figure 3.10. *Required solids density for equality of measured and calculated volumes versus applied pressure*

specific volume of water in hemp bast fibres decreases to 0.87 cm^3/g at 100 bar and the specific volume in NaOH treated fibres decreases to 0.88 cm^3/g, which is respectively 13 % and 12 % lower than the specific volume of free water. The compressibility of water at 20°C is 49·10^{-6} bar^{-1} at 13 bar and 43·10^{-6} bar^{-1} at 200 bar [63], which corresponds with a maximum volume decrease of 0.5 % when water is compressed from 1 to 100 bar. The observed contraction can therefore not be attributed to compression of the liquid. The decrease in specific volume of the liquid can only be explained by movement of the water molecules to places between the molecules of the cell wall components, which are not accessible at ambient pressure. More places might become accessible for water molecules when the pressure is increased, but a maximum is obtained at higher pressures. From the developed model it can be calculated that a maximum of 0.11 gram of water per cm^3 dry fibre can be located on places which are not accessible at ambient pressures and this maximum is obtained at pressures higher than 50 bar. For fibres treated with NaOH a maximum of 0.12 grams of liquid per cm^3 dry fibre is obtained. The fact that NaOH treated fibres can contain more liquid at places which are not accessible at ambient pressures can be explained by different proportions of cell wall components in water and NaOH treated fibres. NaOH decomposes the lignin in the cell wall and so NaOH treated fibres contain less lignin and relatively more cellulose. As NaOH-treated fibres can contain more liquid we might conclude that cellulose contains more places which become accessible for water at higher pressures than lignin. Although NaOH-treated fibres can contain more liquid at spaces which are not accessible at ambient pressure, a lower overall contraction observed in comparison with water-treated fibres, because of the lower dry matter content achieved with NaOH-treated fibres.

Difference between volumetric as well as gravimetric swelling between fibres immersed in water and fibres immersed in a NaOH-solution at atmospheric pressure has been reported before in other studies. Results from our experiments show that also under pressure the volumetric as well as the gravimetric swelling of fibres is higher when treated with a NaOH-solution compared to when treated with water (Fig. 3.7). Moreover the results show that the fibres swollen by the NaOH-solution fill a higher percentage of the total space compared to water swollen fibres. This is probably due to a higher flexibility of the fibres when treated with NaOH.

3.5 Conclusions

The volume of swollen fibres under pressure is shown to be lower than the volume of dry fibres plus the volume of absorbed water. Observed contraction degrees are higher than previously reported under atmospheric pressures. Contraction is attributed to a decrease in specific volume of the liquid in the fibre with pressure, because then water molecules migrate to places which are inaccessible to water molecules at ambient pressure. Experiments show that the specific volume of water in hemp bast fibre decreases to 0.87 cm^3/g at 100 bar and to 0.88 cm^3/g at 100 bar when treated with NaOH.

NaOH treated fibres become more accessible for water when pressurized. From these results it is concluded that cellulose is to a larger extent responsible for contraction than lignin. Removal of lignin by NaOH results in a more flexible cell wall, so that the swollen fibres fill 84 % of the total space instead of a maximum of 79 % at 100 bar filled by swollen fibres when treated with water. This results in higher volumetric swelling values under pressure for fibres immersed in a 0.2 M NaOH-solution compared to fibres in water.

51

3.6 Nomenclature

b	constant in relation between a and P	-
c	constant in relation between a and P	-
C	contraction degree	%
k(P)	relation between ratio of absorbed liquid volume and total solid volume and applied pressure	-
M	mass	g
P	pressure	bar
Q	ratio between specific volumes of absorbed and free liquid	-
V	volume	cm^3
x	dry matter content (fraction)	-
ΔV_f	fibre volume increase by absorption of volume $V_{l, a}$	cm^3
ρ	density	g/cm^3
φ	volume fraction	-

subscripts

a	absorbed
bf	between the fibres
c	calculated
f	fibre
fl	fibrous liquid; liquid in the fibre cell wall
l	liquid
s	solid
t	total

3.7 References

1. van Roekel, G.J., Lips, S.J.J., Op den Kamp, R.G.M. and Baron, G. (1995): Extrusion pulping of true hemp bast fibre (Cannabis sativa L.), Tappi Conference, Chigago, USA, p. 477-485.
2. van Roekel, G.J. (1995): Chemimechanical pulping of fibre hemp, Bioresource Hemp, Frankfurt a/M, Germany.
3. van Roekel, G.J. (1996): Bulk papermaking applications for bast fibre crops using extrusion pulping, PIRA International, Peterborough, England, p. paper 26, 29 pp.
4. Seth, R.S. (1996): Optimizing reinforcement pulps by fracture toughness, Tappi J. 79: 1, 170-178.
5. de Jong, E., van Roekel, G.J., Snijder, M.H.B. and Zhang, Y. (1999): Towards industrial applications of bast fibre pulps; their potential as a nonwood source is discussed, Pulp Paper Canada 100: 9, T270-T273.

6.   Snijder, M.H.B., Wissing, E. and Modder, J.F. (1997): Polyolefins and engineering plastics reinforced with annual plant fibers, 4th Int. Conf. Woodfiber-plastic Composites, Madison (Wisconsin), USA, p. 181-191.

7.   Herrera-Franco, P.J. and Aguilar-Vega, M. (1997): Effect of fiber treatment on the mechanical properties of LDPE-henequen cellulosic fiber composites, J. Appl. Pol. Sci. 65: 1, 197-207.

8.   Heijenrath, R. and Peijs, T. (1996): Natural-fibre-mat-reinforced thermoplastic composites based on flax fibres and polypropylene, Adv. Pol. Let. 5: 3, 71-75.

9.   Mieck, K.-P., Nechwatal, A. and Knobelsdorf, C. (1995): Faser-Matrix-Haftung in Kunststoffverbunden aus thermoplastischer Matrix und Flachs, 2a, Angew. Makromol. Chem. 225, 37-49.

10.   Sanadi, A.R., Caulfield, D.F., Jacobson, R.E. and Rowell, R.M. (1995): Renewable agricultural fibers as reinforcing fillers in plastics: mechanical properties of kenaf fiber - polypropylene composites, Ind. Eng. Chem. Res. 34, 1889-1896.

11.   Matthews, J.M. (1947): "Textile fibres, their physical, microscopical and chemical properties". John Wiley & Sons, New York.

12.   Kirby, R.H. (1963): "Vegetable fibres, botany, cultivation and utilization". Interscience Publishers Inc., New York.

13.   Rance, H.F. (1980): "The raw materials and processing of papermaking". Elsevier Scientific Publishing Company, Amsterdam.

14.   Uhmeier, A. and Salmén, L. (1996): Influence of strain rate and temperature on the radial compression behavior of wet spruce, J. Eng. Mat. Technol. 118: 3, 289-294.

15.   Andersson, S.R. and Rasmuson, A. (1997): Dry and wet friction of single pulp and synthetic fibres, J. Pulp Paper Sci. 23: 1, J5-J11.

16.   Allan, G.G., Carroll, J.P., Devakula, M.L.P., Gaw, K., Joseph, A.A. and Pichitlamken, J. (1997): The effect of filler location on the drainage, pressing, and drying of pulp and paper, Tappi J. 80: 8, 175-179.

17.   Buyevich, Y.A. and Nustrov, V.S. (1993): Nonlinear flow in fractured porous media, Transport in Porous Media 12, 1-17.

18.   Filippov, V.I., Emel'yanov, Y.A., Lunev, V.D. and Kurochkina, M.I. (1983): Calculation of the expression zone in screw devices for separation of suspensions, J. Appl. Chem. USSR 56: 2, 417-420.

19.   Ghaddar, C.K. (1995): On the permeabilitty of unidirectional fibrous media: A parallel computational approach, Phys. Fluids 7: 11, 2563-2586.

20.   Egenes, T.H. and Helle, T. (1992): Transport and drainage processes in a screw press as affected by material characteristics, 78th Annual Meeting, Technical Section, CPPA, p. B173-B181.

21.   Schwartzberg, H., Huang, B.W., Abularach, V. and Zaman, S. (1980): In "Food process engineering", P. L. e. al., ed.,, p. 434-437.

22.   Shirato, M., Murase, T., Hayashi, N., Miki, K., Fukushima, T., Suzuki, T., Sakakibara, N. and Tazima, T. (1978): Fundamental studies on continuous extrusion using a screw press, Int. Chem. Eng. 18: 4, 680-688.

23.   Wei, H., Kumar, P., Ramarao, B.V. and Tien, C. (1996): Drainage and fine particle retention in a forming incompressible fibrous mat, J. Pulp Paper Sci. 22: 11, j446-j451.

24.   Sitkei, G. (1986): "Mechanics of agricultural materials". Elsevier, Amsterdam.

25.   Ottestam, C., Engstrand, P., Htun, M., Sjogren, B. and Olander, K. (1991): A modified method for measuring the swelling properties of mechanical WRV pulps, Int. Mech. Pulping Conf., p. 87-89.

26. Salmén, L. (1990): Thermal expansion of water-saturated wood, Holzforschung 33: 1, 17-19.

27. Katz, S., Liebergott, N. and Scallan, A.M. (1981): A mechanism for alkali strengthening of mechanical pulps, Tappi J. 64: 7, 97-100.

28. Katz, S. and Scallan, A.M. (1983): Ozone and caustic soda treatments of mechanical pulp, Tappi J. 64: 1, 85-87.

29. Zanuttini, M. (1995): Alkaline treatment of sugar cane bagasse. Swelling and properties of chemimechanical pulps, Cellulose Chem. Technol. 29: 6, 751-759.

30. Grignon, J. and Scallan, A.M. (1980): Effect of pH and neutral salts upon the swelling of cellulose gels, J. Appl. Polym. Sci. 25: 11, 2829-2843.

31. Ferrús, R. and Pagés, P. (1977): Water retention value and degree fo crystallinity by infrared absorption sprectroscopy in caustic-soda-treated cotton, Cellulose Chem. Technol. 11, 633-637.

32. Kim, N.-H., Sugiyama, J. and Okano, T. (1989): The behavior of cellulose fibers in the early stage of alkaline swelling, Mokuzai Gakkaishi 35: 5, 387-391.

33. de Groot, B., van der Kolk, J.C., van der Meer, P., van Dam, J.E.G. and van 't Riet, K. (1997): Alkaline swelling of hemp woody core chips, J. Wood Chem. Tech. 17: 1-2, 187-208.

34. Jenkins, L.M. and Donald, A.M. (1997): Use of the environmental scanning electron microscope for the observation of the swelling behaviour of cellulosic fibres, Scanning 19: 2, 92-97.

35. Stone, J.E. and Scallan, A.M. (1967): The effect of component removal upon the porous structure of the cell wall of wood II. Swelling in water and the fiber saturation point, Tappi J. 50: 10, 496-501.

36. Bendzalova, M. and Pekarovicova, A. (1996): Accessibility of swollen cellulosic fibres, Cellulose Chem. Technol. 30: 1-2, 19-32.

37. Laivins, G.V. and Scallan, A.M. (1996): The influence of drying and beating on the swelling of fines, J. Pulp Paper Sci. 22: 5, J178-J184.

38. Scallan, A.M. and Carles, J.E. (1972): The correlation of the water retention value with the fibre saturation point, Svensk Papperstid. 75: 17, 699-703.

39. Stone, J.E. and Scallan, A.M. (1968): A structural model for the cell wall of water-swollen wood pulp fibres based on their accessibility to macromolecules, Cellulose Chem. Technol. 2, 343-358.

40. Babiak, M. and Kúdela, J. (1995): A contribution to the definition of the fibre saturation point, Wood Sci. Techn. 29, 217-226.

41. Nedelcheva, M.P. and Stoilkov, G.V. (1982): Influence of the polyelectrolytes retained on the ability of the cellulose to swell and on the electrokinetic properties, Svensk Papperstid., R61-R63.

42. Ni, Y. and van Heinigen, A.R.P. (1997): The swelling of pulp fibers derived from the ethanol-based organosolv process, Tappi J. 80: 1, 211-213.

43. Szwarcsztajn, E. and Przybysz, K. (1975): Investigatinos of water retention value (wrv) of beaten cellulose fibres, Cellulose Chem. Technol. 9, 597-607.

44. Stamm, A.J. (1971): Review of nine methods for determining the fibre saturation points of wood and wood products, Wood Sci. 4, 114-128.

45. Alince, B. (1988): In "Cellulose Wood Chemistry and Technology", C. Schuerch, ed.,, p. 379-388.

46. Filby, E. and Maass, O. (1932): The volume relations of the system cellulose and water, Can. Res. J. 7, 162-177.

47. Hatakeyama, T., Yamamoto, S., Hirose, S. and Hatakeyama, H. (1988): In "Cellulose and Wood Chemistry and Technology", C. Schuerch, ed.,.

48. Hermans, P.H. (1946): "Contribution to the physics of cellulose fibres; a study in sorption, density, refractive power and orientation". Elsevier Publishing Company, Amsterdam.

49. Seifert, J. (1972): Die Volumenkontraktion zwischen Holz und Wasser (The volume contraction between wood and water), Holz Roh-Werkstoff 30, 332-342.

50. Stamm, A.J. and Seborg, R.M. (1935): Adsorption compression on cellulose and wood, I, J. Phys. Chem. 39, 133-142.

51. Valko, E.I. (1946): In "Cellulose and Cellulose Derivatives", E. Ott, ed., Interscience Publishers Inc., New York.

52. Weltzien, W. (1929): "Chemische und physikalische Technologie der Kunstseide". Akademische Verlagsgesellschaft m.b.H., Leipzig.

53. Gunderson, D.E. (1989): In "Mechanics of cellulosic and polymeric materials", R. W. Perkins, ed.,, New York, p. 157-165.

54. Gunderson, D.E. (1991): Method for measuring mechanosorptive properties, J. Pulp Pap. Sci. 17: 2, J53-J59.

55. Kubát, J. and Nyborg, L. (1962): Influence of mechanical stress on the sorption equilibrium of paper, Svensk Papperstidning 65: 18, 698-702.

56. Mukudai, J. and Yata, S. (1988): Verification of Mukudai's mechano-sorptive model, Wood Sci. Technol. 22: 1, 43-58.

57. Simpson, W.T. (1971): Moisture changes induced in red oak by transverse stress, Wood and fiber 3: 1, 13-21.

58. Treloar, L.R.G. (1953): The absorption of water by cellulose, and its dependence on applied stress, Transactions of the Faraday Soc. 49, 816-823.

59. Van der Put, T.A.C.M. (1989): Theoretical explanation of the mechano-sorptive effect in wood, Wood Fiber Sci. 21: 3, 219-230.

60. Lindström, T. (1986): In "Paper structure and properties", J. A. Bristow and P. Kolseth, ed., Marcel Dekker Inc., New york, p. 75-97.

61. Laivins, G.V. and Scallan, A.M. (1994): Removal of water from pulps by pressing; Part 1: Inter- and intra-wall water, Tappi J. 77: 3, 125-131.

62. Alince, B. (1964): Zur Frage der Dichtebestimmung der Cellulosematerialen, Das Papier 18, 55-62.

63. Perry, R.H. (1984): "Perry's chemical engineers' handbook". McGraw-Hill Book Co, Singapore.

Chapter 4

Drainage through swollen hemp bast fibres during compression

Summary

This paper studies the drainage of water and sodium hydroxide solutions through a column of hemp fibres in order to predict the conditions at which mechanical pulping processes become restricted by flow resistance. The results have been analysed by regression techniques of different models in order to find the best model to describe drainage through hemp bast fibres in the desired pressure and time range.

Drainage experiments with hemp bast fibres were conducted at pressures up to 27 MPa and at sodium hydroxide concentrations up to 2 M. It was shown that the drainage process significantly slowed down with higher sodium hydroxide concentrations. A higher pressure slightly enhances the drainage process.

It was concluded that a model that includes a compressibility equation for the solid network is required when high pressures are applied during drainage.

Swelling appeared to be a very important parameter in the drainage process. Models which neglect fibre swelling, predict drainage processes that are about 50,000 times faster than experimentally observed. The Kozeny-Carman model for flow through porous media has been extended with a proper swelling model. This model correctly describes the decrease of volumetric swelling with pressure: The decrease of volumetric swelling with pressure is small at low pressure as compression of the fibre network at low pressure mainly results in fibre bending and slippage. The initial swelling is higher with higher sodium hydroxide concentrations. However, a more flexible cell wall at higher sodium hydroxide concentration results in a more rapid decrease of swelling with network pressure. The degree of volumetric swelling becomes negligible at high pressure.

4.1 Introduction

Refining and extrusion are processes used to defibrate and fibrillate wood chips and fibre bundles in order to produce pulp. Fibres are repeatedly compressed during refining or extrusion causing a separation of the fibres (defibration) and damage to the fibre wall, resulting in fibrillation and flexibilisation of the fibres. However, only a small part of the total energy consumed during those processes appears to be necessary for the desired change in the fibre properties [1-4]. It is worth studying the fundamentals of energy dissipation by fibres during deformation as mechanical pulping processes consume large amounts of energy. The

pulping processes could be optimised, when knowing the mechanism behind energy absorption, in order to obtain the desired fibre changes with a minimum of energy consumption.

A study of the mechanism of hemp fibre compression at large deformation revealed that at high strain rates and large deformations, the liquid expression from the fibre mass causes the total pressure to increase more rapidly than predicted by the compressibility of the fibres [5]. This pressure increase is attributed to a liquid pressure increase, as the compression rate becomes faster than the rate of liquid expression. From this point, the energy consumed during further compression is mainly used for liquid expression instead of for fibre processing. It is better to avoid too high strain rates or too low permeability, as flow limitation is undesirable.

The fundamentals of liquid expression from hemp fibre pulp are studied and described in this paper in order to predict when compaction becomes controlled by liquid flow.

4.1.1 Drainage through a compressible fibre network

The removal of water from fibre networks has been extensively studied. The most important applications in the paper and pulp industry are the flow through fibre beds during sheet formation and wet pressing. Research on the fundamentals of wet pressing has been reviewed [6,7]. The driving force in drainage is the hydrodynamic pressure gradient caused by either mechanical compaction or gravity. Models describing the flow through fibre networks are mostly based on Darcy's law [6-19]. This empirical relation gives the relation between the pressure gradient and liquid flow rate:

$$q = -\frac{KA}{\mu}\frac{\partial \sigma_l}{\partial x} \qquad\qquad [4.1]$$

The permeability K depends strongly on the geometrical structure of the porous medium. A frequently used model that has implemented a relation between the permeability and structure parameters is the Kozeny-Carman model [7,9-11,13-17,20]. This model assumes laminar flow through cylindrical pores perpendicular to the surface and includes the porosity, specific surface area and shape factor of the material:

$$K(\varepsilon, S_v) = \frac{\varepsilon^3}{kS_v^2(1-\varepsilon)^2} \qquad\qquad [4.2]$$

The Kozeny factor, k, is characterised by the shape and orientation of the material. For fibre networks both porosity and the orientation of the fibres influence the Kozeny factor. The Kozeny factor was found to be 3.07 for a bed of glass fibres oriented nearly parallel, 6.04 for fibres oriented perpendicular to the direction of flow and 4.5 when the fibres were oriented at random [21]. At high porosities, i.e. above 0.86, the Kozeny factor was found to strongly depend on porosity [22]. The Kozeny-Carman model also shows the frequently observed decrease of permeability during compaction caused by a decrease in porosity. In addition to the so-called pore models, drag and orifice models are used to describe flow through textile materials [20]. In drag models a system of cylinders is present in a continuous fluid phase and in orifice models, mostly used for woven fabrics, flow through a narrowing and subsequently

widening flow channel is modelled. However, the models are developed for oriented fibres and are not directly applicable to fibre networks with random orientation.

4.1.2 Swelling

Models for fluid flow through porous media assume liquid flow through the spaces which are not occupied by the solid matrix. A significant amount of liquid is located in the fibre cell wall causing swelling of the fibres, as natural fibres are highly hygroscopic. This liquid might flow through the cell wall and, when swollen fibres are compressed, into the pores. Moreover, fibre swelling significantly decreases the porosity of the fibre mass and thus causes the permeability to become lower than calculated from dry fibre geometry. An example of this is the permeability of cotton fabrics being 55-220 times lower than the permeability calculated from models based on dry fibre geometry [23]. This deviation is probably not only because of swelling but might also be caused by the presence of fibrils on the surface of the cotton fibres. Jönnson and Jönnson [10,11] use the swollen volume of the fibres as incompressible volume while in practice the extent of swelling decreases when the fibre wall is compressed during deformation.

McDonald and Kerekes [24-26] incorporated the liquid in the fibre by developing a model based on the idea that the loading supported by the network is itself a hydraulic pressure since fibres contain a great deal of water. They model liquid expression from a fibre mass of decreasing permeability, instead of decreasing porosity, resulting in the following equation to describe the water removal from a wet web of wood fibres:

$$\frac{m}{m_0} = \left(1 + \left(\frac{nf\sigma_l t}{m_0}\right)\right)^{-\frac{1}{n}}$$ [4.3]

The factor n, is called the compressibility factor representing the relation between the depth of the fibre mat, porosity, hydrodynamic specific surface and moisture content. The permeability decreases faster with decreasing moisture content at higher values of n. Compressibility of the solid part is not included. The factor f, the permeability factor, represents permeability in the initial uncompressed condition.

A correct drainage model allows liquid flow through the small pores in the fibre cell wall and from the cell wall into the interstices. Although a much lower permeability causes the flow through the porous fibre wall to be negligible compared to the flow along the fibres, flow from the fibre wall into the interstices by compression of the fibre wall might play an important role. The amount of liquid present in the fibre wall is described with the volumetric swelling of the fibres:

$$W = \frac{V_f - V_s}{V_s}$$ [4.4]

in which V_f and V_s are respectively the swollen and non-swollen fibre volume. The true porosity matrix is defined as the fraction of the space between the swollen fibres from the total volume, V_t:

$$\varepsilon = 1 - \frac{V_f}{V_t} \qquad\qquad [4.5]$$

while the overall porosity, ϕ, is defined as the volume fraction of liquid:

$$\phi = 1 - \frac{V_s}{V_t} \qquad\qquad [4.6]$$

Combination of Eq. 4.4, 4.5 and 4.6 results in the following relation between the true porosity, ε, and the overall porosity, ϕ:

$$\varepsilon = 1 - (1 + W)(1 - \phi) \qquad\qquad [4.7]$$

If the cell wall contains no liquid, W equals 0 and ϕ equals ε.

The effect of pressure on the volumetric swelling phenomenon has been researched by Westenbroek et al. [27] for hemp bast fibres in water and in 0.2 M NaOH up to 6 MPa. In general it was concluded that the degree of volumetric swelling decreases with increasing solid matrix pressure. At atmospheric pressure fibres soaked in sodium hydroxide exhibit a higher volumetric swelling than fibres soaked in water. This difference diminishes at higher network pressure.

The addition of sodium hydroxide results in a decomposition of the lignin, increased swelling of the fibre wall, and may also result in a change in fibre cellulose structure. Only the effect of sodium hydroxide on volumetric swelling has been studied, because now we are only interested in the effect of sodium hydroxide on the drainage through the fibres.

4.1.3 Compressibility of the solid matrix

During drainage by compression, mechanical loads deform the solid matrix resulting in an increased resistance to liquid flow due to a decreased porosity. The network pressure is a supporting load and does not contribute to water removal. In general El-Hosseiny [7] concludes that in modelling wet pressing the total pressure, σ_t, is taken to be the sum of hydraulic pressure, σ_l, and the network pressure, σ_s:

$$\sigma_t = \sigma_s + \sigma_l \qquad\qquad [4.8]$$

The relationship between porosity in a porous medium and the network pressure is often termed the compressibility. In wet pressing some authors assume the relation between stress and strain to be linear elastic [28], while others assume the compressional behaviour to be non-linear [6,7,10,11,13,15]. As pressures applied on fibres during mechanical pulping by extrusion (up to 30 MPa) are much higher than those during wet pressing (up to 0.5 MPa) the non-linearity of the solid network compressibility is important. This non-linearity is often described with the general compressibility equation [6,10,11,15]. The drainage theory of McDonald and Kerekes [24-26] excludes the compressibility of the network.

The compressibility of the hemp bast fibre network has been investigated in a previous study [5]. The combined effect of fibre bending, fibre slippage and fibre wall compression has been summarised by expressing the experimental data in the form of a power law equation:

$$\sigma_s = \left(\frac{\rho}{\gamma}\right)^{\frac{1}{N}}$$

[4.9]

γ and N were found to depend on temperature, strain rate and pre-treatment.

The drainage of hemp bast fibre mats was studied experimentally and the results are compared with three different models in order to determine which theory best describes the drainage phenomena. Firstly, our experimental curves have been compared with the decreasing permeability model of McDonald and Kerekes [24-26] (Eq. 4.4) by adjusting the values of the permeability and the compressibility factor. Secondly our experimental results have been compared with the Kozeny-Carman model, and thirdly with a combination of the Kozeny-Carman and a swelling model.

4.2 Materials and Methods

Experiments were conducted to study the drainage of water and sodium hydroxide solutions through hemp bast fibres. Hemp (Cannabis sativa L., Felina 34) bast fibres were cut to an average length of 33 mm. For each experiment 20 gram of fibres (on dry basis) was used. The fibres were soaked for at least 4 hours in water, 0.05 M, 0.2 M, 1 M or 2 M NaOH at 20 °C before each experiment. This time period is taken to be sure that the equilibrium in swelling had been reached.

4.2.1 Apparatus

In Figure 4.1 a schematic drawing of the apparatus is given. The apparatus consists of a block containing a cylindrical boring of 30 mm diameter, fitted with a removable porous bottom. The flow resistance over this bottom can be considered negligible as the bottom has a high porosity (> 60 %) and a thickness of 4 mm. The boring can be filled with fibres and a plunger can be placed on top of the fibres in the boring. With a vertical hydraulic cylinder operating on the plunger normal pressures up to 60 MPa can be applied to the fibres. During the experiment the hydraulic cylinder maintains a constant pressure on top of the fibres, implying that the speed of compression depends on the drainage speed. Liquid pressed out from the bottom flows either via the porous bottom or via the edge of the plunger to the outside of the boring. The volume change versus time can be recorded by on-line data-acquisition equipment.

4.2.2 Method

Drainage was studied at pressures of 9, 18 and 27 MPa. Although pressures achieved during extrusion pulping are not clear yet, it is assumed that the pressure range applied in our drainage experiments covers the pressure range obtained during extrusion pulping. Measurement was started at the moment when pressure build-up was fully developed. Slower drainage because of a lower permeability or a lower pressure gradient therefore resulted in a higher initial moisture content.
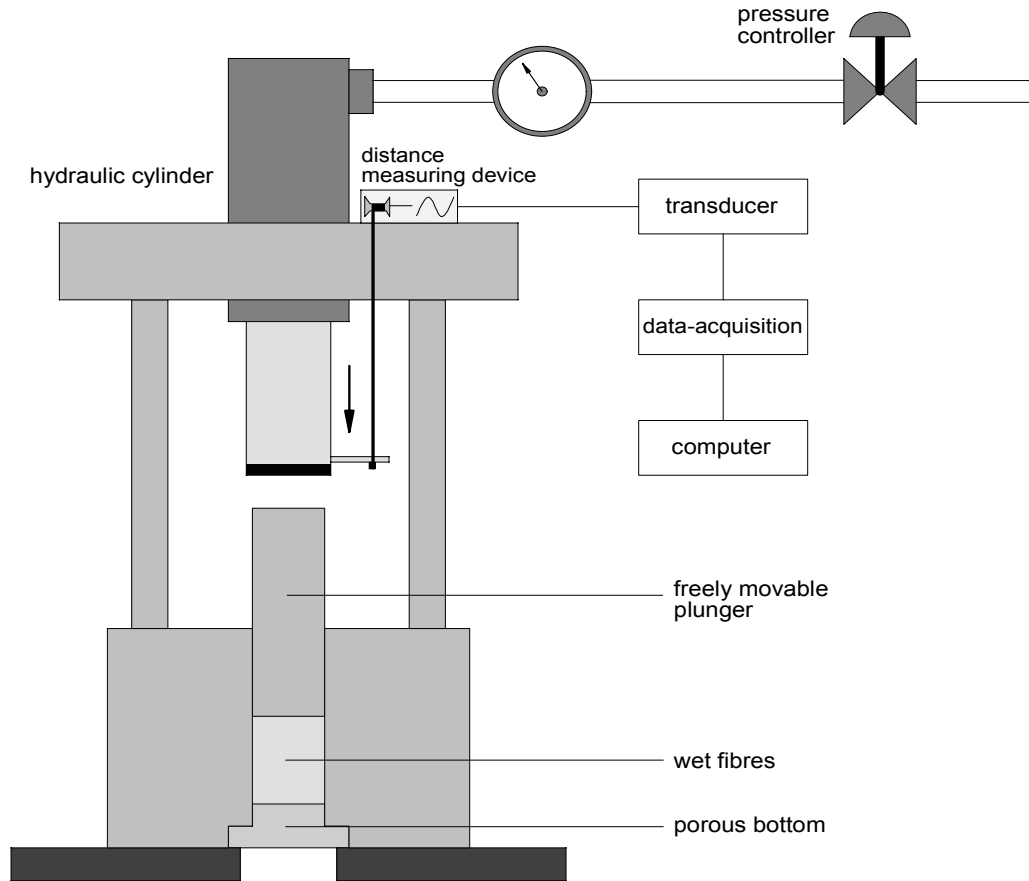
Figure 4.1. Experimental setup

The total residence time in the reversed screw element varies with throughput and screw speed during extrusion. The drainage has been studied for a period of 10 seconds, as the maximum compression time in the reversed screw element of the extruder is 10 seconds (at a very low screw speed of 6 rpm).

In processing the experimental results it was assumed that the compression speed during the experiment was completely limited by the drainage speed. The volume change versus time during the experiments has been recorded by on-line data-acquisition. After each experiment the fibre mass was removed from the boring, the fibres were weighed and the dry matter content was determined. When combining these data with the volume data taken during the experiments, the change in moisture content during the experiment, m(t), could be calculated from:

$$M_{s,e} = \frac{1}{1+m_e} M_{t,e}$$

[4.10]

$$m(t) = \frac{M_{t,e} - M_{s,e} + (V_t(t) - V_{t,e})\rho_l}{M_{s,e}}$$

[4.11]

The Kozeny-Carman model

The total model without volumetric swelling is comprised of relationships describing:
1. the flow of liquid through the porous matrix (Eq. 4.1 and 4.2);
2. the mass balance for the liquid;

$$\frac{\partial \phi}{\partial t} = \frac{1-\phi}{A}\frac{\partial q}{\partial x} \tag{4.12}$$

   (the derivation of the mass balance is provided in Appendix B)
3. the distribution of solid and liquid pressure (Eq. 4.8); and
4. the relation between overall porosity and solid pressure (Eq. 4.9).

The model with volumetric swelling is comprised of two extra relationships:
5. a relation between volumetric swelling and solid pressure; and
6. a relation between overall porosity, volumetric swelling and real porosity (Eq. 4.7).

Substituting the Kozeny-Carman equation (Eq. 4.1 and 4.2) into the mass balance (Eq. 4.12) results in:

$$-\frac{\partial}{\partial x}\left(\frac{\varepsilon^3}{k\mu S_v^2 (1-\varepsilon)^2}\frac{\partial \sigma_l}{\partial x}\right) = \frac{1}{1-\phi}\frac{\partial \phi}{\partial t} \tag{4.13}$$

Initial condition:

At t=0 there are assumed to be no porosity-gradients:

$$\phi(x,0) = \phi_0 \qquad\qquad \text{for } 0 < x < L \tag{4.14}$$

Boundary conditions:

The liquid can drain at the top and at the bottom of the cylinder:

$$\sigma_l = 0 \qquad\qquad \text{at } x = 0 \text{ and } x = L \tag{4.15}$$

The speed of the moving boundary depends on the rate of liquid expression at the top and at the bottom:

$$\frac{dL}{dt} = \frac{1}{A}\left(q(0,t) + q(L,t)\right) \qquad \text{for } t > 0 \tag{4.16}$$

Numerical solution of the model

The model consisting of a non-linear partial differential equation subjected to a moving boundary was solved by an explicit method of finite differences for which the fibre mass was divided into N layers. The necessary discrete equations where obtained by using the difference quotient approximation and by double differentiation of Stirling's interpolation formula [29]. The model solution is iterative and is programmed in Delphi. The model solution has been checked by repeating the simulations with 2N and 3N layers. The resulting drainage curves were the same. The numerical method is presented in Figure 4.2.

63
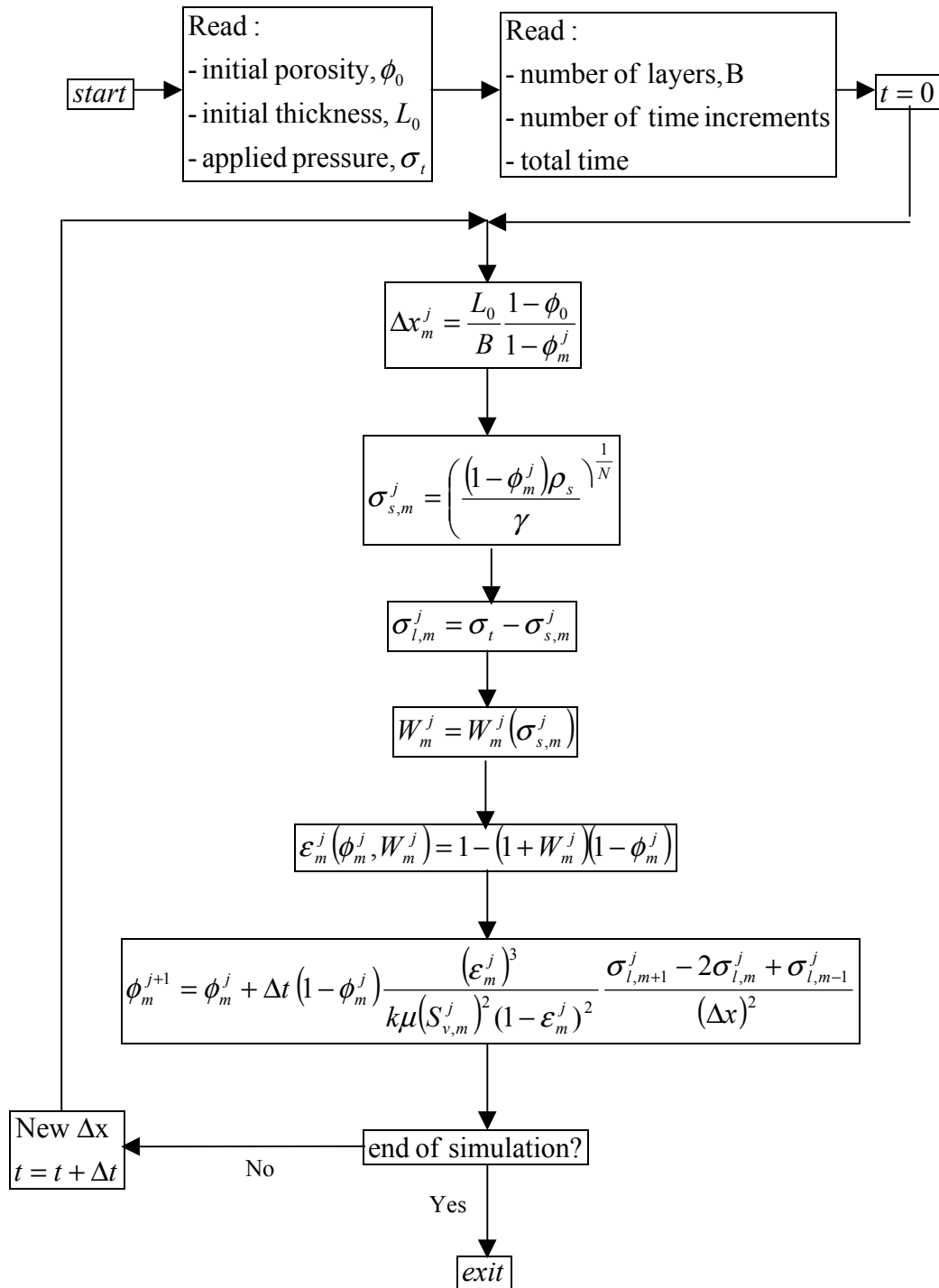
Figure 4.2. *Logic flow diagram of the numerical solution of the model*

For cylindrical fibres the specific surface area, S_v, equals 4/D. The diameter, D, of elementary hemp bast fibres varies between 16 and 50 µm, with an average of 22 µm [30]. Technical fibres, bundles of elementary fibres glued together, might show a lower value for Sv as not all elementary fibre surface area is accessible for liquid. The viscosity of the liquid, µ, is taken to be the viscosity of water at 20 °C, 10-3 Pa.s [31] as the drainage experiments are performed at 20°C. The viscosity is significantly lower at higher temperatures (0.28·10-3 at 100°C) resulting in higher drainage rates. Viscosity measurements on the drained liquids after pretreatment with different concentrations of sodium hydroxide solutions have revealed that the viscosity differences with water are negligible. The parameters for the compressibility and swelling models are taken from Westenbroek et al. [5,27].

4.3 Results and Discussion

An initial fast drainage, limited by the piston speed, takes place under negligible pressure. This is followed by a rapid increase of pressure as flow resistance limits the drainage. The pressure build-up took about 0.7 seconds during all experiments. The drainage measurement was started when the pressure build-up was fully developed. The initial moisture ratio and the moisture ratio during the experimental compression could be determined on basis of the final dry matter content and the volume versus time curve. Each experiment has been repeated at least three times. The experiments appeared to be reproducible within ± 5 %.

Typical drainage curves (moisture content versus time) for different NaOH-concentrations are shown in Figure 4.3. The drainage rate decreases with increasing NaOH-concentration and the initial moisture content significantly increases with sodium hydroxide concentration (Fig. 4.4). A higher applied pressure slightly increases the drainage rate (data not shown). The applied pressure shows no significant influence on the initial moisture content at low NaOH-concentrations, at concentrations higher than 1 M the initial moisture content slightly decreases with applied pressure (Fig. 4.4).

The drainage curves have been modelled consecutively according to
1. the decreasing permeability model of McDonald and Kerekes [24-26]
2. the Kozeny-Carman model (neglecting fibre swelling)
3. an extended Kozeny-Carman model including fibre swelling.
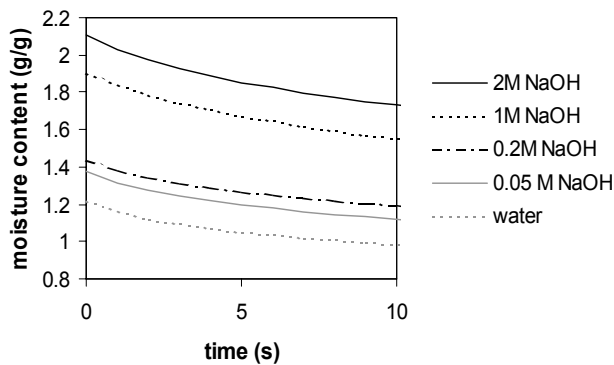
Figure 4.3. Experimental drainage curves at different NaOH-concentrations, applied pressure: 9 MPa
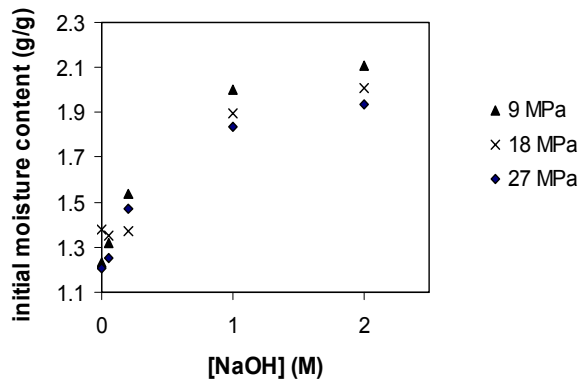
Figure 4.4. Initial moisture ratio versus NaOH-concentration
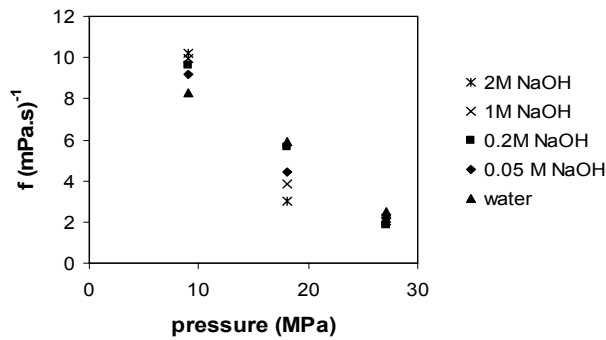
Figure 4.5. *Permeability factor versus pressure*
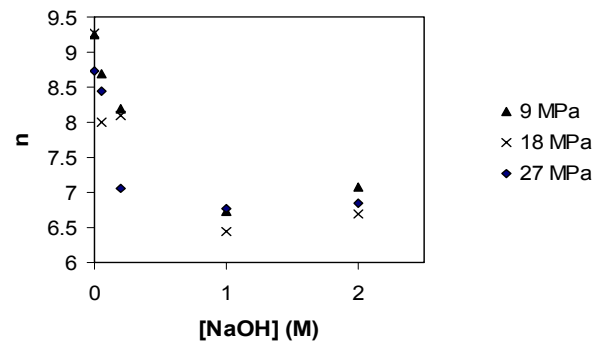
Figure 4.6. *Compressibility factor versus NaOH-concentration*

The model required should be valid for a wide pressure range. Model parameters might depend on sodium hydroxide concentration, but are preferred to be constant with pressure.

1. Decreasing permeability model

The compressibility factor, n, and the permeability factor, f, have been adjusted in order to obtain the best description with the decreasing permeability model. A higher value for n results in a curve, which is steeper in the beginning and less steep in the end. A higher value for f is similar to a higher value of P and results in a lower curve. Both parameters effect the ultimate moisture ratio that can be obtained.

The permeability factor clearly decreases with pressure, while the effect of the sodium hydroxide concentration is not significant (Fig. 4.5). The compressibility factor shows a sharp decrease with NaOH concentration, but reaches a minimum at concentrations near 1 M (Fig. 4.6). The applied pressure has no significant influence on the compressibility factor.

Decrease of the compressibility factor with NaOH-concentration means a slower decrease in permeability (by decreasing column height and porosity) with decreasing moisture content at higher NaOH-concentrations.

It is expected that a higher swelling caused by a higher sodium hydroxide concentration results in a lower permeability, as the permeability depends on the porosity of the medium. However, instead of a dependence on the hydroxide concentration the permeability factor shows a dependence on the pressure. Although the permeability factor might as well depend on the geometry of the fibre mass, like the Kozeny factor, it is not expected that the pressure dependence of the permeability factor can be attributed to the small geometry changes of the fibre mass during compression. Although the experimental curves are well simulated by the model curves, there is no unique relation valid for the whole pressure range as f strongly depends on pressure.

In the model of McDonald and Kerekes the permeability factor represents the permeability of the web in the initial uncompressed condition suggesting that f depends on the initial moisture content. While this initial moisture content strongly depends on sodium hydroxide concentration the effect of NaOH on f appears negligible. Moreover, while the pressure has no significant effect on the initial moisture content the influence on f is strong.

It can be suggested that the absence of a contribution of the solid pressure in the model causes the required permeability factor to depend on pressure. McDonald and Kerekes show a

possibility for inclusion of the compressibility of the network by an introduction of a dependence of the depth of the fibre mat, L, on the maximum pressure, pmax, on the network:

$$\frac{L}{L_0} \cong p_{max}^{h}$$

[4.17]

This ultimately results in the following equation:

$$\frac{m}{m_0} = \left(1 + \left(\frac{nf p_{max}^{h} Pt}{m_0}\right)\right)^{-\frac{1}{n}}$$

[4.18]

If p_{max} is taken to be the applied pressure the exponent h should have the value of -1.3 in order to obtain permeability factors that are approximately constant with pressure, while the similar exponent in the compressibility equation for hemp fibres is found to be -0.4. The influence of sodium hydroxide still is negligible.

The decreasing permeability model developed for wood fibres therefore appears unable to describe drainage through hemp bast fibres over wide pressure range when the compressibility of the network is not included. At high pressures and strains the decreasing permeability model should include a model describing the compressibility of the material.

2. Kozeny-Carman model

The Kozeny-Carman model is applied to the experimental results while adjusting the value of the Kozeny factor. The experimental curves are well described with the Kozeny-Carman model without swelling up to 15 seconds of drainage time (Fig. 4.7), but the required Kozeny factors (Table 4.1) are significantly higher than the theoretical factors that are between 3 and 6.

3. Kozeny-Carman model extended with a fibre swelling model
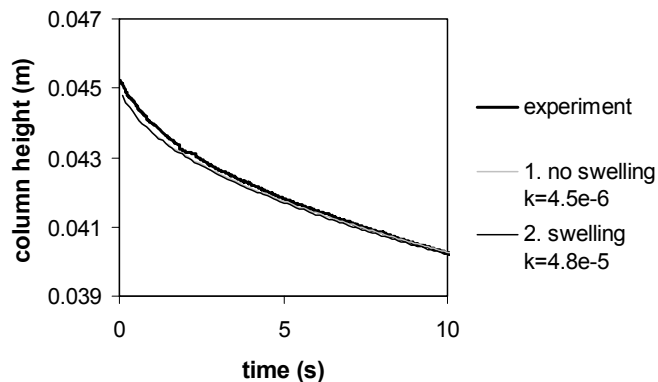
Figure 4.7. *Experimental and model swelling curves. Model with Kozeny-Carman equation. 1. excluding swelling; 2. including swelling (Westenbroek, 1999), fibres in water, σ_t=9.0 MPa*

Relations for dependence of swelling on solid pressure have been developed by Westenbroek et al. [27] for water and 0.2 M NaOH. As those relations are valid up to 6 MPa we have only applied them to the experiments performed here at the lowest pressure (9 MPa). Inclusion of this swelling model in the Kozeny-Carman model yields curves similar to the Kozeny-Carman model without swelling (Fig. 4.7). Required Kozeny factor values decrease with inclusion of this swelling model (Table 4.1), but are still far beyond the theoretical values.

Table 4.1. *Required Kozeny factors for simulation of experimental results with the Kozeny-Carman equation.*

Liquid	Applied pressure (MPa)	Required Kozeny factor	
		No swelling	Swelling according to Westenbroek et al. (1999)
Water	9.05	$2.2 \cdot 10^5$	$4.8 \cdot 10^4$
Water	18.1	$3.7 \cdot 10^5$	not measured
Water	27.2	$5.3 \cdot 10^5$	"
0.05 M NaOH	9.05	$1.8 \cdot 10^5$	"
0.05 M NaOH	18.1	$4.2 \cdot 10^5$	"
0.05 M NaOH	27.2	$6.7 \cdot 10^5$	"
0.2 M NaOH	9.05	$2.5 \cdot 10^5$	$1.6 \cdot 10^4$
0.2 M NaOH	18.1	$3.2 \cdot 10^5$	not measured
0.2 M NaOH	27.2	$8.3 \cdot 10^5$	"
1 M NaOH	9.05	$3.5 \cdot 10^5$	"
1 M NaOH	18.1	$6.2 \cdot 10^5$	"
1 M NaOH	27.2	$9.1 \cdot 10^5$	"
2 M NaOH	9.05	$3.4 \cdot 10^5$	"
2 M NaOH	18.1	$9.1 \cdot 10^5$	"
2 M NaOH	27.2	$11.1 \cdot 10^5$	"

From this it can be concluded that the volumetric swelling is higher than previously reported. The swelling parameters in the previous study were determined at zero liquid pressure, as it was assumed that the solid pressure only determined the volumetric swelling.

However, the present drainage experiments suggest that the liquid pressure also influences the volumetric swelling. Moreover, Westenbroek et al. determined swelling after hours of relaxation, causing the measured solid pressure to be much lower than before relaxation. The actual volumetric swelling before relaxation is probably higher.

The swollen fibre cell wall is probably not directly deformed during compaction of the fibre network, but a first result of compression will be bending and slippage of the fibres and at higher pressures the fibre cell wall will be compressed as well. The swelling equation needs to be adjusted in order to simulate the drainage process with a Kozeny factor of 4.5 (in accordance to the Kozeny factor found for fibres randomly oriented [21]). The swelling curve needs to have a small slope at low pressures followed by a strong decrease with swelling and at higher pressures the swelling approaches zero. Higher sodium hydroxide concentrations require a model with a higher initial swelling and a faster subsequent decrease of swelling with pressure. These phenomena are achieved when the actual swelling curve is approached with the following mathematical equation (Fig. 4.8):

$$W = \frac{\psi \dfrac{c_1}{\sigma_s}}{\dfrac{c_1}{\sigma_s} + c_2 \sigma_s}$$

[4.19]

At low pressures the slope of the swelling curve according to Eq. 4.19 is nearly horizontal (Fig. 4.8). The fibre saturation point, ψ, determines the initial swelling and depends on the sodium hydroxide concentration (Fig. 4.8). The slope of the swelling curve at each pressure is more negative when the initial swelling is higher (Fig. 4.8). At high pressures the slope becomes nearly horizontal again and the swelling degree approaches zero (Fig. 4.8).

Swelling curves described with Eq. 4.19 do not exactly model the experimental curves (Fig. 4.9), but give a good idea of the swelling behaviour of the fibres during drainage up to about 8 seconds and are valid for a wide pressure range at a given sodium hydroxide concentration. Exact modelling of the experimental curves requires more complicated mathematical equations to describe a slightly higher initial swelling and lower swelling at high pressures.

Our experiments have been performed with smooth, hardly fibrillated fibres. It is expected that the swollen fibrils of more fibrillated fibres will have a better occupation of the small pores between the fibres, which decreases porosity and permeability. Wet pressing in papermaking involves beaten and fibrillated short wood fibres. Since in that case swollen fibres and fibrils will optimally occupy the space, the liquid will mainly flow through the fibres instead of through the interstices between the fibres. Such a medium might be better modelled with a decreasing permeability model according to McDonald and Kerekes. It is therefore suggested that the theory required to model flow through fibres depends on the length and smoothness of the fibres and on the pressure and strain applied. For long smooth fibres resulting in a swollen network in which flow through fibres is negligible compared to liquid flow through the interstices, drainage is best described with the Kozeny-Carman equation. For small beaten pulp fibres the space will almost entirely be filled by swollen fibres and flow is better modelled through the swollen fibres by means of the decreasing
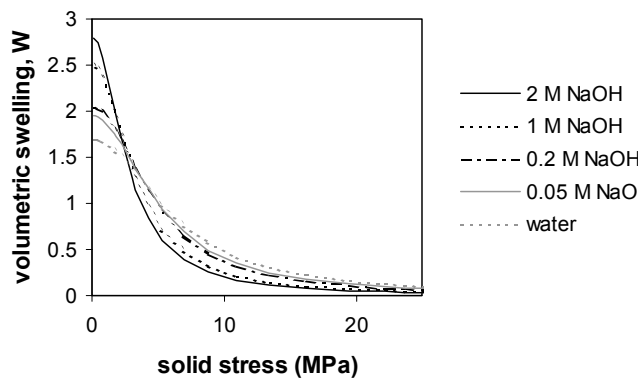
Figure 4.8. Relation between volumetric swelling and network pressure at different NaOH-concentrations
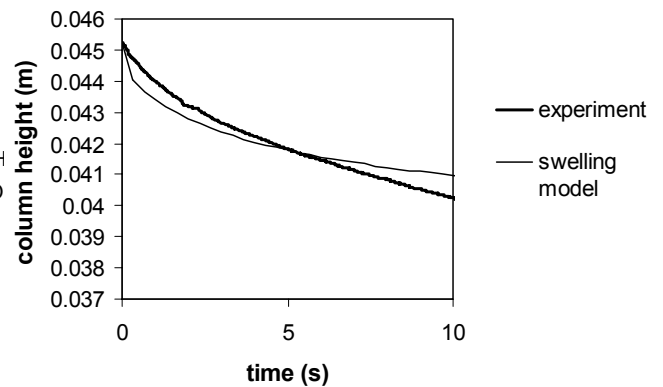
Fig. 4.9. Experimental and model swelling curves. Model with Kozeny-Carman equation, swelling according to Fig. 4.8.

permeability model developed by McDonald and Kerekes [24-26]. At high applied pressures and strains compressibility of the solid network should always be included.

The Kozeny Carman-model extended to include volumetric swelling, and described by Eq. 4.19, can now be used to determine the conditions during mechanical pulping, at which compression becomes limited by flow resistance. These conditions depend on the sodium hydroxide concentration, the initial moisture content and the geometry of the compression space. During extrusion, the screw speed at which compression becomes limited will be lower at higher sodium hydroxide concentration, higher initial moisture content or with a smaller compression 'chamber'.

4.4 Conclusions

Modelling of drainage at high pressures and strains requires inclusion of a relation for the compressibility of the solid matrix. Proper modelling of drainage through natural fibres also requires a model describing the relation between volumetric swelling and network pressure. The drainage is well described with the Kozeny-Carman model for flow through porous media, extended with a model that properly describes the dependence of volumetric swelling on pressure. The developed mathematical equation for swelling indicates that the decrease of volumetric swelling with pressure is small at low pressure, as compression of the fibre network at low pressure mainly results in fibre bending and slippage. This initial swelling increases significantly with sodium hydroxide concentration, which is described with the fibre saturation point. This results in a lower porosity and thus slower drainage. However, the subsequent decrease in swelling with network pressure starts earlier and is steeper for higher sodium hydroxide concentrations because of a more flexible cell wall, which results in a lower volumetric swelling at higher pressures.

These results can be used to predict the extrusion conditions at which the process becomes dependent on liquid expression. Important in this is the combination between throughput and screw speed. Fibres soaked in sodium hydroxide might show slower drainage because of high swelling during the first compression, but faster drainage when repeatedly compressed. While during the first compression a lot of energy is spent on drainage, during the next compression this energy might be significantly reduced. Therefore, the number of repetitions during extrusion pulping, which determine the residence time of the pulp in the extruder is of great importance.

4.5 Nomenclature

A	cross-sectional area	m^2
c_i	(positive) parameters in the relation between volumetric swelling and solid stress	-
D	fibre diameter	m
e	strain	-
f	permeability factor in decreasing permeability model	$kPa^{-1}s^{-1}$
h	exponent in compressibility equation used by McDonald and Kerekes	-
k	Kozeny factor	-
K	permeability of the porous material	m^2
L	thickness of the porous material	m
m	moisture content (liquid mass per solid mass)	-
M	mass	kg
n	compressibility factor in decreasing permeability model	-
N	exponent in compressibility equation	-
q	liquid flow rate	$m^3.s^{-1}$
S_v	specific surface of the porous material	m^{-1}
t	time	s
V	volume	m^3
W	volumetric swelling = $(V_f - V_s)/V_s$	-
x	distance from the bottom	m

γ	parameter in the compressibility equation	-
ε	true porosity	-
μ	viscosity of the fluid	Pa.s
ρ	density	$kg.m^{-3}$
σ	pressure	Pa
ϕ	overall porosity	-
ψ	fibre saturation point (atmospheric pressure)	$m^3.m^{-3}$

Subscripts

0	initial
e	at end of experiment
f	swollen fibres
l	liquid
m	layer number
max	maximum
r	reference
s	solid
t	total
v	void space

Superscript

j	time step number

4.6 References

1.   van den Akker, J.A. (1958): In "Trans. Fund. Res. Symp.", F. Bolan, ed.,. BPBMA, London, UK, p. 435-446.
2.   May, W.D. (1973): A theory of chip refining - the origin of fibre length, Pulp Pap. Mag. Can. 74: 1, 70-78.
3.   Tam Doo, P.A. and Kerekes, R.J. (1989): The effect of beating and low-amplitude flexing on pulp fibre flexibility, J. Pulp Paper Sci. 15: 1, J36-J42.
4.   Martinez, D.M. and Kerekes, R.J. (1994): Forces on fibers in low consistency refining, Tappi J. 77: 12, 119-125.
5.   Westenbroek, A.P.H., van Roekel, G.J., de Jong, E., Weickert, G. and Westerterp, K.R. (1999a): Compressibility of hemp bast fibres, to be published in Nordic Pulp Pap. Res. J.
6.   Wahlstrom, P.B. (1969): Our present understanding of the fundamentals of pressing, Pulp Paper Mag. Can. 70: 10, 76-96.
7.   El-Hosseiny, F. (1991): Mathematical modelling of wet pressing of paper; A review of literature, Nordic Pulp Paper Res. J. 6: 1, 30-34.
8.   Andersson, L. and Back, E.L. (1981): The effect of temperature up to 90°C on dewatering of wet paper webs, evaluated in a press simulator, Tappi Engineering Conference.
9.   Ghaddar, C.K. (1995): On the permeabilitty of unidirectional fibrous media: A parallel computational approach, Phys. Fluids 7: 11, 2563-2586.
10.   Jönnson, K.A.-S. and Jönnson, B.T.L. (1992): Fluid flow in compressible porous media I: Steady-state conditions, AIChE J. 38: 9, 1340-1348.
11.   Jönnson, K.A.-S. and Jönnson, B.T.L. (1992): Fluid flow in compressible porous media II: Dynamic behavior, AIChE J. 38: 9, 1349-1356.
12.   Li, Z., Ni, Y. and van Heiningen, A.R.P. (1998): Flow-through characterization of mechanical pulp pads, Annual Meeting, Technical Section, CPPA,, Montreal, Canada, p. B345-B354.
13.   Sayegh, N.N. and Gonzalez, T.O. (1995): Compressibility of fibre mats during drainage, J. Pulp Paper Sci. 21: 7, J255-J261.
14.   Skartsis, L., Kardos, J.L. and Khomani, B. (1992): Resin flow through fiber beds during composite manufacturing processes. Part I: Review of Newtonian flow through fiber beds, Pol. Eng. Sci. 32: 4, 221-230.
15.   Wilder, H.D. (1960): The compression creep properties of wet pulp mats, Tappi 43: 8, 715-720.
16.   Preziosi, L., Joseph, D.D. and Beavers, G.S. (1996): Infiltration of initially dry deformable porous media, Int. J. Multiphase Flow 22: 6, 1205-1222.
17.   Zhu, S., Pelton, R.H. and Collver, K. (1995): Mechanistic modelling of fluid permeation through compressible fiber beds, Chem. Eng. Sci. 50: 22, 3557-3572.
18.   Bird, R.B., Stewart, E.S. and Lightfoot, E.N. (1960): "Transport phenomena". John Wiley & Sons, Inc., New York.
19.   Back, E.L. (1979): Consolidation - a look into the future (including hot press nips), Paper Techn. Industry 20: 9, 304-309.
20.   Gooijer, H. (1998): Flow resistance of textile materials, PhD Thesis, Textile technology, University of Twente, Enschede.
21.   Sullivan, R.R. and Hertel, K.L. (1940): The flow of air through porous media, J. Appl. Phys. 11, 761-765.
22.   Ingmanson, W.L., Andrews, B.D. and Johnson, R.C. (1959): Internal pressure distributions in compressible mats under fluid stress, Tappi 42: 10, 840-849.

23.   van den Brekel, L.D.M. (1987): Hydrodynamics and mass transfer in domestic drum-type fabric washing machines, Delft University, Delft.

24.   Kerekes, R.J. and McDonald, J.D. (1991): A decreasing permeability model of wet pressing: theory, Tappi J. 74: 12, 150-156.

25.   McDonald, J.D. and Kerekes, R.J. (1991): A decreasing permeability model of wet pressing: applications, Tappi J. 74: 12, 142-149.

26.   McDonald, J.D. and Kerekes, R.J. (1995): A decreasing-permeability model of wet pressing with rewetting, Tappi J. 78: 11, 107-111.

27.   Westenbroek, A.P.H., de Jong, E., van Roekel, G.J., Weickert, G. and Westerterp, K.R. (1999b): Swelling of hemp bast fibres under pressure, to be published in J. Pulp Paper Sci.

28.   Caulfield, D.F., Young, T.L. and Wegner, T.H. (1982): The role of web properties in water removal by wet pressing, Tappi J. 65: 2, 65-69.

29.   Wylie, C.R. and Barrett, L.C. (1985): "Advanced engineering mathematics". McGraw-Hill Book Company, Singapore.

30.   Kocurek, M.J., Hamilton, F. and Leopold, B. (1987): "Pulp and paper manufacture, Volume 3: Secondary fibres and non-wood pulping". Joint Textbook Committee of the Paper Industry, Canada.

31.   Weast, R.C. (1988): "Handbook of Chemistry and Physics". CRC Press, Inc., Boca Raton, Florida.

Chapter 5

Flowability of hemp bast fibres at high consistency
A new concept in pulp rheology

Summary

Modelling and optimisation of the processing of high consistency fibre masses requires knowledge of the rheology of the material. This study is based on a new concept regarding the fibre mass as a solid material using the theory of granular materials.

The shear strength of dry and high consistency hemp bast fibres (50-90% d.m.) has been studied using an apparatus developed to operate at pressures up to 30 MPa. The shear strength increases with normal pressure and with dry matter content. The internal friction coefficient for dry fibres is 0.46, with a permanent structural strength of 1.3 MPa. The wall friction coefficient for dry fibres with stainless steel is 0.05 with an adhesional stress of 0.20 MPa. Wall friction for wet fibres is negligible. For wet fibres the shear strength increases linearly with dry matter content with a proportionality constant of 0.29 MPa/% for the range of dry matter contents studied.

5.1 Introduction

Wood chips or fibre bundles are processed into pulp in extrusion pulping and refining. By changing process conditions pulps of different quality can be obtained. A good description of the rheology of the fibres flowing in the apparatus is required for optimisation and modelling of these processes in order to obtain the desired pulp quality with a minimum of chemicals and energy consumption. During flow through the apparatus the fibres often have a consistency higher than 40%.

A survey of the rheology of fibres leads to fibre suspensions and composites. A suspension of cylindrical fibres having a length L and a diameter D is non-dilute, when a fibre cannot rotate freely without encountering other fibres: at concentrations higher than $1/L^3$. If spacing between fibres becomes of order D (at a concentration of $1/DL^2$), the fibre motion is so restricted that the suspension ceases to be a fluid. Below this concentration the system behaves as a viscoelastic liquid [1] and above this concentration it behaves as an elastic solid material [2]. The orientation distribution of the rods in the 'solid' elastic material is not random anymore, when the concentration approaches $1/D^2L$.

It is generally believed that, at medium and high consistencies and long fibres, the network is so strong that fibres move in plug flow. Moreover, the networks won't break uniformly in the model viscometers developed for liquids. In this case the plug of material slips along the wall and the determined stress will be the wall shear stress, which is the stress at the wall needed before the plug starts to move [3,4]. This wall shear stress is based on the friction between the fibre mass and the wall and depends both on the roughness of the wall and the kind of fibre.

Above a critical concentration the network strength exhibited by the fibre suspensions arises from frictional forces resulting from elastic fibre bending. Normal forces are imposed on the contact points between the fibres. Lord [5] divides the field of fibre friction into three categories: 1. friction between two single fibres; 2. friction between a single fibre and a fibre assembly, and 3. friction between fibre assemblies. The first and second category have been studied extensively on cotton and several synthetic fibres [5-10], less work has been carried out on the frictional forces between fibre assemblies [5,11,12]. Lord [5] notes that the pattern of fibres parallel to the shear plane strongly influences the frictional behaviour, but the exact effect of orientation is still unknown and the effect of fibres perpendicular to the shear plane has never been investigated. Moreover, it is mentioned that macroscopic forces on a fibrous system are transmitted by the fibres in a complicated way [8], but none of the authors mentions a method to calculate pressures on the fibres at different locations in a fibrous system. Moreover, at higher normal forces the required shear forces exceed the fibre tensile strength, so that shearing will lead to breaking of the fibre instead of a moving along the surrounding fibres.

At this point it appeared necessary to investigate the rheology of high consistency pulp. The ability to extend low and medium consistency pulp models to higher consistencies has been investigated. It revealed that both empirical [13-17] and fundamental models [18-21] for suspensions and composites are based on the pure liquid viscosity corrected for the presence of fibres. The high consistencies, which are encountered during extrusion and refining, are beyond the validity range of these models and use of an extension of those models still assumes liquid flow properties. Furthermore, the fundamental models are based on rigid rods, do not include fibre friction and model equations are too complicated to lead to mathematically solvable systems when applied to complicated flow regimes. Extension to flexible fibres, fibre friction and high consistencies will make the models even more complicated.

The properties of solids and liquids differ so much that the mechanisms of flow of these phases are quite unlike. First of all, solids can transfer shear stresses under static conditions, they have a static angle of friction greater than zero, whereas liquids do not [22]. This is why solids form piles whereas liquids form level surfaces. Secondly many solids, when consolidated, possess cohesive strength and retain a shape under load [22]. Thirdly, the shear stresses, which occur in a slowly deforming bulk solid, can usually be considered independent of the rate of shear and dependent on the mean pressure acting within the solid. The situation is reversed in a liquid; the shear stresses are dependent on the rate of shear and independent of the mean pressure [22].

Therefore, in order to obtain the right model to describe the flow of high consistency fibre masses, the fundamentals behind solid flow have been studied for its applicability to fibres at high consistency.

5.1.1 Solid flow

The rheology of granular materials has been evaluated on the basis of interparticle friction. Both granular material and high consistency fibre masses consist of macroscopic particles interacting with each other according to classical mechanics. Moreover, like fibres, granular materials can contain liquids.

The yield or shear strength should be considered in discussing the flow-no flow criteria of a solid [22]. An unconsolidated solid has no yield strength, but, when pressures arise under the weight of the superimposed mass, particles are brought closer together causing the material to consolidate and gain strength. The higher the pressure the greater the consolidation and the strength of the material. The shear strength of a material is the maximum shear stress on a surface in the material before the material ruptures. The wall shear strength is the stress needed at the wall before a plug of particles starts to move in the apparatus.

Being composed of natural fibres, which do not interact mechanically as do metallic atoms, a unique value of the shear strength cannot be given. Coulomb [23] provided the first comprehensive description of shear strength for soil. He stated that the limit of shear resistance is composed of two components, namely cohesion and friction. Cohesion is that part of resistance that can be measured by the direct rupture of two parts of a body in tension. Cohesion does not depend on perpendicular pressure on the rupture surface [24]. Friction, on the other hand, is a process wherein shear resistance depends upon the perpendicular pressure on the sliding surface. The shear resistance of many materials is proportional to normal pressure on a particular plane within a material. Coulomb's law can be expressed as follows:

$$\tau = c + \sigma_n \tan \phi \qquad [5.1]$$

The tangent of the angle of internal friction, $\tan \phi$, is the coefficient of friction commonly used when computing the sliding resistance of one material body over another. In this application, the coefficient is that of frictional strength on an internal surface, and is the constant of proportional increase in shear strength with increasing normal pressure on the surface. The angle of internal friction may depend on the dry matter content and on fibre properties. The term c, normally denoted as the cohesional strength of a material, describes the presence of any kind of structural strength.

At a flat boundary between the fibre mass and another material, such as steel, the shear strength is generally less than the internal strength, and different parameters must be used. The following equation is employed to describe friction between the fibre mass and the wall [24]:

$$\tau_w = c_w + \sigma_n \tan \delta \qquad [5.2]$$

We studied the shear strength parameters of hemp bast fibres in order to be able to use the solid flow model in our development of an extrusion pulping model for natural fibres. Although variation in surface smoothness and flexibility among fibre kinds will lead to varying values of the friction parameters, the mechanism behind internal strength and external friction is the same for all kind of fibres. More flexible fibres or fibres with a higher surface roughness will lead to higher shear strength values.

77

5.2 Materials and Methods

Experiments were conducted to study the shear strength parameters of hemp bast fibres. Experiments have been conducted with dry fibres (91% dry matter) and with fibres soaked in water and sodium hydroxide solutions. To avoid the influence of fibre orientation on the shear plane the hemp bast fibres (*Cannabis sativa* L., Felina 34) were chopped to 2.85 mm and subsequently milled with a hammermill equipped with a 3 mm sieve. For each experiment 80 grams of fibres (on dry basis) were used. The treated fibres were soaked for at least 4 hours in water or 0.2 M NaOH at 20 °C before each experiment.
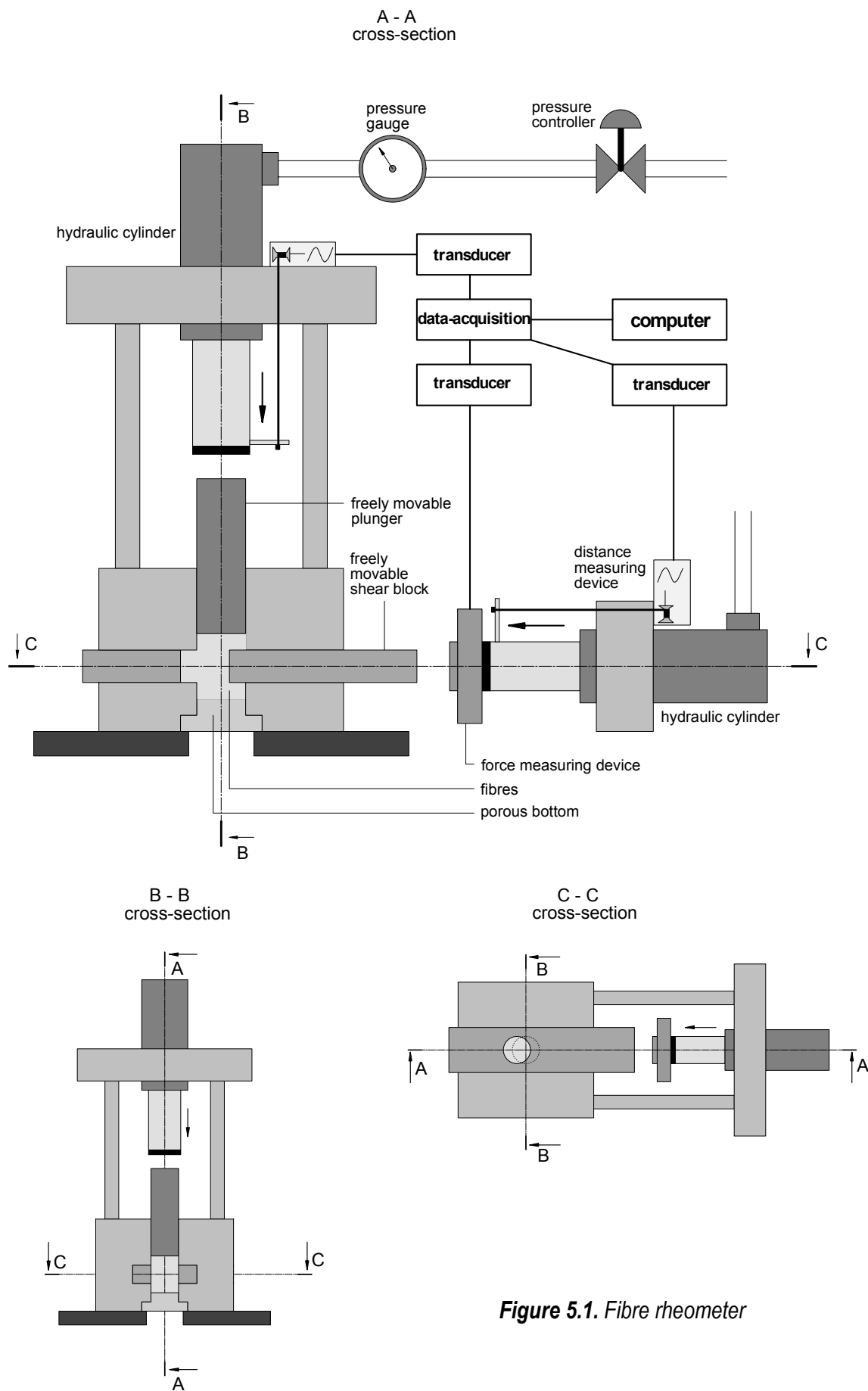
5.2.1 Apparatus

The angle of internal friction of granular materials is commonly measured using the direct shear box originally devoloped by Jenike [22]. This measuring device consists of two or three concentric round or square rings, in which samples are placed and which can be moved horizontally relative to each other while vertically loading the material upto a few bars. As the shape of fibres demands a higher consolidation pressure compared to granular materials and as pressures encountered in apparatuses processing high consistency pulps are higher (up to 30 MPa) than those applied in the Jenike shear box, a measuring device needed to be developed especially to determine the shear strength of fibre masses.

The developed 'fibre rheometer' is based on the principle of laboratory devices developed to measure the shear strength of granular materials. Schematically represented in Figure 5.1 the 'fibre rheometer' is designed to measure the shear strength of fibre networks under high normal pressures up to 30 MPa.

The apparatus consists of a stainless steel block containing a cylindrical boring of 40 mm diameter, which is fitted with a removable porous bottom. The boring can be filled with fibres and a plunger can be placed on top of the fibres in the boring. With a vertical hydraulic cylinder operating on the plunger normal pressures up to 30 MPa can be applied to the fibres. During the experiment the hydraulic cylinder maintains a constant pressure on top of the fibres. In a rectangular groove made in the bottom half of the block a shear block containing the same boring can move by means of a horizontal hydraulic cylinder, which operates up to a shear stress of 40 MPa on the shear planes. The force and speed of the press and shear cylinder are adjustable. Plunger displacement, shear block displacement and shear stress are recorded versus time by on-line data-acquisition equipment.

5.2.2 Method

The fibres were placed in the boring and the required pressure is applied. The shear strength was studied at normal pressures of 5 to 25 MPa and each experiment has been performed five times. Although pressures achieved during extrusion pulping are not clear yet, it is assumed that the pressure range applied in our experiments covers the pressure range obtained during extrusion pulping. At the moment when pressure build-up was fully developed the shear block was pressed out of the block by means of the horizontal cylinder. Simultaneously the shear block displacement and the force applied on the shear block were recorded. Data were processed to obtain curves of the shear force versus increasing shear displacement for different vertical loads. One measurement, including proper filling of the boring, pressing, shearing and removing the fibres from the apparatus takes about 20 minutes.

A - A
cross-section

B
pressure
gauge

pressure
controller

hydraulic cylinder

transducer

data-acquisition

computer

transducer

transducer

freely movable
plunger

freely
movable
shear block

distance
measuring
device

C

C

hydraulic cylinder

force measuring device

fibres

porous bottom

B

B - B
cross-section

C - C
cross-section

A

B

C

C

A

A

A

B

A

Figure 5.1. Fibre rheometer

79

In order to study the influence of the dry matter content, experiments were performed with soaked fibres. These fibres were drained for different time periods before shearing, to obtain dry matter contents in accordance with those obtained during compression of fibres in refining or extrusion. Each experiment was performed three times. Liquid pressed out flowed either via the porous bottom or via the edge of the plunger or the rectangular groove to the outside of the boring. After each experiment the fibre mass was removed from the boring, the fibres were weighed and in the case of wet fibres the dry matter content was determined.

5.3 Results and Discussion

5.3.1 Wall friction

A pressure gradient appeared to exist in the column during the experiments with dry fibres. This phenomenon is similar to what is observed in silo's containing granular solid materials, namely that the bottom load does not increase linearly with the filling height [25-27]. This pressure gradient is caused by wall friction.

Wall friction of hemp bast fibres with the stainless steel block was determined by measuring the stress gradient over the total column by adding a stress sensor at the bottom of the column. Stress gradients were determined at five different applied pressures up to 22.7 MPa. Assuming a constant density over the column (the effect of pressure on density in the range of pressures encountered in the column is negligible) a force balance results in the following equation (Appendix C):

$$\sigma_z = \frac{1}{C_1}\left(\left(C_1\sigma_0 - C_2\right)\cdot e^{-C_1 z} + C_2\right)$$ [5.3]

with $C_1 = \dfrac{4\nu\tan\delta}{Z}$ and $C_2 = \rho g - \dfrac{4c_w}{Z}$

According to the Taylor expansion at low z this equation can be approximated by the following linear equation:

$$\sigma_z = \sigma_0 - \left(C_1\sigma_0 - C_2\right)z + o(z)$$ [5.4]

o(z) denotes the error made by using this first order Taylor-expansion instead of Eq. 5.3 and is defined by:

$$o(z) \le \frac{1}{2!}\sigma''_{z_{max}}\left(z_{max}\right)^2$$ [5.5]

The Poisson-ratio, ν, is a parameter typical for solids. It is defined as the ratio of the strain in the lateral direction to the strain in the axial direction. For massive solids the Poisson ratio often has a value of about 0.4 [28]. Forces are only borne and transferred by the solid part of the porous structure, a fraction (1-ε) of the total volume. This leads to the following relation between the Poisson ratio of the total structure and the porosity:

$$\nu = 0.4(1-\varepsilon)$$ [5.6]
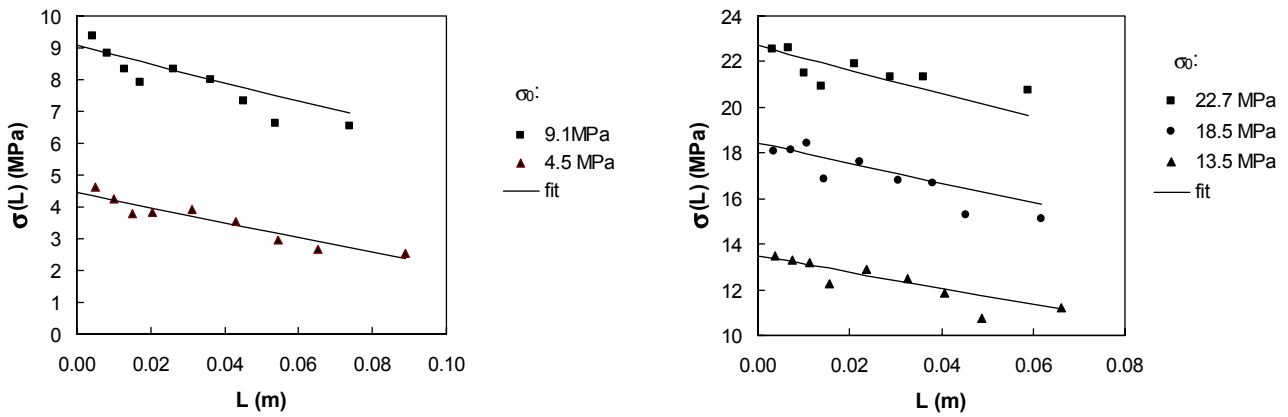
Figure 5.2. *Pressure gradient in a column with dry fibres (91% d.m.) by wall friction, at different applied pressures, fit according to Eq. 5.3. Each point is an average of ten independent measurements.*

The porosity can be calculated from the bulk density of the fibre mass, depending on the applied pressure, and the density of hemp bast fibres, which is measured to be 1.5 g/cm^3 (Helium pycnometer results). The Poisson ratio becomes 0.4 when the porosity of the fibre mass becomes zero.

The pressure at the bottom of the column was measured at nine different column heights (5 to 80 grams of fibres) for five different applied pressures, while all experiments have been performed ten times. For each pressure the average experimental results have been fit into Eq. 5.4 by adjusting the values of C_1 and C_2, while requiring the same values for tanδ and c_w at each applied pressure (Fig. 5.2). From the resulting C_1, C_2 and density values the wall friction coefficients for dry hemp bast fibres (91 % dry matter) with stainless steel could be calculated (Table 1):

tanδ = 0.05 ± 0.02

c_w = 0.20 ± 0.05 MPa

Table 5.1. *Experimental results to determine wall friction*

Applied pressure, P (MPa)	Density, ρ (kg/m^3)	Porosity, ε (-)	Poisson ratio, ν (from Eqn. 5.6) (-)	C_1 (m^{-1})	C_2 (N.m^{-3})
4.5	730	0.51	0.19	0.97	- $2.0 \cdot 10^7$
9.1	870	0.42	0.23	1.16	- $2.0 \cdot 10^7$
13.5	970	0.35	0.26	1.29	- $2.0 \cdot 10^7$
18.5	1055	0.30	0.28	1.50	- $2.0 \cdot 10^7$
22.7	1120	0.25	0.30	1.55	- $2.0 \cdot 10^7$

81

With the parameters above the error made by using the first order Taylor expansion (Eq. 5.4) instead of Eq. 5.3 can now be calculated for each pressure by means of Eq. 5.5:

$\sigma_0 = 4.5$ MPa $o(z) = 0.07$ MPa

$\sigma_0 = 9.1$ MPa $o(z) = 0.10$ MPa

$\sigma_0 = 13.5$ MPa $o(z) = 0.14$ MPa

$\sigma_0 = 18.5$ MPa $o(z) = 0.20$ MPa

$\sigma_0 = 22.7$ MPa $o(z) = 0.24$ MPa

As these error values are acceptable, we can continue using the first order Taylor expansion.

As no pressure gradients were observed in the column filled with wet fibres wall friction with wet fibres is assumed to be negligible in the examined pressure and dry matter range.

5.3.2 Shear strength

On the shear force - displacement curve for each vertical load the failure point is determined. This point is taken to be the point of maximum shear force, F_s. In order to estimate the strength parameters the failure shear force values are plotted against the normal loads. The best fit straight line through the points corresponding to individual shear tests has the slope tan ϕ and intercept c on the shear force axis.
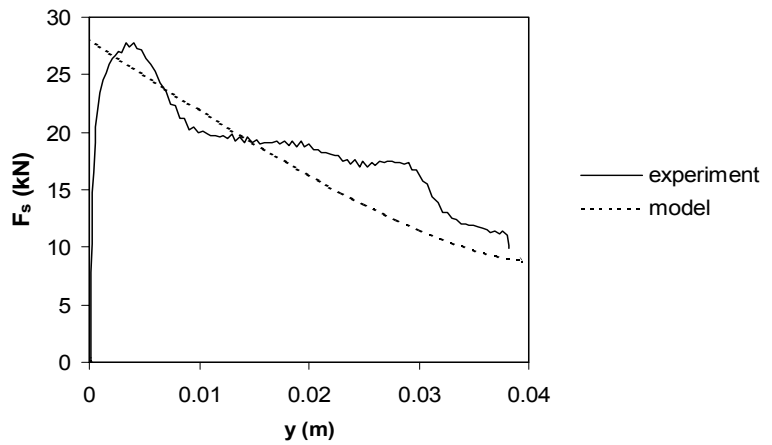

Figure 5.3. *Typical shear force-displacement curve for dry fibres (91% d.m.), 22.7 MPa*

A typical force-displacement curve (Fig. 5.3) shows that the shear force increases sharply in the beginning, reaches a maximum and than decreases with displacement. This decrease is caused by a decreasing internal shear plane surface area. The surface area of both internal shear planes, S_i, as a function of the shear block displacement, y, can be expressed by the following relation (Appendix D):

$$S_i = Z^2 \arccos\left(\frac{y}{Z}\right) - y\sqrt{Z^2 - y^2}$$ [5.7]

When part of the fibres is pressed out, the remaining fibres shear along the shear block, whereas the removed plug shears along the apparatus in the rectangular groove. As with the decreasing area of internal fibre-fibre shear planes, the surface area between the fibres and walls increases, and part of the measured friction is in fact wall friction. As both the remaining fibres and the removed plug of fibres shear along the apparatus, the surface area for wall friction increases twice as fast as the decrease in internal shear surface (Fig 5.4). The friction of the shear block with the apparatus is negligible compared to fibre-wall and fibre-fibre friction.

82
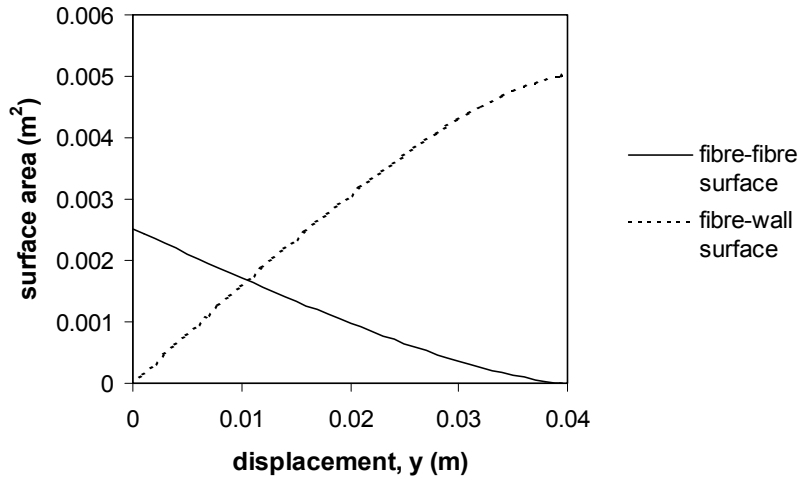
Figure 5.4. *Surface area of internal and external shear planes versus shear block displacement*

With Eq. 5.4 and the calculated wall friction parameters the pressure on the two shear planes before shearing can be calculated from the applied pressure and the column height. The force needed to move the shear block depends on the shear strength of both shear planes:

$$F_s = A(\tau_a + \tau_b) = A(2c + (\sigma_a + \sigma_b)\tan\phi) \qquad [5.8]$$

With A=1.26·10^{-3} m^2, plotting F_s against ($\sigma_a + \sigma_b$) (Fig. 5.5) yields, both the structural strength and the static friction coefficient:

c   = 1.3 ± 0.5 MPa
tanϕ = 0.46 ± 0.03
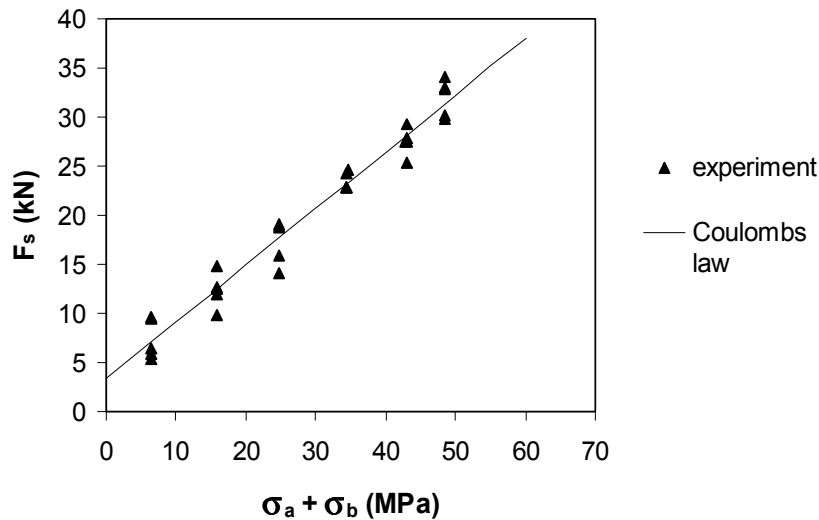
Figure 5.5. *Shear force versus normal pressure on the shear planes for dry fibres (91% d.m.), σ_a and σ_b are the normal pressures on resp. shear plane a and b.*

83

Combination of the equations and parameters for internal friction, external friction and the change of internal and external shear plane areas with displacement yields a curve for the shear force versus displacement (Fig. 5.3). As this curve reasonably covers the experimental curve, it can be concluded that the dynamic and static coefficients are in the same range.

5.3.3 Soaked fibres

Dry matter content was varied by draining for different time periods and by varying the applied pressures. Differences in shear strength between experiments therefore might be caused both by pressure and dry matter content. Fibres were soaked in water or in a 0.2M sodium hydroxide solution.

The influence of both applied pressure and sodium hydroxide appears to be negligible compared to the influence of dry matter content (Fig. 5.6). The shear strength can be described with the following relation:

$$\tau = -(13 \pm 3) + (0.29 \pm 0.05) * d.m.(\%) \quad [MPa] \quad\quad [5.9]$$

Although sodium hydroxide does not directly influence shear strength, fibres in sodium hydroxide show slower drainage resulting in a lower dry matter content for a given pressing duration. Therefore they would be expected to exhibit a lower shear strength in actual extrusion operation at similar initial dry matter contents.

A small liquid layer between the fibres lubricates the shear displacement within the studied range of dry matter contents. A lower dry matter content increases thickness of this layer and decreases shear resistance. Apparently the thickness of the liquid layer has more influence on the shear strength than the applied pressure or sodium hydroxide concentration.
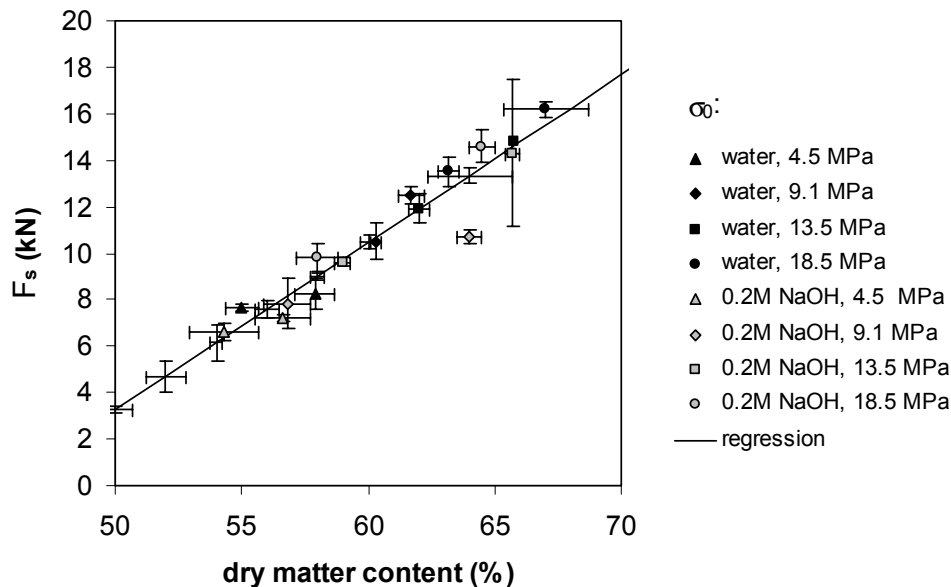
Figure 5.6. Shear strength versus dry matter content. Each point is an average of three independent measurements.

Calculation of the shear strength on an internal plane in the fibre mass is possible with the described theory if the normal stress or pressure acting on that plane is known beforehand. Stresses are, however, often known to be acting on certain surfaces of the material which are not coincident with the failure or sliding planes. In such cases it is necessary to be able to calculate stresses on surfaces of different orientations or angles to the horizontal in the material.

Mohr [28,29] showed how this can be accomplished in any solid material as long as equilibrium can be maintained at all points in the body considered. Shear and normal stresses can be calculated on different planes in the material with use of Mohr's circle of stresses. This enables the determination of places where the shear stress exceeds the shear strength and the fibre strength, provided that the shear strength parameters are known.

5.4 Conclusions

The most important phenomena in the rheological behaviour of high consistency pulp can be described with theories from solid flow. Internal friction and wall friction can be described with Coulomb's law. By means of a new measuring device especially developed for determination of the shear strength of fibres at high normal pressures it is determined that the shear strength of dry fibres increases linearly with normal pressure. For wet fibres the influence of normal pressure is negligible compared to the influence of dry matter content. The shear strength increases linearly with dry matter content in the range 50-68% d.m. Addition of sodium hydroxide has a negligible influence on the shear strength of wet fibres. The theory developed in this study is believed to be valid for all kinds of high consistency fibre masses, while the values of the friction parameters might vary. More flexible fibres or fibres with a higher surface roughness are expected to lead to higher shear strength values. However, experiments with other kind of fibres are needed to prove the validity of the developed theory for those fibres.

In modelling of the processing of high consistency pulp the described theories of granular flow can be used to determine flow criteria and the location of shear planes in the material. Processes can therefore be optimised in order to decrease energy consumption necessary for defibration, fibrillation, flexibilisation and cutting of the fibres. A better comprehension of the phenomena in pulps containing long fibres still requires further investigation of the effect of fibre length and orientation on the shear strength.

5.5 Nomenclature

A	=	cross-sectional area	m^{-2}
c	=	cohesional strength	Pa
D	=	fibre diameter	m
d.m.	=	dry matter content	%
F	=	force	N
g	=	gravitational acceleration = 9.81	$m.s^{-2}$
L	=	fibre length	m
O	=	circumference	m
R	=	surface area of triangle	m^2
S	=	surface area	m^2
$\tan\phi$	=	internal friction coefficient	-
$\tan\delta$	=	wall friction coefficient	-
W	=	surface area of wedge of circle	m^2
x	=	height of triangle	m
y	=	displacement of shear block	m
Z	=	column diameter	m
δ	=	boundary surface angle of friction	-
ε	=	porosity	-
ν	=	Poisson ratio	-
ρ	=	density	$kg.m^{-3}$
σ	=	stress	Pa
τ	=	shear strength	Pa
ϕ	=	angle of internal friction	-

Subscripts

a	=	shear plane a
b	=	shear plane b
H	=	at the bottom of the column
i	=	internal shear plane
n	=	normal
s	=	shear
w	=	wall
y	=	y-direction
z	=	z-direction
0	=	at the top of the column

5.6 References

1.   Doi, M. and Edwards, S.F. (1978): Dynamics of rod-like macromolecules in concentrated solution. Part I, J. Chem. Soc., Faraday Trans. 2 74: 3, 560-570.
2.   Doi, M. and Kuzuu, N.Y. (1980): Nonlinear elasticity of rodlike macromolecules in condensed state, Polym. Sci.: Polym. Phys. Ed. 18, 409-419.
3.   Singh, K.M. and Stenuf, T.J. (1986): Determination of wall shear stress of medium and high consistency pulps, Tappi Engineering Conference, Book 2, Atlanta, USA, p. 589-591.
4.   Longdill, G.R. and Duffy, G.D. (1988): The shear behavior of medium concentration wood pulp suspensions, Appita 41: 6, 456-461.
5.   Lord, E. (1955): Frictional forces between fringes of fibres, J. Textile Inst. 46, P41-P58.
6.   El Mogahzy, Y.E. and Gupta, B.S. (1993): Friction in fibrous materials. Part II: Experimental study of the effects of structural and morphological factors, Textile Res. J. 63: 4, 219-230.
7.   de Jong, H.G. (1993): Yarn-to-yarn friction in relation to some properties of fiber materials, Textile Res. J. 63: 1, 14-18.
8.   Andersson, S.R. and Rasmuson, A. (1997): Dry and wet friction of single pulp and synthetic fibres, J. Pulp Paper Sci. 23: 1, J5-J11.
9.   Postle, L.J. and Ingham, J. (1952): The relation between external pressure and inter-fibre forces in untwisted slivers, J. Text. Inst. 43, T87-T90.
10.   Cox, D.R. (1952): The relation between external pressure and inter-fibre forces in untwisted slivers, J. Text. Inst. 43, T87-T90.
11.   Martindale, J.G. (1947): An instrument for the measurement of the forces operating between fibres during drafting, J. Text. Inst. 38, T151-T166.
12.   Morrow, J.A. (1931): The frictional properties of cotton materials, J. Text. Inst. 22, T425-T440.
13.   Burgers, J.M. (1938): In "Second report on viscosity and plasticity". Nordemann, New York, p. 113-184.
14.   Blakeney, W.R. (1966): The viscosity of suspensions of straight rigid rods, J. Colloid Interface Sci. 22, 324-330.
15.   Rosinger, E.L.J., Woodhams, T. and Chaffrey, C.E. (1974): Shear flow behavior of complex asbestos fibril dispersions, Trans Soc. Rheol. 18: 3, 453-466.
16.   Maschmeyer, R.O. and Hill, C.T. (1977): Rheology of concentrated suspensions of fibers in tube flow II; An exploratory study, Trans. Soc. Rheol. 21: 2, 183-194.
17.   Utracki, L.A. and Fisa, B. (1982): Rheology of fiber- or flake-filled plastics, Polymer Composites 3: 4, 193-211.
18.   Batchelor, G.K. (1970): The stress system in a suspension of force-free particles, J. Fluid Mech. 41: 3, 545-570.
19.   Batchelor, G.K. (1971): The stress generated in a non-dilute suspension of elongated particles by pure straining motion, J. Fluid Mech. 46: 4, 813-829.
20.   Dinh, S.M. and Amstrong, R.C. (1984): A rheological equation of state for semiconcentrated fiber suspensions, J. Rheology 28: 3, 207-227.
21.   Cintra, J.S., Jr. and Tucker III, C.L. (1995): Orthotropic closure approximations for flow-induced fiber orientation, J. Rheol. 39: 6, 1095-1122.
22.   Jenike, A.W. (1967): "Storage and flow of solids". University of Utah, Utah.

23. Coulomb, C.A. (1776): Essai sur une application des règles des maximis et minimis à quelques problèmes de statique relatifs à l'architecture., Academie royale des Sciences: Mémoires de Mathématique et de Physique, presentés à l'Academie royale des Sciences, par divers savants, et lus dans les Assemblées 7, 343-382.

24. McKyes, E. (1989): "Agricultural engineering soil mechanics". Elsevier, Amsterdam.

25. Janssen, H.A. (1895): Versuche über Getreidedruck in Silozellen (Tests of grain pressure in elevator cells), Zeitschrift des Vereins deutscher Ingenieure 39, 1045-1049.

26. Broersma, G. (1972): "Behaviour of granular materials". Stam Technical Publications, Culemborg.

27. Haaker, G. (1994): Powder flow properties, Lecture notes, Stockholm, Sweden, Skandinavisk Teknikförmedling International AB.

28. Gere, J.M. and Timoshenko, S.P. (1984): "Mechanics of materials". PWS-Kent Publishing Company, Boston.

29. Mohr, O. (1914): Welche Umstände bedingen die Elastizitätsgrenze und den Bruch eines Materiales, Z. Ver. Dtsch. Ing. 44, 1524-1530.

Chapter 6

Extrusion pulping
Relation between process conditions and pulp quality

Summary

Extrusion pulping is used in producing natural fibre products for bulk applications or reinforcement in paper and board applications. Different product properties can be achieved by changing process conditions and screw configurations. The effect of screw speed, throughput, temperature and pre-treatment on the energy consumption and quality of the product has been studied. Extrusion pulp products have been analysed for several strength and optical properties in order to obtain qualitative predictions.

Defibration, shortening and fibrillation of the fibres cannot always be achieved independently. For special product requirements post-processing by beating, refining or a second extrusion step might be necessary. An important parameter in relating pulp properties to extruder conditions appeared to be the filling degree, which has been defined as the ratio between throughput and screw speed. When the filling degree is decreased (by either decreasing the throughput or increasing the screw speed), fibres remain in the extruder during a higher number of screw revolutions and therefore obtain a higher number of impacts. This causes a higher energy consumption, breaking length and beating degree and a reduced tear index. The specific energy consumption also appeared to increase with decreasing throughput (at constant filling degree). This mainly results in lower tear strength. Pre-treatment with sodium hydroxide instead of water does not influence the specific energy consumption but appears to increase breaking length, burst index and tear strength, because of improved bonding and higher fibre length. Decreasing the process temperature does not affect the specific energy consumption, but increases breaking length and beating degree of the product.

6.1 Introduction

Extrusion pulping is a mechanical or chemimechanical pulping method in which fibres are processed by means of compression and shear forces. The basic principles of this pulping method have been developed over the last 25 years, with successful results in pilot and industrial applications to annual plants including cotton, hemp and flax [1-7]. The original BiVis (French for twin screw) process [8-11] was designed with two pulping extruders in series, the first for impregnation and partial cutting, the second for bleaching and additional cutting. The extrusion process for hemp bast fibres evaluated in this study was derived from the BiVis process, but uses only one extruder without bleaching. Further, the fibrous material is subjected to cold water or alkaline impregnation before entering the process. The

experimental screw elements have been specially developed for the processing of the fibres. This extrusion pulping process, for which a patent is pending, can be used for producing several paper qualities from wood and non-wood fibres [12-14]. Our attention was mainly focused on bast fibres, because of the excellent ability of extrusion pulping to process very long cellulosic fibres and fibre bundles (of up to 1.5 m) to a pulp with a controlled fibre length and narrow fibre length distribution.

The main screw element used in extrusion pulping processes is the reversed screw element (RSE). This is an element with threads, whose pitch is opposite to those screws which transport the material towards the outlet of the extruder. This results in accumulation and compression of the fibres in the space between the transport screws and the RSE's. The high compression and shear forces cause defibration, fibrillation and shortening of the fibres. Machined slots are regularly distributed in the threads of the RSE, through which the fibres can eventually pass forward.

For papermaking purposes chemical pulping was traditionally used for bast fibres like hemp, flax, seedflax, jute, kenaf, ramie and others. Such processing yields a very high quality pulp with exceptional properties. Because of the high cost of such pulps, applications have been limited to specialities including teabag and filter papers, cigarette and similar papers, technical papers and specialty printing and writing papers. In a comparison between chemical and extruder mechanical pulping of bast fibres, van Roekel [13] concluded that extruder mechanical pulping provides a much higher yield (typically 80%) and a much lower use of chemicals. Moreover, extrusion pulping also allows cutting to a desired fibre length, so the pulps can be handled by bulk papermaking systems without additional beating. Extruder mechanical pulps, however, possess lower strengths than chemical pulps, and some lignin (< 4%) is still maintained in the fibre. In comparison to alkaline peroxide bleached mechanical softwood pulp and a softwood kraft pulp, extruded fibres appeared to show a higher tear strength, a lower tensile strength and a lower dewatering rate [13]. However, van Roekel performed his extrusion experiments at constant process conditions. Change of process conditions may significantly influence the product properties and energy consumption. Moreover, while bast fibres are suitable as raw material for printing and writing grade paper they are also suitable as reinforcing material in recycled board. Further, they are suitable for use in composites and construction materials to replace wood and glass because of their high tensile strength. Different fibre properties required for the different paper or reinforcement applications can be achieved by changing the process conditions and screw configurations.

Effect of morphology and chemical composition on paper properties

Wood fibres and bast fibres have different papermaking abilities, because of differences in both morphology and chemical composition. Average values for morphological properties and chemical composition have been summarised for spruce, aspen, flax bast and hemp bast fibres (Table 6.1).

Strength properties

In general, paper strength properties increase with fibre length, l, [15-23]. For wood fibres it is generally believed that this effect is more pronounced in the tear strength than in the tensile and burst strengths [15,16,18,19,21-23]: for wood fibres the tensile strength was found to be proportional to the square root of the fibre length, $l^{0.5}$, burst strength to l and tear strength to $l^{1.5}$ [19]. In general it is found that the effect of beating on softwood fibres is at

Table 6.1. Morphology and chemical composition of selected wood and non-wood fibres [18-20,24-33]

	Length (mm)	Diameter (μm)	Aspect ratio	Wall fraction (%)	Cellulose (%)	Hemi-cellulose (%)	Pectin (%)	Lignin (%)
Spruce	3.5	36	100	33	43	29		27
Aspen	1.0	21	50	40	53	31		16
Hemp bast	20	20	1000	50-80	60-70	10-15	1-3	4
Flax bast	28	21	1350	> 90	70-80	12-18	1-3	3

first a small increase followed by a decrease in tear strength as a result of a decrease in fibre length [16]. Beating of shorter hardwood fibres generally results in an increased tear strength as a result of increased bonding [16]. As bast fibres are much longer than wood fibres, the tear strength in particular will be higher, and processing will lead to a lower tear strength because of a decrease in average fibre length.

Paper strength also depends on the chemical composition, strength of the individual fibres, degree of bonding and the bond strength. Paper strength improves with increased fibre strength, which is often measured as the zero span tensile strength of the paper. For wood fibres, paper strength was also found to increase with decreasing coarseness of the fibres (determined by fibre width and wall thickness), since low coarseness implies more fibres per unit weight, a larger total specific surface and usually better collapsibility [18,23]. Coarseness of wood fibres was found to influence tensile strength with an exponent of -0.6, burst strength with a factor of -1.0 and tear strength with a factor of -0.3 [34]. However, Seth and Page [22] conclude that among fibres of similar length and strength, coarser fibres make sheets of higher tear resistance, as sheets of lower density are obtained. However, Stationwala et al. [35] note that higher coarseness and lower flexibility do not necessarily imply a lower sheet density. Although it seems clear that coarser fibres yield lower tensile and burst strengths, the effect of coarseness on tear strength is not clear.

Hemp bast fibres are distinguished from wood fibres by a thicker cell wall and a very small lumen [33,36] and thus a higher coarseness. The hemp bast fibre is rigid and not collapsible [33,36]. The high coarseness of the hemp bast fibres in comparison with most wood fibres negatively affects most of its strength properties. In mechanical pulping of wood or non-wood fibres the coarseness of the produced fibres also depends on the degree of defibration achieved during the process.

Mechanical treatment increases the surface area capable of hydrogen bonding, provided that it is carried out in a manner which facilitates swelling of the fibres [19]. Beating in water at alkaline conditions therefore generally favours rapid strength developments, in comparison with neutral or acidic media [19]. Mechanical pulping also results in fragmentation and fibrillation of fibres. For wood fibres, mechanical pulping appears to differ from beating, because of the presence of large amounts of lignin, which restricts fibre swelling [19]. As the amount of lignin in bast fibres is significantly less (3-5%), mechanical pulping of bast fibres might approach the process of beating more. This is facilitated by alkaline pre-treatment of the fibres [37].

Fines in pulp consist of fibrils, very short fibres, cell wall fragments, and middle lamellae [18]. These components are important for bonding and light scattering. In general, fines increase bonding and strength properties as they increase the specific surface area. Tear strength, however, might be reduced at higher fines content, as a consequence of a lower average fibre length. Different mechanical treatments produce different kinds of fines. Fines produced during refining appear to be less coarse and have a much larger specific surface area than fines produced during grinding [35]. The fines produced during refining therefore have a greater positive effect on strength properties than those from grinding [35].

For wood fibres it is clear that hemicellulose content plays an important role in paper bonding [18,19], as it promotes swelling and facilitates fibrillation and increases bond strength [19]. Hemicellulose therefore affects those strength properties that mainly depend on bond strength, such as tensile and bursting strength [18]. Although the hemicelluloses of bast fibres differ from the hemicelluloses present in wood fibres [25,38], it is expected that the lower hemicellulose content of bast fibres compared to wood fibres will result in a lower bond strength and less fibrillation. Decreases in the degree of polymerisation of hemicellulose results in reduced interfibre bond strength. Bast fibres at same lignin content as wood fibres have a much higher degree of polymerisation [38]. Decreases in the degree of polymerisation of cellulose reduce fibre strength, and therefore all strength properties, tear strength in particular [19].

Lignin has been shown to restrict swelling and decrease the adhesion forces between fibres because of its hydrophobic nature and its dominant location at the fibre surfaces [19]. In removing lignin, swelling of the fibre during beating occurs more rapidly, the fibres become more flexible, surface enlargement can occur, and interfibre bonds of good strength can be formed [19]. Fibres with a higher lignin content will result in a paper with a higher thickness and therefore a higher stiffness. Because of the low lignin content the composition of bast fibres resembles the composition of chemical wood fibres. However, the higher coarseness of the hemp bast fibres prevents the fibres from becoming as flexible as wood fibres, except maybe after severe beating.

Surface properties

Coarse long fibres adversely affect surface smoothness and increase porosity [18]. Fibrillation and fines decrease porosity and contribute to the creation of a smooth surface suitable for printing [18,39]. As hemicellulose enhances fibrillation and flexibilisation of the fibres, it increases surface smoothness and decreases porosity. Lignin increases fibre stiffness resulting in decreased paper smoothness and increased porosity of the paper. As smoothness and porosity are not affected by fibre strength the polymerisation degree of cellulose has no influence.

Optical properties

The brightness of a paper increases with scattering and decreases with absorption; the material appears darker at higher light absorption [40]. Absorption is directly related to molecular groups that give colour. Removal of lignin during the pulping process results in a decrease in absorption. The scattering coefficient, s, is a measure of the specific surface area in the paper that reflects light. In general scattering increases with decreasing particle size and increases with the fibre specific surface [40,41]. Light can reflect from the internal surfaces of uncollapsed lumens or from unbonded external fibre surfaces, since a bonded interface

between fibres is not a discontinuity [41]. Fibre possibilities can be combined in the following equation [18]:

$$s \propto \frac{2 - \text{collapse} - \text{RBA}}{\text{fibre thickness}} \qquad\qquad [6.1]$$

where collapse is the fraction of lumen surface closed by internal bonding and RBA is the relative bonded area. RBA is the fraction of external fibre surface made transparent by interfibre bonding. As hemp bast fibres are hardly collapsible [36] the effect of internal bonding by lumen collapse will be negligible. For chemical pulps the scattering coefficient decreases with beating, as bonding is increased, and thus with increasing tensile strength. For mechanical pulps the scattering coefficient increases with increasing tensile strength, as new surfaces are formed [18,40]. The thickness of a mechanical pulp fibre depends on the degree of defibration and is a function of energy input and pulping conditions. Fines increase light scattering [18,35,40]. Although fines produced in different mechanical processes influence strength and dewatering in different ways, Stationwala and co-workers [35] show that the scattering coefficient of a sheet depends only on the amount of fines, independent of their morphology. This, however, seems contradictory to Eq. 6.1, which suggests a higher scattering for fines with a higher specific surface area and lower coarseness. Apparently fines with a high specific surface and low coarseness, as produced by the peeling-off mechanisms during refining contribute more to the relative bonded area than coarse fines, as produced by groundwood pulping, which can also be noticed from the higher tensile strengths of refiner pulps. Although the chemical composition of hemp bast fibres resembles that of chemically pulped wood fibres, the scattering behaviour of hemp bast fibres will resemble that of mechanical pulp fibres, since the high coarseness prevents the formation of a dense web and promotes light scattering. Opacity of the paper increases when scattering is increased [18,40]. While the presence of lignin decreases the strength and increases stiffness of the paper, it increases opacity and light scattering [18].

The influence of extrusion conditions and pre-treatment on specific fibre product properties has been studied for hemp bast fibres and is discussed in this paper. With use of this information we should be able to optimise the process to obtain required fibre qualities at a minimum of energy and chemical consumption.

6.2 Materials and methods

Experiments were conducted to study the influence of process conditions and screw configurations on the product properties and energy consumption of hemp bast fibre extrusion. The hemp bast fibres (*Cannabis sativa* L.) were chopped to an average length of 33 mm to allow manual feeding to the extruder. The fibres were impregnated with water or 0.2 M NaOH in a 1:11 dry fibre:liquid ratio at room temperature for 16 hours. After impregnation the liquid was allowed to drain through a perforated screen. After draining, the impregnated fibres were preheated with saturated steam at atmospheric pressure for 30 minutes.

fibres

effluent   **water**

pulp

RSE

steam
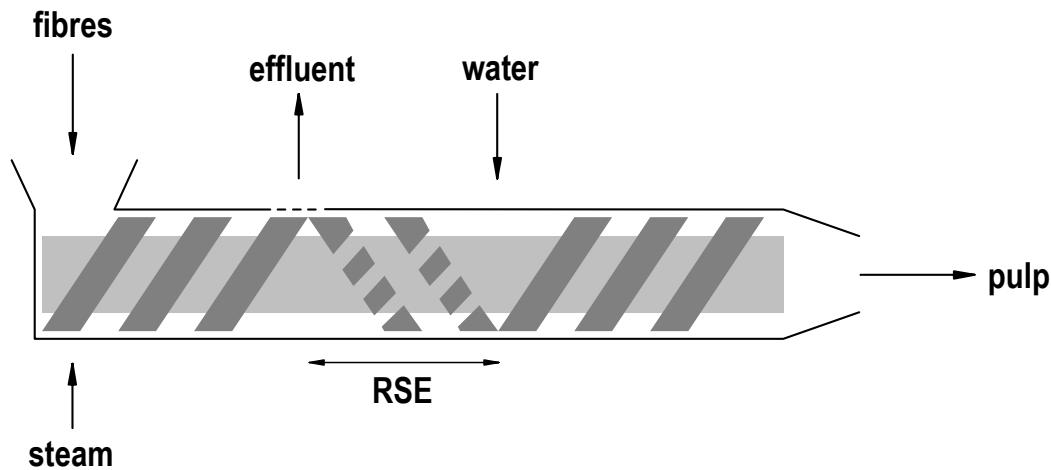
Fig. 6.1. *Side view diagram of the extruder*

6.2.1 Equipment

A Clextral BC45 corotating twin-screw extruder with a screw diameter of 55 mm and a total axis length of 1.25 m (Fig. 6.1) was used in these experiments. The extruder consists of a system of two corotating intermeshing screws with trapezoidal threads in a binocular-shaped barrel. The initial transport screws move the fibrous material from the feed inlet into the barrel. The subsequent RSE's form a relatively short screw section with a reversed pitch, imparting compression and high shear to the fibres. Fibres can eventually pass forward through the slots machined in the RSE threads, and are carried towards the outlet by means of transport screws. Excess water squeezed out by the pressure generated in the RSE is allowed to drain from the machine through a 0.11 mm slit filter located in the top of the barrel. The combination of transport screw, RSE and filter constitutes one defibration zone. Our experiments were been performed with only one defibration zone, in order to relate fibre changes directly to the process conditions and screw configurations of one defibration zone. The extruder can be set up to hold a maximum of four separate defibration zones, enabling a higher extent of shortening, defibration and fibrillation during one run.

6.2.2 Method

Screw configuration and speed were set on the extruder before each experiment. The extruder was preheated to and kept at the desired temperature by means of heating elements on the extruder, using magnetic induction and a temperature control system. For the experiments performed at 100°C additional heating of the pulp was provided with steam injection directly behind the feed inlet. The fibres were fed in regular portions to obtain a constant feed rate and allow a stable process. Water was added to the extruder directly behind the RSE to avoid dense knots in the product. The system was allowed to stabilise for a few minutes until the motor load, evaluated by on-line data-acquisition, remained constant, indicating a constant flow of pulp to the RSE.

The pulp temperature was recorded by data-acquisition. The average pulp throughput was determined by weighing the product that had exited the extruder in a set amount of time. The mass of the product was corrected for dry mass by measuring the dry matter content by drying the pulp at 105 °C for 16 hours. Specific energy consumption was calculated from the dry matter throughput and the motor load, adjusted for the motor load with transport screws only. The experimental set-up is given in Table 6.2.

Table 6.2. Experimental conditions

Study of the effect of throughput and screw speed (45 experiments):	
Temperature, T	100 °C
Pitch	35 mm
Throughput (on dry matter basis), Q	0.25 - 36 kg/hr
Screw speed, W	6 – 336 rev./min. (rpm)
Impregnation	0.2 M NaOH
Study of the effect of temperature (+ 5 experiments):	
Temperature	**30 °C**
Pitch	35 mm
Impregnation	0.2 M NaOH
Study of the effect of impregnation (+ 14 experiments):	
Temperature	100 °C
Pitch	35 mm
Impregnation	**Water**
Study of the effect of pitch of transport screw before RSE (+ 6 experiments):	
Temperature	100 °C
Pitch of transport screw before RSE	**15, 25 and 50 mm**
Impregnation	0.2 M NaOH

Laboratory evaluation

Pulps were disintegrated in a Messmer laboratory disintegrator according to ISO 5263-1979 standard. The beating degree was determined according to the Schopper-Riegler method ISO 5267/1-1979. Laboratory sheets for evaluation were formed according to ISO 5269/1-1979. The sheets were tested for several strength and optical properties according to standards at 23 °C, 50% RH:

- Breaking length - km (ISO 1924/1-1983)
- Tear index - mNm^2/g (ISO 1974-1974)
- Burst index - kPam^2/g (ISO 2758-1983)
- Thickness - μm (ISO 534-1988)
- Zero span tensile strength - N (specified test procedure zero-span measurements)
- Scattering coefficient - m^2/kg (Tappi T425 om-91)

Data from the experiments were analysed to obtain relations between the extrusion operating conditions variables and the measured pulp properties. The experimental data were analysed using multiple linear regression by means of Genstat 5 Release 3.2 [42]. The assumptions underlying the analysis (constant variance and normal distributed residual error) were examined and appeared to be justified for all responses except the beating degree [43]. For the beating degree a log-transformation was applied to the data before analysis.

In addition experiments were performed to determine the residence time distribution of the fibres in the extruder at different process conditions. The residence time of fibres in the defibration zone was measured by tracking the time needed to process a chopped-up standard

red A4 sheet of paper with the raw material. The samples taken during extrusion were analysed both visually and by measuring the redness of the papers produced from the samples. The redness was measured by comparing the difference in reflectance values at 540 nm with a standard red A4 sheet of paper and a blank sample.

6.3 Results

### 6.3.1 Relations between process conditions and product properties

In this section the results are analysed for relationships between the product properties and the process conditions during extrusion. During the experiments for the determination of the effect of screw speed, W, and throughput, Q, only those two independent input parameters have been varied. The filling degree, D, is defined as the ratio between throughput and screw speed, and denotes the mass of fibres that is compressed during each revolution. Since the filling degree compared to the screw speed appeared to be a more effective parameter to describe the mechanism of the extrusion process, the filling degree is taken instead of screw speed as a parameter for the regression analysis. The maximum filling degree that can be achieved depends on the screw speed and the maximum power of the extruder used.

Table 6.3. *Results of the multiple linear regression analysis*

Parameter	Model
Specific energy cons.	$$P = 1049 - 36\,Q - 244\,D + 10.6\,QD \qquad \text{[kWh/ton]}$$ $st.error \quad 97 \qquad 9.6 \qquad 52 \qquad 3.5$ $$R^2 = 53\%$$
Dry matter content	$$\phi = 19.0 + 20.7\,D + 0.0211\,P \qquad \text{[\%]}$$ $st.error \quad 7.3 \qquad 4.6 \qquad 0.0055$ $$R^2 = 58\%$$
Beating degree	$$\ln \beta = 2.32 + 0.201\,D + 4.02 \cdot 10^{-3}\,P - 1.68 \cdot 10^{-6}\,P^2 - 1.36 \cdot 10^{-3}\,DP \qquad \text{[°SR]}$$ $st.error \quad 0.17 \qquad 0.049 \qquad 0.43 \cdot 10^{-3} \qquad 0.21 \cdot 10^{-6} \qquad 0.16 \cdot 10^{-3}$ $$R^2 = 87\%$$
Paper thickness	$$H = 176.0 + 1.48 \cdot 10^4\,\frac{1}{P} \qquad [\mu m]$$ $st.error \quad 5.9 \qquad 0.16 \cdot 10^4$ $$R^2 = 68\%$$
Breaking length	$$\tau = 2.882 + 0.07\,D + 3.56 \cdot 10^{-3}\,P - 1.86 \cdot 10^{-6}\,P^2 - 1.55 \cdot 10^{-3}\,DP \qquad \text{[km]}$$ $st.\,error \quad 0.074 \qquad 0.11 \qquad 0.99 \cdot 10^{-3} \qquad 0.48 \cdot 10^{-6} \qquad 0.37 \cdot 10^{-3}$ $$R^2 = 75\,\%$$
Burst index	$$\zeta = 2.13 + 0.411\,D + 4.11 \cdot 10^{-3}\,P - 1.80 \cdot 10^{-6}\,P^2 - 2.63 \cdot 10^{-3}\,DP \qquad \text{[kPa m}^2\text{/g]}$$ $st.error \quad 0.28 \qquad 0.094 \qquad 0.74 \cdot 10^{-3} \qquad 0.35 \cdot 10^{-6} \qquad 0.30 \cdot 10^{-3}$ $$R^2 = 78\%$$
Tear index	$$\sigma = 37.4 - 0.0382\,P + 0.97\,Q - 0.0203\,Q^2 + 1.64 \cdot 10^{-5}\,P^2 \qquad \text{[mN m}^2\text{/g]}$$ $st.error \quad 3.3 \qquad 0.0077 \qquad 0.27 \qquad 0.0078 \qquad 0.43 \cdot 10^{-5}$ $$R^2 = 80\,\%$$
Scattering coefficient	$$s = 15.9 - 1.21\,D + 0.0188\,P - 8.6 \cdot 10^{-6}\,P^2 + 7.1 \cdot 10^{-3}\,DP \qquad \text{[m}^2\text{/kg]}$$ $st.error \quad 1.5 \qquad 0.46 \qquad 0.0040 \qquad 1.9 \cdot 10^{-6} \qquad 1.5 \cdot 10^{-3}$ $$R^2 = 84\%$$

For the Clextral BC45 this implies that the product of specific power consumption, P (kWh/ton) and filling degree, D (g/r) is smaller than 1600.

The results of the regression analysis are presented in Table 6.3. All relations presented are significant at the 95% level. The equations are used to illustrate the relations between process conditions and product properties.
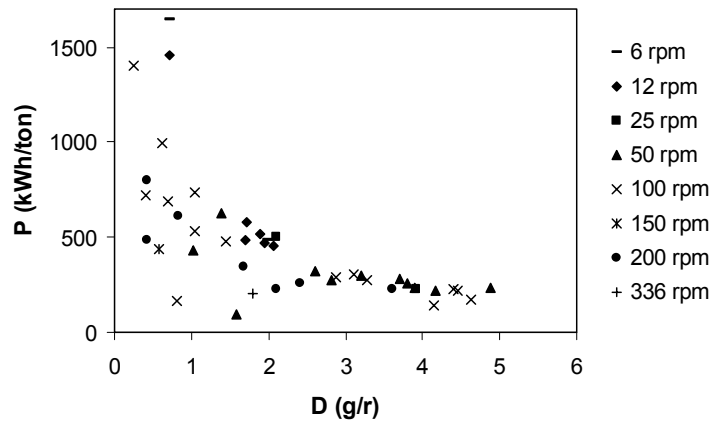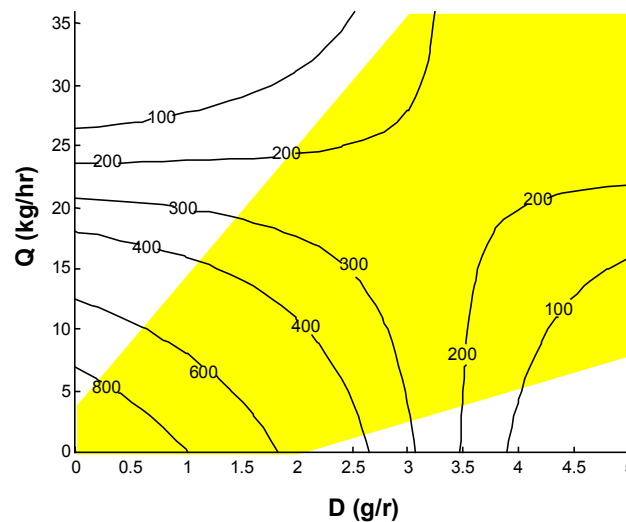

Fig. 6.2. *Specific energy consumption versus filling degree during extrusion at different screwspeeds*

In general the *specific energy consumption*, P, seems to decrease with filling degree, but a slight dependence on screw speed also appeared (Fig. 6.2). Multiple linear regression revealed that the specific energy consumption can be best described by the combination of throughput and filling degree:

$$\underset{st.error}{P} = 1049 \underset{97}{} - 36 \underset{9.6}{Q} - 244 \underset{52}{D} + 10.6 \underset{3.5}{QD} \qquad [\text{kWh/ton}]$$
$$R^2 = 53\%$$

[6.2]

The values below the coefficients denote the standard error in the coefficients. R^2 denotes the percentage of variance the model accounts for. 53% of the variance in the experimental data of the specific energy consumption can be accounted for by the model. A contour plot of
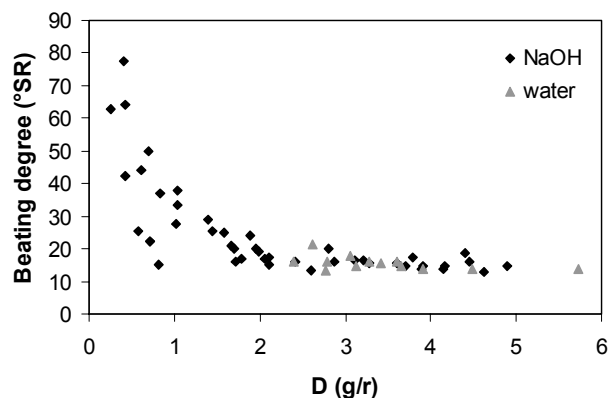

Fig. 6.3. *Specific energy consumption (kWh/ton) versus filling degree, D, and throughput, Q.*
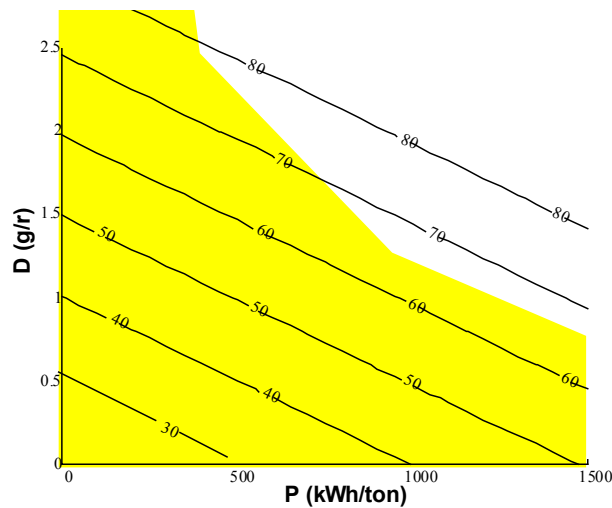
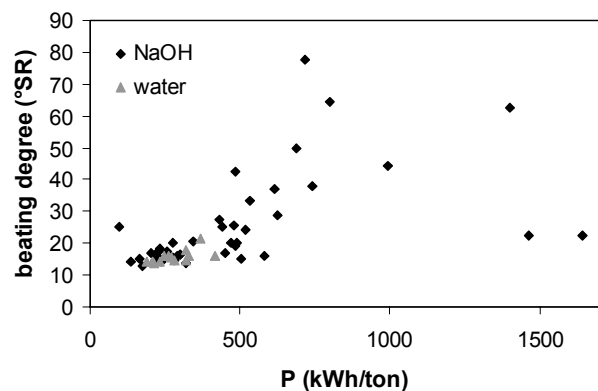***Fig. 6.4.*** *Dry matter content (%) versus specific energy consumption, P, and filling degree, D*

this model shows that at throughputs up to 20 kg/hr the specific energy consumption decreases with filling degree, while at higher throughput an increase with filling degree is observed (Fig. 6.3). Similarly, at filling degrees up to 3.1 grams per revolution the specific energy consumption decreases with throughput, while at higher filling degree an increase with throughput is observed (Fig. 6.3). The model is only valid in the shaded area of the graph, which represents the range of process conditions during the experiments that are used to develop the model.

Pulp and paper properties are often related to the amount of energy consumed during mechanical pulping. However, the specific energy consumption required to reach a certain value for a given property will depend on the process conditions. In order to visualise this dependency the examined pulp and paper properties have also been related to the specific energy consumption. Since only two independent parameters have been varied during the experiments, the properties have been related to a combination of two parameters. For each property the best combination out of filling degree, throughput and specific energy consumption is chosen.

***Fig. 6.5.*** *Beating degree of the pulp versus filling degree, D*

Fig. 6.6. *Beating degree of the pulp versus specific energy consumption, P*

98
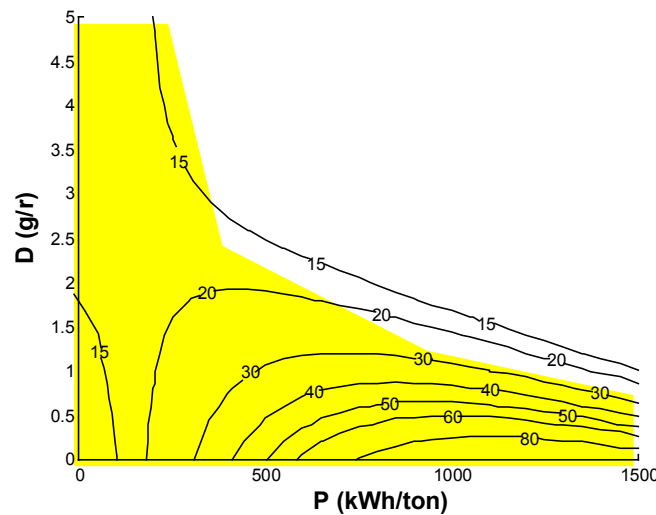
Fig. 6.7. *Beating degree of the pulp (°SR) versus filling degree, D, and specific energy consumption, P*

The dry matter content of the material leaving the RSE has been determined for 18 experiments. Multiple linear regression revealed that the *dry matter content*, ϕ, of the material leaving the RSE can be best described by the combination of filling degree and specific energy consumption (Table 6.3). At constant specific energy consumption the dry matter content strongly increases with filling degree, while at constant filling degree the dry matter content increases with specific energy consumption (Fig. 6.4).

From experimental results the *beating degree*, β, seemed to decrease with filling degree to a minimum of about 13 °SR (Fig. 6.5), while no direct relationship between beating degree and specific energy consumption was found (Fig. 6.6). According to multiple linear regression of the experimental data the beating degree, β, is related to the combination of the filling degree and the specific energy consumption (Table 6.3). At low specific energy consumption the effect of filling degree on the beating degree is negligible (Fig. 6.7), while at higher specific energy consumption the beating degree clearly decreases with increasing filling degree (Fig. 6.7). At high filling degree the effect of specific energy consumption on the beating degree is low.
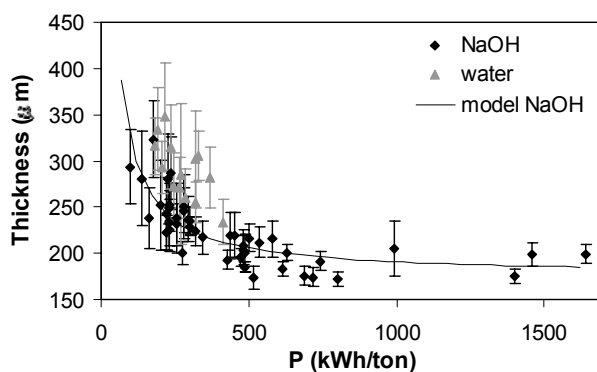
Fig. 6.8. *Paper thickness versus specific energy consumption, P*
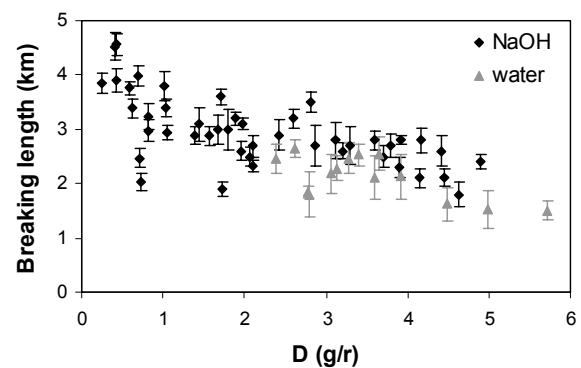
Fig. 6.9. *Breaking length versus filling degree, D*

99
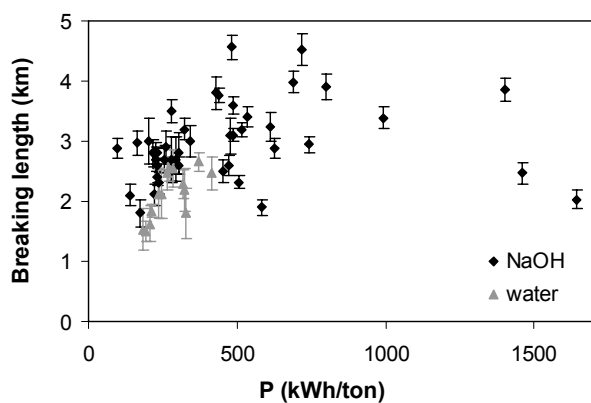
Fig. 6.10. *Breaking length versus specific energy consumption, P*
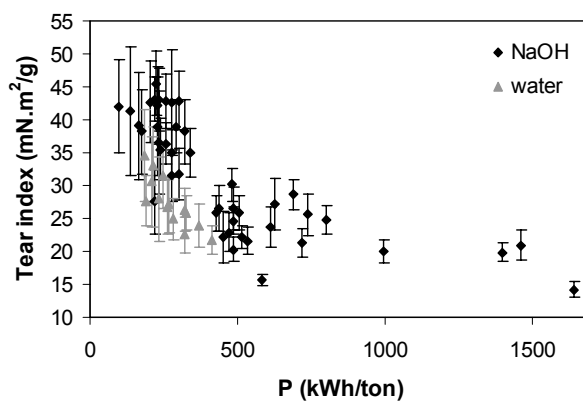
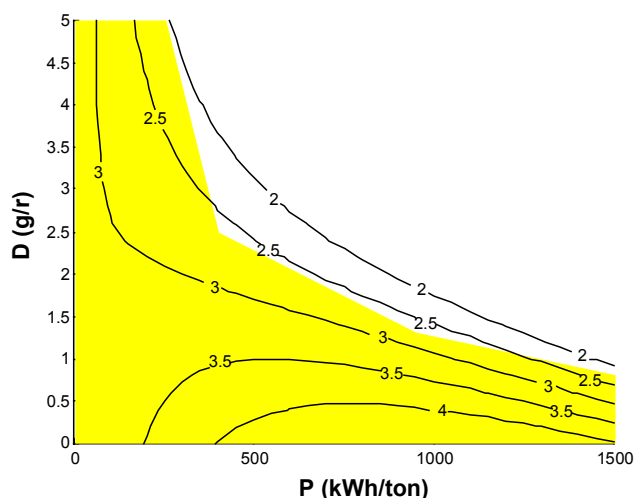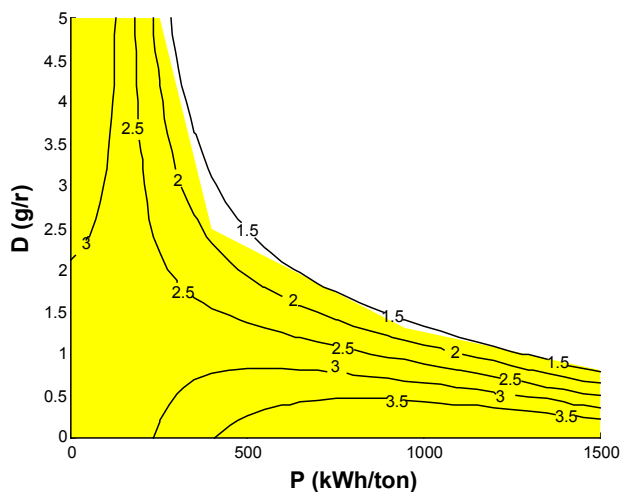
Fig. 6.13. *Tear index versus specific energy consumption, P*

Fig. 6.11. *Breaking length (km) versus filling degree, D, and specific energy consumption, P*

Fig. 6.12. *Burst index (kPa.m²/g) versus filling degree, D, and specific energy consumption, P*

100

Experimental results show that the *paper thickness*, H, decreases with specific energy consumption to a minimum of about 170 μm (Fig. 6.8). At high specific energy consumption the effect is less significant. Multiple linear regression of the experimental data also revealed that the paper thickness mainly depends on specific energy consumption (Table 6.3).

Similar to the beating degree the *breaking length*, τ, seems to decrease with filling degree (Fig. 6.9), while no direct relation is found for the specific energy consumption (Fig. 6.10). Multiple linear regression of the experimental data revealed that the breaking length depends on a combination of specific energy consumption and filling degree (Table 6.3, Fig. 6.11). The effect of filling degree on the breaking length is low at a specific energy consumption up to 400 kWh/ton, while at higher specific energy consumption the breaking length strongly decreases with increasing filling degree.

No significant effect of the extrusion conditions on either the *zero-span tensile strength* or the *strain at breakage* was found.

Multiple linear regression revealed that the *burst index*, ζ, depends on the combination of specific energy consumption and filling degree (Table 6.3, Fig. 6.12). At specific energies up to 250 kWh/ton the effect of filling degree on the burst index is negligible, while at higher specific energy consumption the burst index strongly decreases with filling degree. At high filling degree the burst index decreases with increasing specific energy consumption, while at low filling degree the burst index increases with specific energy consumption.

From experimental results it seems that the *tear index*, σ, decreases with specific energy consumption (Fig. 6.13), while no clear direct relationship is observed between the tear index and the filling degree (Fig. 6.14). Multiple linear regression revealed that the tear index can be best described with the combination of throughput and specific energy consumption (Table 6.3, Fig. 6.15). The effect of the throughput on tear index appears weak, while the effect of specific energy consumption is strong. As the model is only valid in the shaded area, the multiplicity of the tear index at certain values of the throughput, as shown by the model, cannot be obtained in practice.
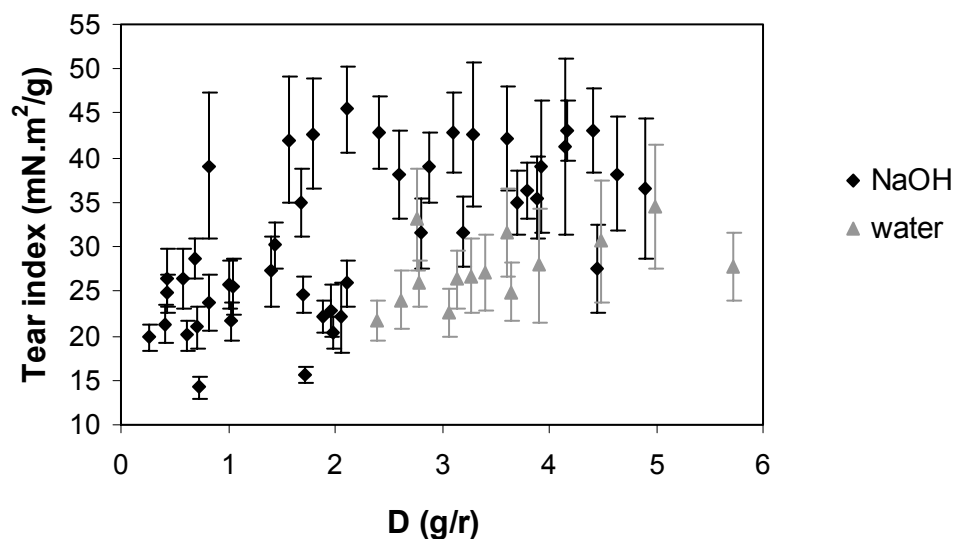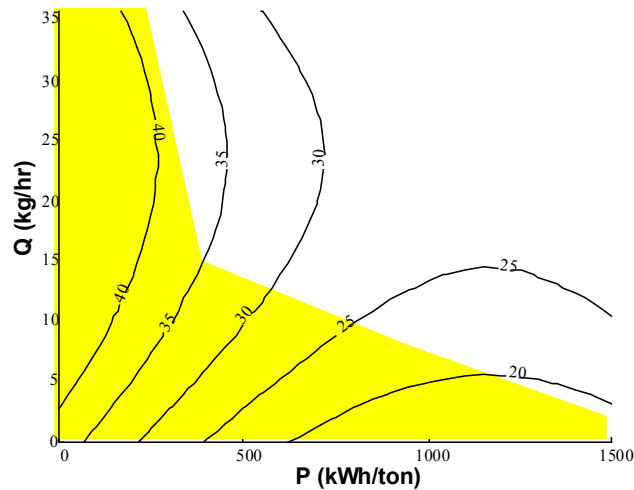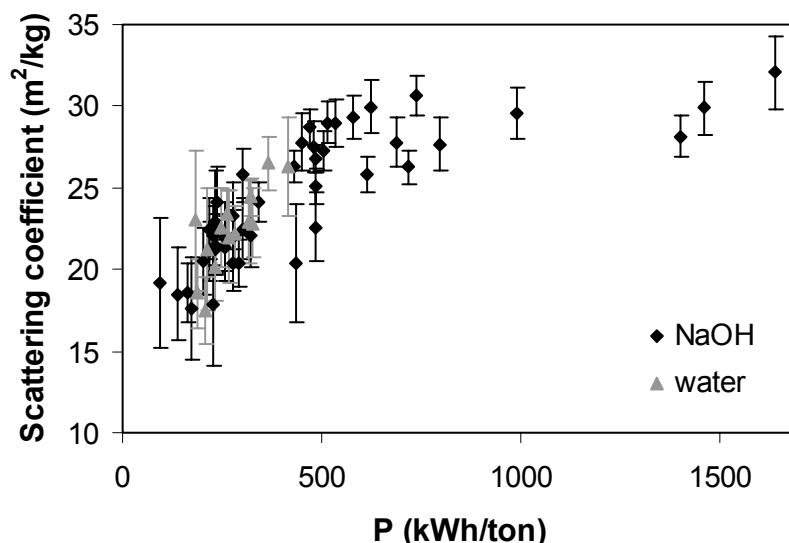

Fig. 6.14. *Tear index versus filling degree, D*

Fig. 6.15. *Tear index (mN.m^2/g) versus specific energy consumption, P, and throughput, Q*

Experimental results show that the *scattering coefficient*, s, increases with specific energy consumption (Fig. 6.16). Multiple linear regression of the experimental data shows that the scattering coefficient depends on both the filling degree and the specific energy consumption (Table 6.3, Fig. 6.17). The influence of specific energy consumption on the scattering coefficient increases with increasing filling degree. At low specific energy consumption the scattering coefficient is hardly influenced by filling degree, at high specific energy consumption scattering increases with increasing filling degree.

The *pitch of the transport screw* just before the RSE appeared to have no significant influence on the pulp and paper properties (data not shown). Use of *sodium hydroxide* instead of water increased tensile, burst and tear strengths (Fig. 6.9 and 6.13), burst strength (data not shown) and decreased sheet thickness (Fig. 6.8), while the specific energy consumption was not influenced (data not shown). The scattering coefficient appeared not to be influenced by sodium hydroxide (Fig. 6.16). *Temperature* had no influence on specific energy consumption (data not shown). A lower temperature resulted in a slightly higher beating degree, tensile and burst strength (Fig. 6.18 A and B). The tear index and the scattering coefficient are not influenced by temperature (Fig. 6.18 C and D).

Fig. 6.16. *Scattering coefficient versus specific energy consumption, P*

The effect of different process conditions on the paper properties has been summarised in Table 6.4.

102
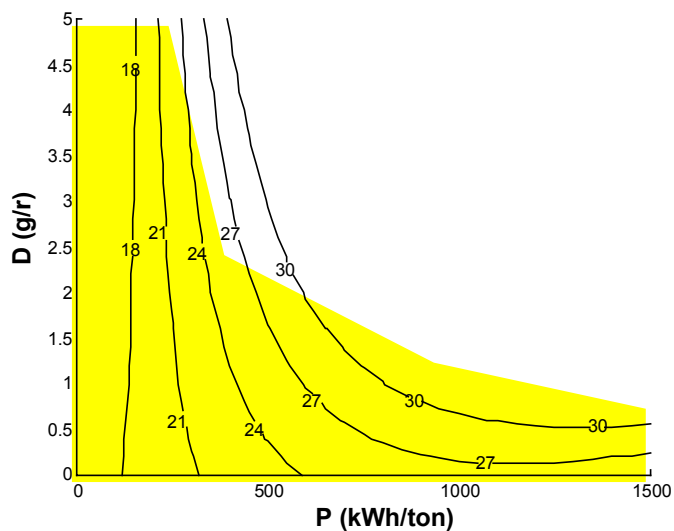
Fig. 6.17. *Scattering coefficient (m²/kg) versus filling degree, D, and specific energy consumption, P*
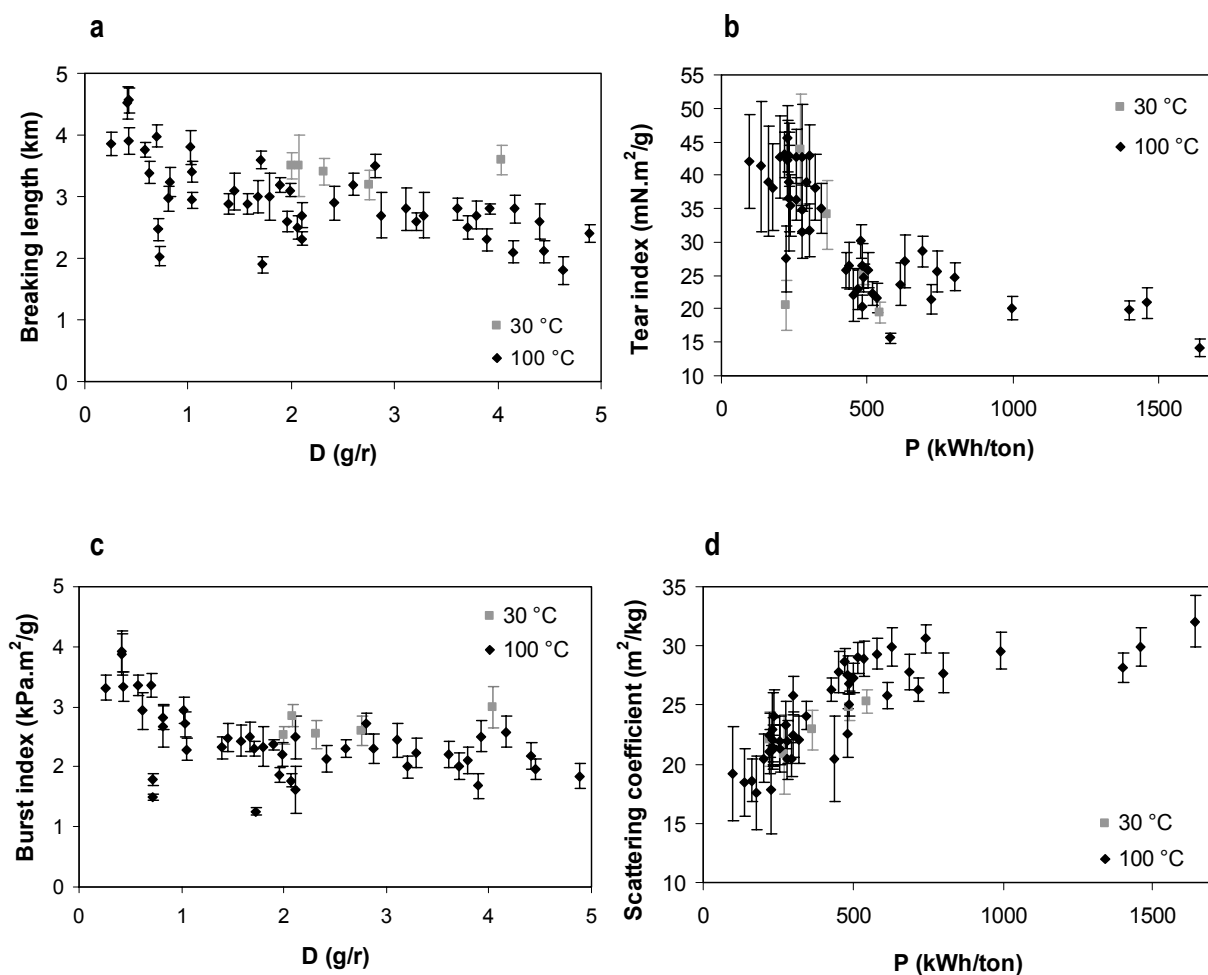
Fig. 6.18a-d. *Influence of process temperature on paper properties, NaOH treated fibres*

103

Table 6.4. *The effect of process conditions on pulp and paper properties*

The first eight columns show the effects of changes in screw speed and throughput on paper properties. Column 9 shows the effect of decreasing temperature and column 10 shows the effect of using water instead of sodium hydroxide as pretreatment liquid.

↑	*increase*		+	*positively affected*
↓	*decrease*		–	*negatively affected*
C	*constant*		+/–	*not affected*

	1	2	3	4	5	6	7	8	9	10
Screw speed	↓	↓	↓↓	↓	↓	↓	↓	C	C	C
Throughput	↓	↓	↓	↓↓	C <25	C >25	↑	↓	C	C
Filling degree	C <2.5	C >2.5	↑	↓	↑	↑	↑	↓	C	C
Temperature	C	C	C	C	C	C	C	C	↓	C
Pretreatment	NaOH	NaOH	NaOH	NaOH	NaOH	NaOH	NaOH	NaOH	NaOH	water
Specific power consumption, P	+	–	0	++	–	+	–	+	0	0
Beating degree	0+	0+	–	+	–	–	–	+	0+	0
Thickness	–	–	0	–	0+	–	+	–	0–	+
Breaking length	0+	0+	–	+	–	–	–	+	+	0–
Burst index	0–	–	–	0+	0–	–	–	+	+	–
Tear index	–	–	0–	——	+	–	+	–	0	0–
Scattering	+	+	0+	+	0	+	0	0+	0–	0
Dry matter content	+	+	+	0	0+	+	0+	0–	n.m.[*]	n.m.[*]

[*]n.m. = not measured
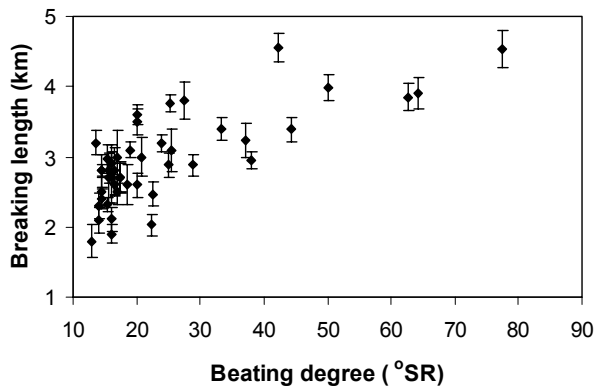
Fig. 6.19. *Breaking length of the paper versus beating degree of the pulp, NaOH treated fibres*
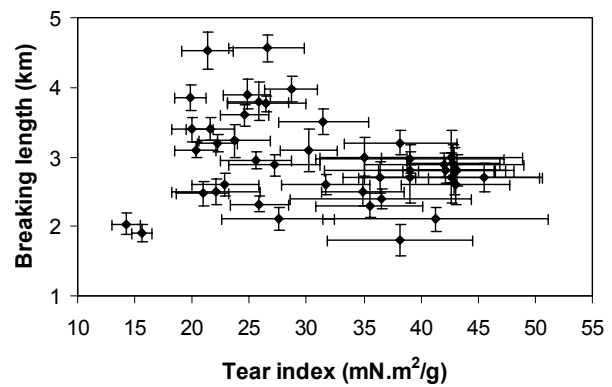
Fig. 6.20. *Breaking length versus tear index of the paper, NaOH treated fibres*

6.3.2 Relations between different product properties

In this section the results are analysed for relationships between the different product properties, in order to elucidate the different mechanisms behind the extruder processing. Plotting the breaking length against the beating degree clearly shows that both parameters are correlated (Fig. 6.19). The breaking length appears to increase with increasing beating degree. However, at higher beating degrees the breaking length hardly increases anymore, suggesting that at these process conditions higher beating degrees are mainly caused by an increasing amount of fines. The breaking length of paper made from extruded hemp bast fibres apparently is influenced by fibrillation in particular, as the degree of fibrillation and the amount of fines formed by extensive fibrillation are the most important fibre properties affecting the beating degree [16].

Plotting the breaking length against the tear strength (Fig. 6.20) shows that there is no significant relation between those strength properties. The two most left points in Figure 6.20 (low tear strength and breaking length) represent samples obtained at extreme conditions. The sample with the lowest tear strength is obtained at low filling degree (0.72 g/r), very low screw speed (6 rpm) and low throughput (0.51 kg/hr) resulting in a high specific energy consumption (Fig. 6.3) (1640 kWh/ton). As fibre length is the most important fibre property affecting the tear strength, it is suggested that the regarded sample has a low fibre length. The second sample of low tear strength is also obtained at low screw speed (12 rpm) and low
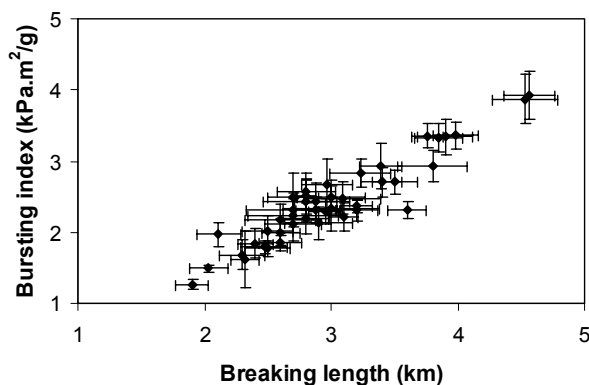
Fig. 6.21. *Burst index versus breaking length of the paper, NaOH treated fibres*
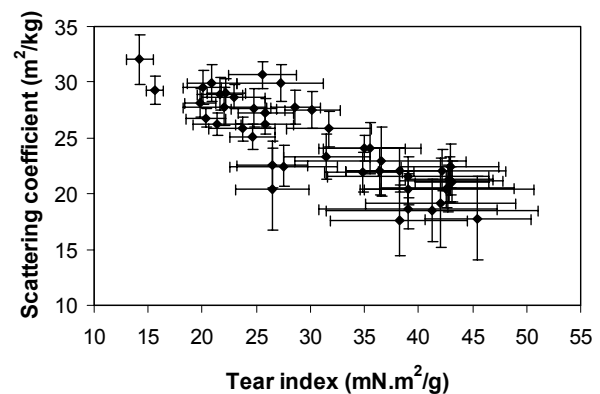
Fig. 6.22. *Scattering coefficient versus tear index of the paper, NaOH treated fibres*

throughput (1.24 kg/hr), but a somewhat higher filling degree (1.72 g/r). These conditions also cause a low tear strength and a low breaking length. From the fact that no direct significant relationship between breaking length and tear strength is shown, it can be concluded that fibrillation (and forming of fines in the form of fibrils) and fibre shortening do no not always happen simultaneously in extrusion pulping.

Plotting the burst strength against the breaking length (Fig. 6.21) shows that these paper strength properties are correlated. The burst strength cannot be directly related to the tear strength (data not shown). Fibre strength apparently does not significantly change by changing extrusion conditions, as zero-span tensile strength hardly changes.

Plotting the scattering coefficient against tear strength (Fig. 6.22) shows that this optical paper property decreases with increasing tear strength. The tear strength is mainly influenced by fibre length, while the scattering coefficient is influenced by the degree of defibration and fibrillation and by the presence of fines. Defibration, fibrillation and fines increase the surface area, while fibrillation and fines from fibrils also increase the bonded area. Because of the strong relation between tear strength and scattering coefficient, it can be suggested that during extrusion pulping fibre shortening often occurs simultaneously with an increase in the amount of fines, whether those fines are fibrils broken from the cell wall or coarse broken fibres.
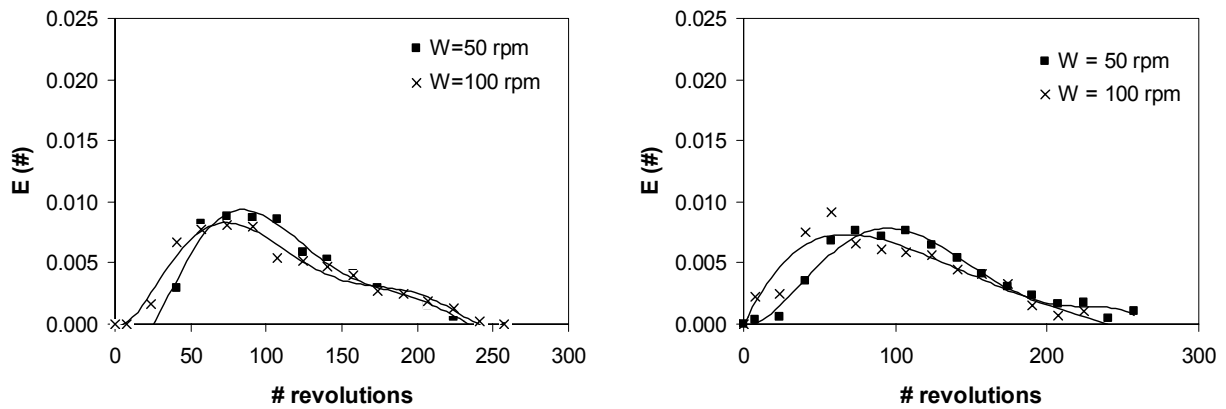
6.3.3 Residence time distribution

The increase in specific energy consumption with decreasing filling degree and decreasing throughput means that under these conditions more energy is consumed per kilogram of fibres. This supports the assumption that fibres accumulate and are pressurised in the space between the transport screws and the RSE's. When the pressure is high enough, and enough fibres have accumulated in this space, part of the fibres are pressed through the slots in the flights of the RSE towards the outlet of the screws. Higher filling degrees mean that more fibres accumulate in this space per revolution and thus fewer revolutions are required to reach a certain pressure. On average the number of revolutions that fibres stay in the RSE-zone becomes lower at higher filling degrees and thus the specific energy consumption becomes lower. This has been verified by examining the residence time distribution (RTD) of fibres in the RSE under different process conditions. It appears that all RTD-curves based on visual perception of redness show a small kink just after the midpoint after which the curve goes to zero (Fig. 6.23 B and 6.24 B). The RTD-curves based on analytical measurement of redness do not have a kink but show a long tail (Fig. 6.23 A and 6.24 A), indicating that part of the red fibres remain in the extruder for very long times. This suggests the presence of a dead zone in the extruder. The fact that visually no red fibres were present in the last samples indicates that at higher residence times fibres are better defibrated and mixed with other fibres.

The average residence time expressed as number of revolutions has been calculated based on the obtained analytical results as well as on the results of visual perception. As from the analytical RTD curves it appears that still some red fibres are present in the last samples taken, the actual average residence time may be somewhat higher. The average number of revolutions that fibres remain in the RSE clearly increases with decreasing filling degree (Fig. 6.23 and 6.25). However, the screw speed and thus the throughput appear to have negligible influence on the residence time when the filling degree is kept constant (Fig. 6.24). In the extruder fibres move at plug flow in the transport screws, while in the RSE zone they are mixed with fibres with a different residence time resulting in axial dispersion. Axial dispersion causes the RTD-curve to become broader. At lower filling degrees the average

number of revolutions that fibres remain in the RSE-zone becomes higher. This results in more axial dispersion and thus broader RTD-curves.
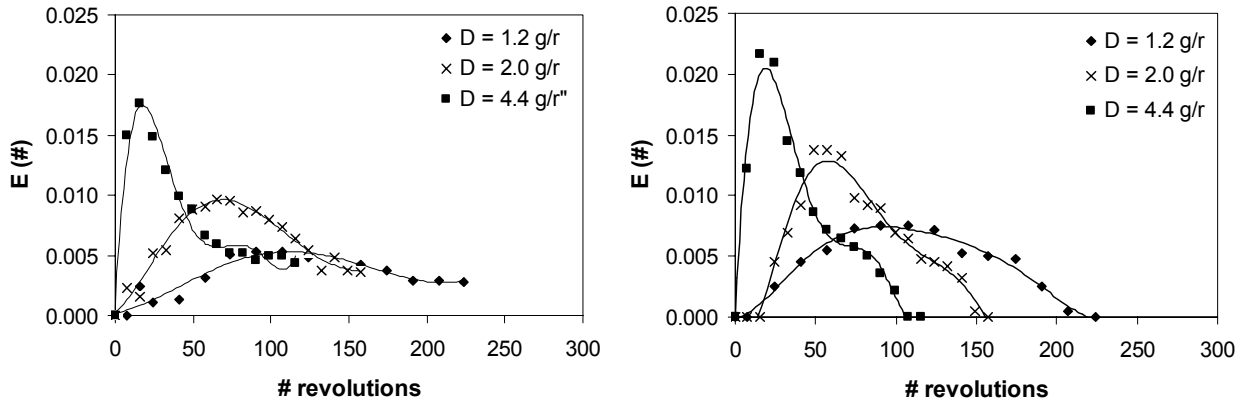
Fig. 6.23. *Residence time distribution of fibres in the RSE-element of the extruder (measured as number of screw revolutions) at different filling degrees, D, and a constant screw speed of 50 rpm*
A: analytical measurement of redness
B: visual perception of redness

Fig. 6.24. *Residence time distribution of fibres in the RSE-element of the extruder (measured as number of screw revolutions) at different screw speeds, W, and constant filling degree of 1.4 g/r*
A: analytical measurement of redness
B: visual perception of redness
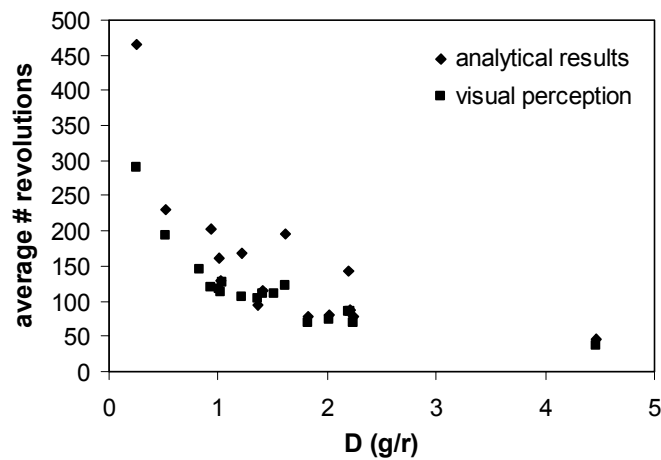
Fig. 6.25. *Average amount of revolutions that fibres remain in the RSE-element versus the filling degree, D*

107

6.4 Discussion

From the relations between the different process conditions, specific energy consumption and the pulp and properties of the product, suggestions can be made regarding the changes in fibre properties achieved at different extruder conditions. There are different ways to change the product properties and the specific energy consumption by changing the process conditions (Table 6.4). The suggestions about the effect of these different process conditions on the fibre properties have been summarised in Table 6.5 and are discussed below.

1. Decreasing both screw speed and throughput and keeping the filling degree constant (< 2.5 g/r);

Beating degree and breaking length are slightly increased when increasing the energy consumption by changing the process conditions according to this option. It can be suggested that a small part of the extra energy consumed is used for fibrillation, as beating degree and breaking length are mainly influenced by the degree of fibrillation and by fines. From the decrease in tear strength accompanying the increase in breaking length it can be suggested that the average fibre length decreases. The small decrease in burst strength might also be caused by a decrease in fibre length. The increase of scattering might be caused by a decrease in fibre length, by the small increase in amount of fines, and by a decrease in fibre thickness (Eq. 6.1), thus by an increase in degree of defibration. An increase of defibration and decrease in fibre length cause the paper thickness to decrease.

2. Decreasing both screw speed and throughput and keeping the filling degree constant (> 2.5 g/r);

This change in process conditions results in a reduction of specific energy consumption. Under these conditions the tear strength is increased and the scattering decreased. It can therefore be suggested that the reduction of specific energy consumption results in a reduction of shortening and defibration of the fibres. However, beating degree, breaking length and burst index appear to be (slightly) increased, suggesting a small increase in fibre fibrillation. The increase in paper thickness might be caused by decreased defibration and increased fibre length.

3. Decreasing both screw speed and throughput while increasing the filling degree;

This change in process conditions results in a reduction of beating degree, breaking length and burst index. The specific energy consumption does not change significantly. Under these conditions it seems that less energy is consumed for fibrillation and production of fines. The decrease in tear strength and the increase in scattering, however, suggest that energy is consumed in cutting and defibration of the fibres.

4. Decreasing both screw speed and throughput while decreasing the filling degree;

A strong increase in specific energy consumption results when the process conditions are changed according to this option, resulting in an increased beating degree, breaking length and scattering and a decreased tear strength. From this it can be suggested that the degree of fibrillation and defibration increase and that the average fibre length reduces, causing a reduced paper thickness.

5. Increasing the filling degree by decreasing the screw speed and keeping the throughput constant (< 25 kg/hr);

Both breaking length and beating degree are reduced when the process conditions are changed according to this option, suggesting a decrease in fibrillation. Tear strength increases suggesting a reduction in the extent of fibre shortening. The scattering is not affected, from which it could be suggested that the degree of defibration increased resulting in a higher specific surface.

Table 6.5. *Suggestions for the effect of process conditions on fibre properties based on experimental results*

↑	increase	+	positively affected
↓	decrease	–	negatively affected
C	constant	+/–	not affected

	1	2	3	4	5	6	7	8	9	10
Screw speed	↓	↓	↓↓	↓	↓	↓	↓	C	C	C
Throughput	↓	↓	↓	↓↓	C <25	C >25	↑	↓	C	C
Filling degree	C <2.5	C >2.5	↑	↓	↑	↑	↑	↓	C	C
Temperature	C	C	C	C	C	C	C	C	↓	C
Pretreatment	NaOH	NaOH	NaOH	NaOH	NaOH	NaOH	NaOH	NaOH	NaOH	water
Fibre shortening	+	–	0+	++	–	+	–	+	0	0+
Defibration	+	–	+	+	+	+	0+	+	–	0–
Fibrillation	0+	+	–	+	–	——	–	+	+	0–
Specific power consumption	+	–	0	++	–	+	–	+	0	0

6. *Increasing the filling degree by decreasing the screw speed and keeping the throughput constant (> 25 kg/hr);*

This change in process conditions results in an increase in specific energy consumption, which apparently does not result in more fibrillation, as beating degree, breaking length and burst index are decreased. It can be suggested that this energy is consumed in cutting of the fibres, as evidenced by the decrease in tear index. The scattering coefficient probably is increased by an increase in fines and in defibration. Paper thickness may be increased because of decreased fibrillation.

7. *Increasing the filling degree by decreasing the screw speed and increasing the throughput;*

Changing the process conditions in this manner results in a reduction of specific energy consumption as well as beating degree and breaking length, and in an increase in the tear index. It could therefore be suggested that the degree of fibrillation is reduced and the average fibre length increased. Scattering does not change, while the amount of fines has been decreased by a decrease in fibrillation and fibre shortening, suggesting an increased degree of defibration. Paper thickness might be increased because of a decreased amount of fines.

8. *Decreasing the filling degree by decreasing the throughput and keeping the screw speed constant;*

The beating degree, breaking length and burst index are increased when increasing the energy consumption according to this option. This suggests an increase of fibrillation and the amount of fines from fibrils. The observed decrease of the tear index and increase of the scattering coefficient probably means a reduction in fibre length and an increase in the degree of defibration. It is suggested that the combination of enhanced fibrillation and defibration and the reduced fibre length, causes the paper thickness to decrease.

9. Decreasing the temperature;

The increased beating degree and breaking length at lower temperatures suggest enhanced fibrillation and improved bonding. Tear index is not influenced, suggesting a limited decrease in fibre length. Scattering is slightly decreased, suggesting improved bonding.

10. Using water instead of sodium hydroxide.

Pre-treatment of the fibres in water instead of sodium hydroxide negatively affects breaking length and burst index, but does not influence the beating degree. Fibrillation is probably hardly affected. Specific energy consumption is not influenced. The tear index decreases, suggesting a decrease in fibre length. However, the scattering coefficient is not affected, suggesting a lower degree of defibration. Paper thickness increases. The increased fibre shortening might be caused by decreased fibre flexibility and increased fibre friction by water pre-treatment. Alkaline pre-treatment increases fibre swelling and decomposes the lignin and pectin, which enhances defibration.

It is suggested that, at constant temperature and constant pre-treatment, the degree of fibrillation increases with filling degree whether the specific energy consumption is increased or not (Fig. 6.7). This would mean that low values of beating degree and breaking length can be achieved at high specific energy consumption when the filling degree is high (at very low screw speed). When the filling degree decreases, the average mass of fibres compressed in the space between the transport screws and the RSE's during one screw turn decreases. This increases the residence time and the number of impacts that the fibres experience in the extruder. It can therefore be suggested that fibrillation and defibration are obtained by repeated compression of the fibres. Moreover, it is observed that increasing the filling degree results in a higher dry matter content (Fig. 6.4).

Figure 6.13 indicates that fibre shortening is increased by increasing specific energy consumption, and thus by decreasing the filling degree or decreasing the throughput. Decreased filling degree results in a higher residence time and more impacts. Decreasing the throughput at constant filling degree, increases the specific energy consumption (Fig. 6.3) and increases the dry matter content (Fig. 6.4). It can be suggested that, because of increased friction forces between the fibres, the higher dry matter content results in increased shortening. At higher filling degree more material is compressed during one revolution, resulting in higher hydraulic forces, increased drainage and increased dry matter content.

The developed relationships can be used to determine the process conditions that should be applied in order to obtain a pulp with certain required properties. For example, if a highly fibrillated pulp is required with a high beating degree and breaking length, the extruder should operate at high specific energy consumption at low filling degree (Fig. 6.7 and 6.11).

When the main goal of extrusion pulping is to shorten the fibres as much as possible, the process should be operated at high specific energy consumption (Fig. 6.15). This can be achieved by decreasing both filling degree and throughput. A highly fibrillated pulp but less shortening should therefore be obtained by applying a low filling degree at high throughput (and therefore high screw speed). Table 6.4 indicates that, when a highly defibrated pulp is required, the filling degree should be increased, while decreasing the screw speed.

From the resulting relationships it is clear that defibration, shortening and fibrillation of the fibres cannot always be achieved at the same time. Therefore in some cases post processing should be applied. This might be performed by a second extrusion step, but extra fibrillation of the fibres, for instance, can also be obtained by post-processing by beating or refining.

110

6.5 Conclusions

The extruder process conditions have a strong influence on the fibre product properties. It appears that specific energy consumption is increased at decreased filling degree (by either increasing the throughput or decreasing the screw speed) and at decreased throughput (at constant filling degree). Decreasing the filling degree increases the number of revolutions that fibres remain in the extruder, and therefore fibres experience more impacts during the extrusion process. This leads to increased specific energy consumption, breaking length and beating degree, and a reduced tear strength. Decreasing the throughput at constant filling degree increases specific energy consumption and dry matter content. Under these conditions the tear strength is reduced. Decreasing the temperature does not affect the specific energy consumption but increases breaking length and beating degree of the product. Alkaline pre-treatment also does not affect the specific energy consumption, but increases fibre swelling and flexibility and decomposes the lignin and pectin. This appears to increase breaking length and burst index, and decreases tear strength.

Defibration, shortening and fibrillation of the fibres cannot always be achieved at the same time. Therefore in some cases post processing should be applied by extrusion at other conditions, by beating or refining.

6.6 Nomenclature

c	(positive) constant	-
D	filling degree	$g.r^{-1}$
d	fibre diameter	m
H	thickness	μm
l	fibre length	m
P	specific energy consumption	$kWh.ton^{-1}$
Q	throughput	$kg.hr^{-1}$
R^2	percentage variance accounted for by the models	%
RSE	Reversed Screw Element	
s	scattering coefficient	$m^2.kg^{-1}$
W	screw speed	rpm
β	beating degree	°SR
ζ	burst index	$kPa.m^2.g^{-1}$
σ	tear index	$mN.m^2.g^{-1}$
τ	breaking length	km
ϕ	dry matter content	%

6.7 References

1. Kurdin, J.A. and Bohn, W.L. (1984): Mechanical pulping by extrusion, Tappi Pulping Conference, San Fransisco CA, USA, p. 265-274.
2. Kurdin, J.A. (1985): New developments in mechanical pulping, South. Pulp Paper, 45-51.
3. de Choudens, C., Angelier, R. and Combette, P. (1984): Pâtes mécaniques de résineux pâtes chimicomécaniques de feuillues, Revue A.T.I.P 38: 8, 405-416.
4. de Choudens, C., Angelier, R. and Lombardo, G. (1987): Pâtes chimico-mécaniques blanchies obtenues par le procédé "BiVis", Revue A.T.I.P 41: 2, 63-68.
5. de Choudens, C. and Angelier, R. (1990): Les Pâtes chimico-thermo-mécaniques blanchies obtenues par le procédé BiVis, Revue A.T.I.P. 44: 3, 137-146.
6. Babé, F. (1995): Fabriquer la pâte à partir de sorgho: opération réussie, Papier, Carton & Cellulose 44: 5-6, 24-25.
7. N'Diaye, S., Rigal, L., Larocque, P. and Vidal, P.F. (1996): Extraction of hemicelluloses from polar, *Populus tremuloides*, using an extruder-type twin-screw reactor: a feasibility study, Bioresource Techn. 57, 61-67.
8. Creusot-Loire (1977): Procédé et machine de fabrication de pâte à papier, France, Patent 75 23911.
9. Creusot-Loire (1980): Procédé et machine de fabrication de pâte à papier, France, Patent 78 26865.
10. de Choudens, C. and Bourne, C. (1979): Procédé pour la fabrication de pâtes papetières mécano-chimiques à haut rendement, France, Patent 77 21024.
11. de Choudens, C., Angelier, R., Combette, P. and Lesas, C. (1989): Procédé de fabrication de pâtes chimicomécaniques ou chimicothermo-mécaniques blanchies, Patent 87 11082.
12. van Roekel, G.J., Lips, S.J.J., Op den Kamp, R.G.M. and Baron, G. (1995): Extrusion pulping of true hemp bast fibre (*Cannabis sativa* L.), Tappi Conference, Chigago, USA, p. 477-485.
13. van Roekel, G.J. (1995): Chemimechanical pulping of fibre hemp, Bioresource Hemp, Frankfurt a/M, Germany.
14. van Roekel, G.J. (1996): Bulk papermaking applications for bast fibre crops using extrusion pulping, PIRA International, Peterborough, England, p. paper 26, 29 pp.
15. Page, D.H. (1969): A theory for the tensile strength of paper, Tappi 52: 4, 674-681.
16. Page, D.H. (1994): A note on the mechanism of tearing strength, Tappi J. 77: 3, 201-203.
17. Page, D.H. (1993): A quantitative theory of the strength of wet webs, J. Pulp Paper Sci. 19: 4, J175-J176.
18. Dence, C.W. and Reeve, D.W. (1996): "Pulp Bleaching- Principles and Practice". Tappi Press, Atlanta.
19. Rydholm, S.A. (1965): "Pulping Processes". John Wiley and Sons, Inc., New York.
20. Smook, G.A. (1982): "Handbook for pulp and paper technologists". Tappi, Atlanta.
21. Instrumentation Studies XLVI (1944): Tearing strength of paper, Paper Trade J. 118: 5, 13-19.
22. Seth, R.S. and Page, D.H. (1988): Fiber properties and tearing resistance, Tappi Journal 2, 103-107.
23. Seth, R.S. (1995): The effect of fiber length and coarseness on the tensile strength of wet webs: a statistical geometry explanation, Tappi J. 78: 3, 99-102.
24. Catling, D. and Grayson, J. (1982): "Identification of vegetable fibres". Chapman and Hall, London.

25. Fengel, D. and Wegener, G. (1984): "Wood; Chemistry, Ultrastructure, Reactions". Walter de Gruyter, Berlin.

26. Gilmour, S.C. (1955): "Paper: Its making, merchanting and usage : the paper merchant's textbook". National Assn. of Paper Merchants, London.

27. Batra, S.K. (1989): In "Handbook of Fibre Science and Technology", M. Lewin and E. M. Pierce, ed., Marcel Dekker Inc., New York, p. 727-807.

28. Kirby, R.H. (1963): "Vegetable fibres, botany, cultivation and utilization". Interscience Publishers Inc., New York.

29. Kocurek, M.J., Hamilton, F. and Leopold, B. (1987): "Pulp and paper manufacture, Volume 3: Secondary fibres and non-wood pulping". Joint Textbook Committee of the Paper Industry, Canada.

30. Matthews, J.M. (1947): "Textile fibres, their physical, microscopical and chemical properties". John Wiley & Sons, New York.

31. Rance, H.F. (1980): "The raw materials and processing of papermaking". Elsevier Scientific Publishing Company, Amsterdam.

32. Hägglund, E. (1951): "Chemistry of Wood". Academic Press Inc., Publishers, New York.

33. Ranalli, P. (1998): In "Advances in hemp research", P. Ranalli, ed., Food Products Press, An Imprint of The Haworth Press, Inc., New York, p. 61-84.

34. Clark, J.d.A. (1962): Effects of fiber coarseness and length, I. Bulk, burst, tear, fold, and tensile tests, Tappi 45: 8, 628-634.

35. Stationwala, M.I., Mathieu, J. and Karnis, A. (1996): On the interaction of wood and mechanical pulping equipment. Part II: Pulp quality, J. Pulp Paper Sci. 22: 6, J202-J207.

36. de Groot, B., van Roekel, G.J. and van Dam, J.E.G. (1998): In "Advances in hemp research", P. Ranalli, ed., Food Products Press, An Imprint of The Haworth Press, Inc., New York, p. 213-242.

37. Allan, G.G. and Ko, Y.C. (1995): The microporosity of pulp, Cellulose Chem. Technol. 29, 479-485.

38. de Jong, E., van Roekel, G.J., Snijder, M.H.B. and Zhang, Y. (1999): Towards industrial applications of bast fibre pulps; their potential as a nonwood source is discussed, Pulp Paper Canada 100: 9, T270-T273.

39. Bos, J.H., Veenstra, P., Verhoeven, H. and de Vos, P.D. (1995): "Het papierboek". VAPA, Apeldoorn.

40. Pauler, N. (1998): "Paper optics". AB Lorentzen & Wettre, Kista.

41. Ingmanson, W.L. and Thode, E.F. (1959): Factors contributing to the strength of a sheet of paper, II Relative bonded area, Tappi 42: 1, 83-93.

42. Payne, R.W., Lane, P.W., Digby, P.G.N., Harding, S.A., Leech, P.K., Morgan, G.W., Todd, A.D., Thompson, T., Tunnicliffe Wilson, G., Welham, S.J. and White, R.P. (1993): "Genstat™ 5 Release 3, Reference Manual". Clarendon Press, Oxford.

43. Draper, N.R. and Smith, H. (1981): "Applied regression analysis". John Wiley & Sons, New York.

Concluding Remarks

The aim of the research described in this thesis was to elucidate the mechanism behind extrusion pulping in order to be able to develop a model that describes the relation between process conditions, screw configuration and product quality. Modelling of the extrusion pulping process is necessary for proper control of required product quality and development of scale up rules. Accurate modelling requires a good description of the constitutive relations of the fibres, for those properties that are important in the processing mechanism.

Models developed for food and polymer processing by extrusion are based on different main mechanisms compared to fibre extrusion. While important mixing and thus axial dispersion takes place by leakage flows of molten polymers between the chambers of one screw or intermeshing screws, fibres move in plug flow and do not mix in the transport screws. Models designed for the extrusion of food and polymers make use of liquid rheology relations, whereas modelling fibre processing requires relations of solid mechanics.

During extrusion pulping, processing appears to be confined to the space formed by the last screw chamber of the transport screw and the first chamber of the Reversed Screw Element (RSE), where fibres are processed by application of high compression and shear forces. The extent of cutting, defibration and fibrillation during extrusion pulping is assumed to depend on the distribution of compressive and shear forces in the extruder. Therefore, the model to be developed should calculate compressive and shear forces on the fibres in the extruder influenced by process conditions and extruder geometry.

The fibrous material processed in extrusion pulping consists of two phases; a solid hydrophilic fibre network and a liquid phase. Therefore, calculation of the compressive and shear forces in the compression chamber of the extruder requires at least relations describing

- the relation between swelling of the fibres by the liquid phase and the applied pressure
- the drainage of impregnation liquids through the fibre network
- the compressibility of the fibre network
- the transfer of forces through the fibre network
- the shear strength of the fibre network

The complicated geometry of the compression space was simplified by modelling it as a cylinder, which may contain several holes of different geometry and position to simulate the effect of the slots in the RSE. The volume decrease versus time of the piston acting on the fibres in the cylinder depends on the screw speed and the screw geometry (Appendix A). This simplified model will be sufficient to calculate compression forces in the fibre network. However, a more complicated three-dimensional model might be necessary for accurate determination of the shear forces in the medium.

The results of the extrusion experiments suggest that fibrillation is increased at lower filling degree (Chapter 6). A lower filling degree has shown to imply a higher average number of revolutions that fibres remain in the RSE, which means a higher average number of impacts on the fibres. Modelling of the second and subsequent compression steps of the fibre network

requires inclusion of the effects of repeated compression (Chapter 3). However, proper modelling also requires a relation for the uptake of liquid by the fibre mass at different conditions. The results of the extrusion experiments also suggest that shortening is increased at higher specific energy consumption (to be achieved by decreasing both filling degree and throughput), and defibration is increased by increasing the filling degree while decreasing the screw speed (Chapter 6). To prove the suggestions of the effects of extrusion conditions on fibre properties, fibre length, degree of defibration and fibrillation should be measured directly. However, proper quantitative measuring techniques are not available (yet) for the relatively long bast fibres.

Extrusion experiments revealed that the specific energy consumption is not decreased when increasing the temperature (Chapter 6). The coefficient of the compressibility equation decreases with temperature resulting in a lower stress over the whole density range (Chapter 3). This implies that less energy is required for compression of the fibre network. This could suggest that other mechanisms during extrusion consume relatively more energy at higher temperature. Although the effect of temperature on swelling is unknown and needs to be determined for proper modelling of the effect of temperature, the decrease of liquid viscosity with increasing temperature might accelerate the drainage. Therefore, the fibres will be dryer after compression and more energy will be consumed in shearing the fibre mass, according to the constitutive relations developed for shear strength (Chapter 5).

Impregnation with sodium hydroxide also appeared to have negligible effect on the specific power consumption (Chapter 6) Because of higher swelling, drainage becomes slower at higher sodium hydroxide concentration causing a higher specific energy consumption for compression (Chapter 4). Slower drainage, however, causes a lower dry matter content after compression, and shear will become easier, resulting in a lower energy consumption for shearing. For both temperature increase and sodium hydroxide impregnation extrusion experiments showed increasing breaking length and beating degree, because of softening of the lignin (Chapter 6). Impregnation with sodium hydroxide resulted in increased tear strength as well, indicating reduced shortening, while this is not observed when increasing the temperature. At higher sodium hydroxide concentration, drainage becomes slower and more energy is consumed in compression of the fibre mass (Chapter 4). However, a great part of this energy is used to compress liquid and is not consumed to increase the stress of the solid (Chapter 2) indicating that fibre shortening mainly increases at higher solid stresses.

The constitutive relations developed in this work should be combined with the geometry model of the 'compression chamber' between the transport screws and the RSE into one model describing the processing of fibres in a corotating twin-screw extruder. However, in order to be able to predict the effect of temperature on processing, the influence of temperature on fibre swelling as well as shear strength needs to be determined.

The model should be extended and optimised with information obtained from simulation of the performed extrusion experiments. This will yield the differences in the distribution of compressive and shear forces that cause the differences in degree of cutting, defibration and fibrillation. By means of this model other geometries might be designed for optimised fibre processing. This can result in an optimised design for RSE's or the design of other 'screw' elements to effectuate improved control of fibre processing of the fibre network with more efficient energy consumption.

Appendix A

Screw geometry model

In this Appendix the geometry of a corotating twin screw extruder with trapezoidal screw elements is outlined in order to obtain a relation describing the volume change versus time of the compression chamber in the twin-screw extruder. A model that describes this volume change is not available in literature.

The compression chamber is formed by the last screw chamber of the transport screw and the first screw chamber of the RSE. The important screw dimensions are drawn in figure A.1. The developed model includes the formula's developed by Tayeb [1] for the volume of a complete screw chamber of one screw during one revolution, without intermeshing flights.

The screw dimensions used for the calculations are based on the trapezoidal elements of the Clextral BC-45 corotating twin-screw extruder, with RSE's having a pitch of 25 mm and transport screws having a pitch of 35 mm.
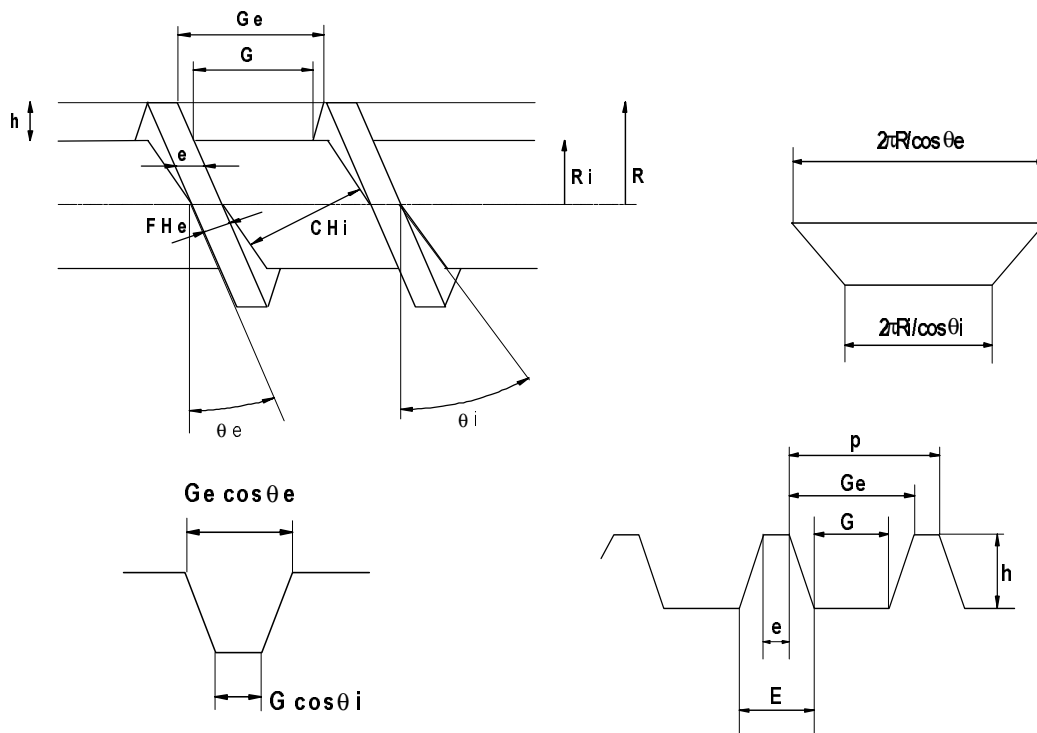
Figure A.1. Screw dimensions

A.1 Reversed Screw Elements

Dimensions of the used RSE's

$D := 55$ outer diameter [mm]

$Di := 34$ inner diameter [mm]

$p := 25$ pitch [mm]

$e := 7.3$ width of the top of the flight [mm]

$E := 12.8$ width of the base of the flight [mm]

Basic calculations of RSE dimensions (see figure A.1)

$R := \dfrac{D}{2}$ outer radius [mm] $R = 27.500$

$Ri := \dfrac{Di}{2}$ inner radius [mm] $Ri = 17.000$

$I := 0.5 \cdot (D + Di)$ distance between the two screws [mm] $I = 44.500$

$h := D - I$ channel depth [mm] $h = 10.500$

$G := p - E$ width of the bottom of the channel [mm] $G = 12.200$

$Ge := p - e$ width of the top of the channel = distance between two flights [mm] $Ge = 17.700$

$\theta i := \operatorname{atan}\left(\dfrac{p}{2 \cdot \pi \cdot Ri}\right)$ internal pitch angle $\theta i = 0.230$

$\theta e := \operatorname{atan}\left(\dfrac{p}{2 \cdot \pi \cdot R}\right)$ external pitch angle $= \gamma$ $\theta e = 0.144$

$\theta t := \operatorname{atan}\left[\dfrac{h}{0.5 \cdot (E - e)}\right]$ angle of trapeziodal flight $\theta t = 1.315$

$\beta := \operatorname{acos}\left(\dfrac{I}{D}\right)$ intermeshing angle $\beta = 0.628$

$CHe := Ge \cdot \cos(\theta e)$ $CHe = 17.518$

$CHi := G \cdot \cos(\theta i)$ $CHi = 11.879$

$FHe := e \cdot \cos(\theta e)$ assistant variables [mm] $FHe = 7.225$

$FHi := E \cdot \cos(\theta i)$ $FHi = 12.463$

The volume of the screw channel during one revolution is calculated according to Tayeb [1]:

$$\text{Vol} := 2 \cdot \pi \cdot h \cdot \frac{Ri}{\cos(\theta i)} \cdot \left(\frac{CHe + CHi}{2} \right) + 4 \cdot \pi \cdot \frac{h}{2} \cdot \left(\frac{R}{\cos(\theta e)} - \frac{Ri}{\cos(\theta i)} \right) \cdot \left(\frac{CHe}{3} + \frac{CHi}{6} \right)$$

$$\text{Vol} = 2.226 \cdot 10^4 \qquad \text{mm}^3$$

Volume of channel and flight during one revolution [mm^3]:

$$\text{Vtotal} := 0.25 \cdot \pi \cdot p \cdot \left(D^2 - Di^2 \right) \qquad\qquad \text{Vtotal} = 3.670 \cdot 10^4 \qquad \text{mm}^3$$

Volume of the flights during one revolution [mm^3]:

$$\text{Vflight} := \text{Vtotal} - \text{Vol} \qquad\qquad \text{Vflight} = 1.444 \cdot 10^4 \qquad \text{mm}^3$$

Volume end of channel and flight

The volume of the end of the channel can be calculated from the ratio between the surface of the channel end and the surface of the middle of the channel during one revolution (Fig. 2). This ratio is denoted by ψ:

$$\psi := \frac{G + Ge}{4 \cdot p} \qquad\qquad \psi = 0.299$$

(G+Ge)/2 is the width of the middle of the channel.
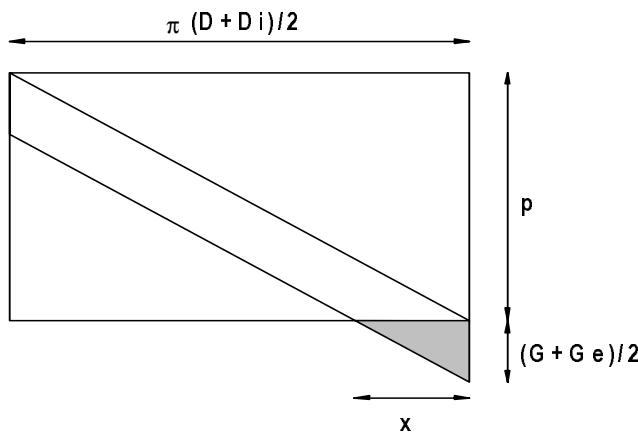
Figure A.2: *fraction of end of channel*
x = π(D+Di)(G+Ge)/4p
surface triangle: x(G+Ge)/4
surface parallelogram: π(D+Di)(G+Ge)/4
ψ = surface triangle / surface parallelogram

The volume of the channel, Vchanend can now be calculated using the same ratio between the volume of the screw ending and the volume during one revolution:

$$Vchanend := Vol \cdot \psi \qquad\qquad Vchanend = 6.655 \cdot 10^3 \quad mm^3$$

The volume of the flightend can be calculated similarly:

$$\psi flight := \frac{E + e}{4 \cdot p} \qquad\qquad \psi flight = 0.201$$

(E+e)/2 is the width of the middle of the flight.

$$Vflightend := Vol \cdot \psi flight \qquad\qquad Vflightend = 4.474 \cdot 10^3 \quad mm^3$$

The intermeshing part

The width of the flight, w, depends linearly on the radial distance from the middle of the screw.
at r = R : w = e
at r = Ri : w = E
This results in the following linear relation for w(r):

$$w(r) := \left(\frac{E - e}{R - Ri} \right) \cdot (R - r) + e \qquad\qquad [mm]$$
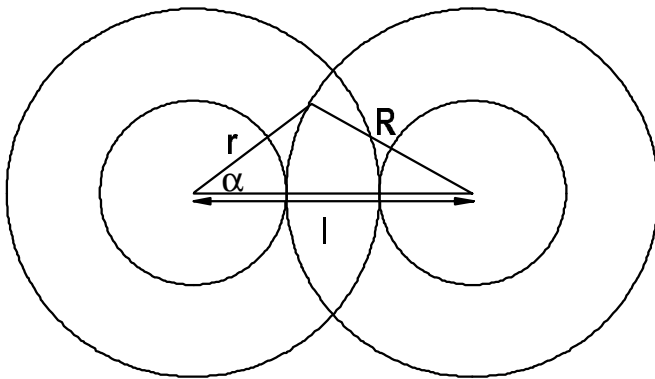
Figure A.3: cross-section of intermeshing screws, calculation of α

Applying the cosinus rule on the triangle drawn in figure 3 results the following relation between angle α, and the radial distance from the middle of the screw, r:

$$\alpha(r) := acos\left(\frac{r^2 + I^2 - R^2}{2 \cdot r \cdot I} \right)$$

Figure A.4: cross-section of intermeshing screws, calculation of curve length cl

This yields the following relation between the curve length, cl (figure 4), and the radial distance from the middle of the screw, r:
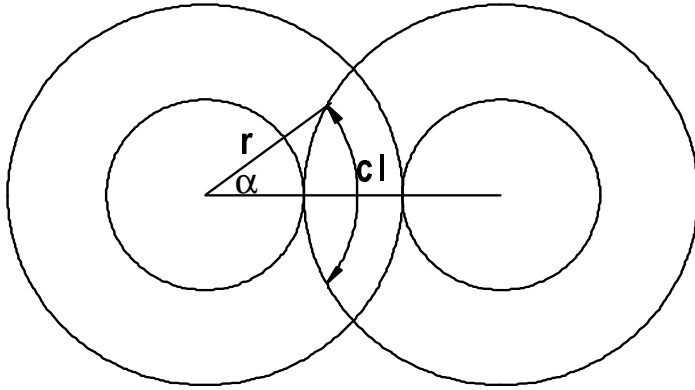
$$cl(r) := 2 \cdot acos\left(\frac{r^2 + I^2 - R^2}{2 \cdot r \cdot I}\right) \cdot r \qquad \text{[mm]}$$

The volume of the intermeshing part of the flight is now defined by:

$$intvol := \int_{Ri}^{R} cl(r) \cdot w(r) \, dr \qquad\qquad intvol = 2.182 \cdot 10^3 \quad mm^3$$

Calculation of the volume of the end of the flight in the intermeshing zone

The volume of the end of the flight that is present in the intermeshing zone depends on the position of the screws at that moment. This position will be indicated with angle θ.
θ equals zero when the base of the flight starts at Q (figure 5).
The angle over which the integration should be performed is not constant, but depends on the radial distance from the centre, r, as well as on the position of the screws, θ. This tangential integration interval will be denoted with $\phi min <$ angle $< \phi max$. The radial integration interval will be denoted with Rmin $< r <$ Rmax.
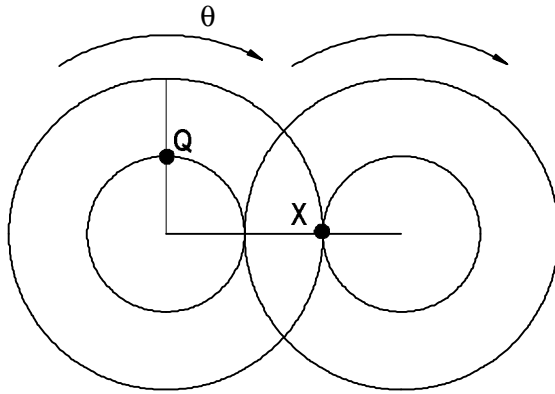
Figure A.5: cross-section of intermeshing screws

Flight is present at point X at the following value for θ:

$$0.5 \cdot \pi - \frac{2 \cdot E \cdot \pi}{p} = -1.646$$

As the flight has a certain thickness, the flight is present over a certain angle interval. The width of this interval depends on the thickness of the flight (figure 6):

$$\xi be(r) := \frac{w(r)}{p} \cdot 2 \cdot \pi$$

$$\xi be(R) = 1.835 \qquad \xi be(Ri) = 3.217$$
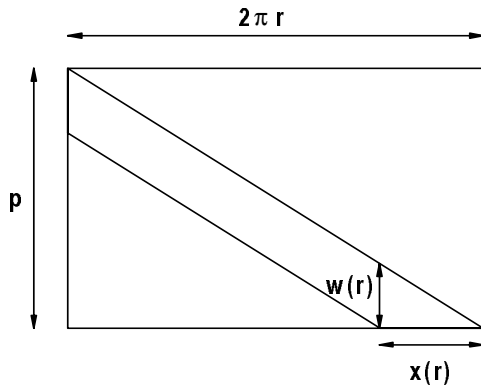
Figure A.6: calculation of the angle interval over which flight is present

$x(r) / w(r) = 2\pi r / p$

$\xi be = x(r) / r$

Definition of the tangential integration interval

The relation between the screw position, θ, and the angle of the integration interval, a, is:

$$\theta(a) := -\xi be(Ri) - a + \frac{3}{2} \cdot \pi$$

$$\xi \phi min(r, a) := 0.5 \cdot \pi - \theta(a) - \frac{(E - w(r)) \cdot \pi}{p}$$

The lower boundary of the tangential integration interval:

$$\phi min(r, a) := if(\xi \phi min(r, a) < 0, 0, \xi \phi min(r, a))$$

The upper boundary of the tangential integration interval:

$$\phi max(r, \theta) := if(\xi be(r) > \alpha(r) + \xi \phi min(r, \theta), \alpha(r) + \xi \phi min(r, \theta), \xi be(r))$$

Definition of the radial integration interval

$$\xi Rmax(a) := R - \frac{p \cdot (R - Ri) \cdot \left(0.5 \cdot \pi - \theta(a) - \frac{E + e}{p} \cdot \pi\right)}{\pi \cdot (E - e)}$$

if $\xi Rmax(\theta) > R$ than flight is present at point X: Rmax:=R
if $\xi Rmax(\theta) < Ri$ than no flight is present at point X: Rmax:=Ri

The upper boundary of the radial integration interval:

$$tiny := 0.00000001$$

$$Rmax(a) := if(\xi Rmax(a) > R, R, if(\xi Rmax(a) < Ri, Ri + tiny, \xi Rmax(a)))$$

$$\xi Rmin(a) := \left[R - (R - Ri) \cdot \left[1 - \frac{(0.5 \cdot \pi - \theta(a)) \cdot p}{(E - e) \cdot \pi}\right]\right] - tiny$$

The lower boundary of the radial integration interval:

$$Rmin(a) := if(\xi Rmin(a) < Ri, Ri, \xi Rmin(a))$$

Definition of the integration functions

$$\text{if1}(r,a) := \text{if}\left[\alpha(r) + \xi\phi\text{min}(r,a) < 0, 0, \left[\frac{-p}{4\cdot\pi}\cdot\left(\phi\text{max}(r,a)^2 - \phi\text{min}(r,a)^2\right) + w(r)\cdot(\phi\text{max}(r,a) - \phi\text{min}(r,a))\right]\cdot r\right]$$

$$r,a) - \phi\text{min}(r,a)\right]\cdot r\right]$$

$$\text{if2}(r,a) := \text{if}(\xi\phi\text{min}(r,a) > 0, 0, \text{if}((-\xi\phi\text{min}(r,a)) > \alpha(r), (w(r)\cdot\alpha(r))\cdot r, (w(r)\cdot-\xi\phi\text{min}(r,a))\cdot r))$$

This gives the following relation between the volume of the intermeshing end of the flight and the angle:

$$\text{Vimend}(a) := \int_{Ri}^{Rmax(a)} \text{if1}(r,a)\ dr + \int_{Rmin(a)}^{R} \text{if2}(r,a)\ dr \qquad [\text{mm}^3]$$

$$a := -1, -0.8 .. 4$$
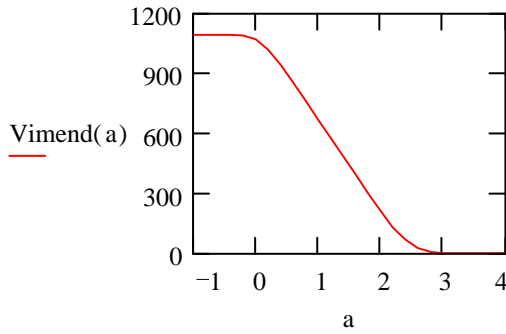
$$2\cdot\text{Vimend}((-2)) = 2.182\cdot10^3 \quad \text{mm}^3$$

$$\text{intvol} = 2.182\cdot10^3 \qquad \text{mm}^3$$

Figure A.7: *Volume of the intermeshing end of the flight versus the angle a*

Volume of the channel related to the screw position

$$b := \frac{G + Ge}{2}$$
width of the channel at r = (R+Ri)/2 (figure 7)
$$b = 14.950 \quad mm$$

$$o(a) := a \cdot \frac{R + Ri}{2}$$
circumference of a fraction of a circle with radius (R+Ri)/2 and angle a
$$[mm]$$

$$x := \frac{b \cdot \pi \cdot (R + Ri)}{p}$$
length of the channel at r = (R+Ri)/2 (figure 7)
$$x = 83.601 \quad mm$$
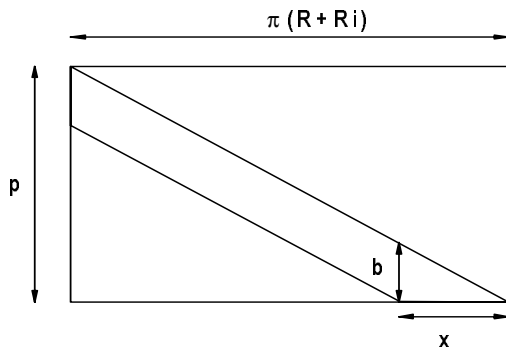
Figure A.8: *dimensions of the screw channel at r=R+Ri*

$$o = 0$$
$$a = 0$$

$$0 < o < x$$
$$0 < a < 2x/(R+Ri)$$

$$o = x$$
$$a = 2x/(R+Ri)$$

$$x < o < \pi(R+Ri)$$
$$2x/(R+Ri) < a < 2\pi$$

$$o = \pi(R+Ri)$$
$$a = 2\pi$$

$$o > \pi(R+Ri)$$
$$a > 2\pi$$
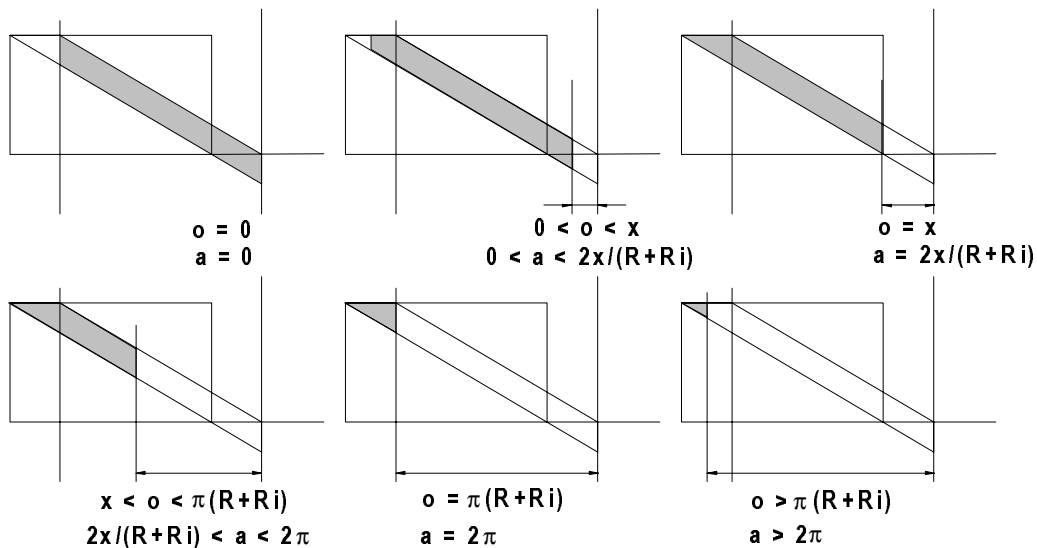
Figure A.9: *Fraction of the screw channel that is part of the compression chamber for different positions of the screws (given by angle, a and the fraction of the circumference of the circle, o)*

The shaded area in figure A.9 shows the fraction, f(a), of the total channel surface, $\ell\pi(R+Ri)$, that is part of the compression chamber at different screw positions. When the screws turn, angle a increases and fraction f(a) increases. At a=0 (o=0) the total channel volume is part of the compression chamber and when a > $2\pi(1+b/p)$ (o > p(R+Ri)+x) the volume of the compression chamber has become zero. The relation between f(a) and a can be described with the following equation:

$$f(a) := \text{if}\left[o(a)>0,\text{if}\left[o(a)<x,\dfrac{-o(a)\cdot b + 0.5\cdot b\cdot x - 0.5\cdot \dfrac{b}{x}\cdot(x-o(a))^2}{b\cdot\pi\cdot(R+Ri)}+1,\text{if}\left[o(a)>\pi\cdot(R+Ri),\text{if}\left[o(a)\right.\right.\right.\right.$$

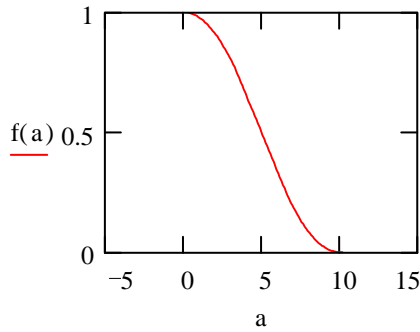$$\left. + Ri\right),\text{if}\left[o(a)>\pi\cdot(R+Ri)+x,0,\dfrac{(x-o(a-2\cdot\pi))^2\cdot 0.5\cdot b}{x\cdot b\cdot\pi\cdot(R+Ri)}\right],\dfrac{-0.5\cdot b\cdot x - (o(a)-x)\cdot b}{b\cdot\pi\cdot(R+Ri)}+1\right],1\right]$$

$a := -1,-0.9..2\cdot\pi+4$

$f(0) = 1.000$

$f(12) = 0.000$

Figure A.10: *Fraction of the total volume of the screw channel that is part of the compression chamber versus the angle a*

The volume of the channel of the RSE versus the angle [mm³]:

$$VRSE(a) := \text{if}\left[a<\xi be(Ri)-\pi,\text{Vol}-\text{intvol},\text{if}\left[a<2\cdot\pi,\text{Vol}\cdot f(a)-\dfrac{\text{intvol}}{2}-\text{Vimend}(a),\text{if}\left[a<2\cdot\pi\cdot\left(1+\dfrac{1}{1}\right.\right.\right.\right.$$

$$\left. a<2\cdot\pi\cdot\left(1+\dfrac{b}{p}\right),\text{Vol}\cdot f(a)-\left(\dfrac{\text{intvol}}{2}-\text{Vimend}(4\cdot\pi-a-\xi be(Ri))\right),0\right]\right]\right]$$

$a := -3, -2.6 .. 2 \cdot \pi + 7$
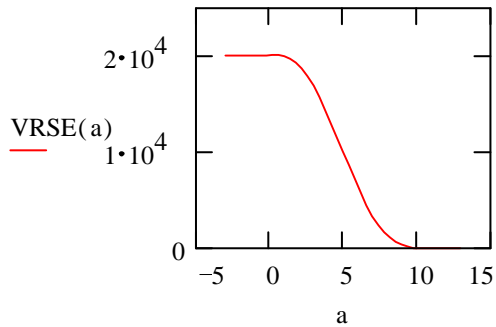
Figure A.11: *Volume of the compression chamber that is part of the RSE versus the screw position*

A.2 Transport screws

$e := 10.25$ mm

$E := 15.6$ mm

$p := 35$ mm

$I := 0.5 \cdot (D + Di)$ $I = 44.500$ mm $\theta i := \operatorname{atan}\left(\dfrac{p}{2 \cdot \pi \cdot Ri}\right)$ $\theta i = 0.317$

$h := D - I$ $h = 10.500$ mm

$G := p - E$ $G = 19.400$ mm

$Ge := p - e$ $Ge = 24.750$ mm $\theta e := \operatorname{atan}\left(\dfrac{p}{2 \cdot \pi \cdot R}\right)$ $\theta e = 0.200$

$CHe := Ge \cdot \cos(\theta e)$ $CHe = 24.257$ mm

$CHi := G \cdot \cos(\theta i)$ $CHi = 18.436$ mm

$FHe := e \cdot \cos(\theta e)$ $FHe = 10.046$ mm $\theta t := \operatorname{atan}\left[\dfrac{h}{0.5 \cdot (E - e)}\right]$ $\theta t = 1.321$

$FHi := E \cdot \cos(\theta i)$ $FHi = 14.824$ mm

$$Vol := 2 \cdot \pi \cdot h \cdot \frac{Ri}{\cos(\theta i)} \cdot \left(\frac{CHe + CHi}{2}\right) + 4 \cdot \pi \cdot \frac{h}{2} \cdot \left(\frac{R}{\cos(\theta e)} - \frac{Ri}{\cos(\theta i)}\right) \cdot \left(\frac{CHe}{3} + \frac{CHi}{6}\right)$$

$Vol = 3.268 \cdot 10^4$ mm³

$Vtotal := 0.25 \cdot \pi \cdot p \cdot \left(D^2 - Di^2\right)$ $Vtotal = 5.138 \cdot 10^4$ mm³

$Vflight := Vtotal - Vol$ $Vflight = 1.870 \cdot 10^4$ mm³

$$\psi := \frac{G + Ge}{4 \cdot p}$$ $\psi = 0.315$

$Vchanend := Vol \cdot \psi$ $Vchanend = 1.031 \cdot 10^4$ mm³

$$\psi flight := \frac{E + e}{4 \cdot p}$$ $\psi flight = 0.185$

$Vflightend := Vol \cdot \psi flight$ $Vflightend = 6.034 \cdot 10^3$ mm³

$$\beta := acos\left(\frac{I}{D}\right)$$ $\beta = 0.628$

The intermeshing part

$$w(r) := \left(\frac{E - e}{R - Ri}\right) \cdot (R - r) + e \qquad \text{[mm]}$$

$$\alpha(r) := acos\left(\frac{r^2 + I^2 - R^2}{2 \cdot r \cdot I}\right)$$

$$cl(r) := 2 \cdot acos\left(\frac{r^2 + I^2 - R^2}{2 \cdot r \cdot I}\right) \cdot r \qquad \text{[mm]}$$

$$intvol := \int_{Ri}^{R} cl(r) \cdot w(r) \, dr \qquad\qquad intvol = 2.850 \cdot 10^3 \qquad \text{mm³}$$

Calculation of the volume of the end of the flight in the intermeshing zone

$$\xi be(r) := \frac{w(r)}{p} \cdot 2 \cdot \pi$$

$$\theta(a) := -\xi be(Ri) - a + \frac{3}{2} \cdot \pi$$

$$\xi \phi min(r, a) := 0.5 \cdot \pi - \theta(a) - \frac{(E - w(r)) \cdot \pi}{p}$$

$$\phi min(r, a) := if(\xi \phi min(r, a) < 0, 0, \xi \phi min(r, a))$$

$$\phi max(r, \theta) := if(\xi be(r) > \alpha(r) + \xi \phi min(r, \theta), \alpha(r) + \xi \phi min(r, \theta), \xi be(r))$$

$$\xi Rmax(a) := R - \frac{p \cdot (R - Ri) \cdot \left(0.5 \cdot \pi - \theta(a) - \frac{E + e}{p} \cdot \pi\right)}{\pi \cdot (E - e)}$$

$\text{Rmax}(a) := \text{if}(\xi\text{Rmax}(a) > R, R, \text{if}(\xi\text{Rmax}(a) < Ri, Ri + \text{tiny}, \xi\text{Rmax}(a)))$

$\xi\text{Rmin}(a) := \left[R - (R - Ri) \cdot \left[1 - \frac{(0.5 \cdot \pi - \theta(a)) \cdot p}{(E - e) \cdot \pi} \right] \right] - \text{tiny}$

$\text{Rmin}(a) := \text{if}(\xi\text{Rmin}(a) < Ri, Ri, \xi\text{Rmin}(a))$

$\text{if1}(r, a) := \text{if}\left[\alpha(r) + \xi\phi\text{min}(r, a) < 0, 0, \left[\frac{-p}{4 \cdot \pi} \cdot \left(\phi\text{max}(r, a)^2 - \phi\text{min}(r, a)^2 \right) + w(r) \cdot (\phi\text{max}(r, a) - \phi\text{min}(\right. \right.$

$\left. \left. r, a) - \phi\text{min}(r, a)) \right] \cdot r \right]$

$\text{if2}(r, a) := \text{if}(\xi\phi\text{min}(r, a) > 0, 0, \text{if}((-\xi\phi\text{min}(r, a)) > \alpha(r), (w(r) \cdot \alpha(r)) \cdot r, (w(r) \cdot -\xi\phi\text{min}(r, a)) \cdot r))$

$\text{Vimend}(a) := \int_{Ri}^{\text{Rmax}(a)} \text{if1}(r, a)\ dr + \int_{\text{Rmin}(a)}^{R} \text{if2}(r, a)\ dr \qquad \text{mm}^3$

$$2 \cdot \text{Vimend}((-2)) = 2.850 \cdot 10^3$$

Volume of the channel related to the screw position

$b := \dfrac{G + Ge}{2}$ [mm] $o(a) := a \cdot \dfrac{R + Ri}{2}$ [mm] $x := \dfrac{b \cdot \pi \cdot (R + Ri)}{p}$ [mm]

$f(a) := \text{if}\left[o(a) > 0, \text{if}\left[o(a) < x, \dfrac{-o(a) \cdot b + 0.5 \cdot b \cdot x - 0.5 \cdot \frac{b}{x} \cdot (x - o(a))^2}{b \cdot \pi \cdot (R + Ri)} + 1, \text{if}\left[o(a) > \pi \cdot (R + Ri), \text{if}\left[o(a) \right. \right. \right. \right.$

$\left. \left. \left. \vdash Ri), \text{if}\left[o(a) > \pi \cdot (R + Ri) + x, 0, \dfrac{(x - o(a - 2 \cdot \pi))^2 \cdot 0.5 \cdot b}{x \cdot b \cdot \pi \cdot (R + Ri)} \right], \dfrac{-0.5 \cdot b \cdot x - (o(a) - x) \cdot b}{b \cdot \pi \cdot (R + Ri)} + 1 \right] \right], 1 \right]$

The volume of the channel of the transport screw versus the angle [mm^3]:

$$\text{Vtransp}(a) := \text{if}\left[a<\xi\text{be}(Ri) - \pi, \text{Vol} - \text{intvol}, \text{if}\left[a<2\cdot\pi, \text{Vol}\cdot f(a) - \frac{\text{intvol}}{2} - \text{Vimend}(a), \text{if}\left[a<2\cdot\pi\cdot\left(1 + \right.\right.\right.\right.$$

$$\text{if}\left[a<2\cdot\pi\cdot\left(1 + \frac{b}{p}\right), \text{Vol}\cdot f(a) - \left(\frac{\text{intvol}}{2} - \text{Vimend}(4\cdot\pi - a - \xi\text{be}(Ri))\right), 0\right]\right]\right]$$

The volume of the compression chamber consisting of the RSE and the transport screw versus the angle:

Vtransp(a) + VRSE(a)

Vtransp(a + 2) + VRSE(a)
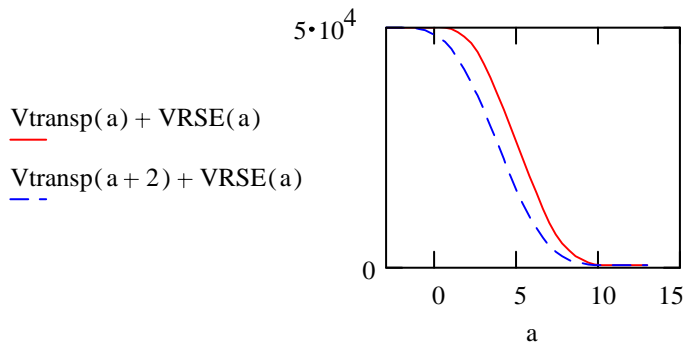
Figure A.12: Volume of the compression chamber versus the angle at two different tangential positions of the RSE with respect to the transport screw

Notation

a	angle of integration interval	
b	width of the channel at r = (R+Ri)	
CHe	assistant variable	mm
CHi	assistant variable	mm
cl	curve length	mm
D	outer diameter	mm
Di	inner diameter	mm
E	width of the base of the flight	mm
e	width of the top of the flight	mm
FHe	assistant variable	mm
FHi	assistant variable	mm
f	fraction of the channel that is part of the compression chamber	
G	width of the bottom of the channel	mm
Ge	width of the top of the channel = distance between two flights	mm

h	channel depth	mm
I	distance between the two screws	mm
intvol	intermeshing volue of the flight	mm^3
o	fraction of the circumference of a circle with radius (R+Ri)/2	
p	pitch	mm
R	outer radius	mm
Ri	inner radius	mm
Rmax	upper boundary of radial integration interval	mm
Rmin	lower boundary of radial integration interval	mm
$V_{chanend}$	volume of the end of the channel	mm^3
V_{flight}	volume of the flight during one revolution	mm^3
$V_{flightend}$	volume of the end of the flight	mm^3
V_{imend}	volume of intermeshing end of the flight	mm^3
Vol	volume of screw channel during one revolution	mm^3
VRSE	volume of the channel of the RSE	mm^3
Vtotal	volume of screw channel and flight during one revolution	mm^3
Vtransp	volume of the channel of transport screw	mm^3
x	length of the channel in tangential direction	mm
w	width of the flight	mm
α	angle	
β	intermeshing angle	
θ	screw position (angle)	
θe	external pitch angle	
θi	internal pitch angle	
θt	angle of trapeziodal flight	
ξbe	angle interval of flight	
ξRmax	assistant variable in calculation of radial integration interval	
ξRmin	assistant variable in calculation of radial integration interval	
ξφmax	assistant variable in calculation of tangential integration interval	
ξφmin	assistant variable in calculation of tangential integration interval	
φmax	upper boundary of tangential integration interval	
φmin	lower boundary of tangential integration interval	
ψ	ratio between surface of channel end and the surface of the middle of the channel during one revolution	
ψflight	ratio between surface of flight end and the surface of the middle of the flight during one revolution	

Reference

[1] Tayeb, J. and Della Valle, F. (1988): Theortetical computation of the isothermal flow throught the reverse screw element of a twin screw extrusion cooker, J. Food Sci. 53: 2, 616-625.

Appendix B

Derivation of the liquid mass balance

The total fibre mass is considered to consist of an constant amount of layers, each containing an equal mass of solid fibres. As no fibres are pressed out from the system, the fibre mass in each layer is constant during drainage. Consider one of those layers with a thickness Δx at a distance x from the bottom. Let q(x) and q(x+Δx) denote the flow rates of the liquid leaving and entering the layer, respectively.

The flow rate of liquid squeezed from a layer, Δq, is equal to the rate of reduction in the volume of its void space:

$$\Delta q = \frac{\partial V_v}{\partial t} \qquad\qquad [B.1]$$

where

$$V_v = A\Delta x\phi \qquad\qquad [B.2]$$

Differentiating Eq. B.2 with respect to time yields:

$$\Delta q = A\Delta x \frac{\partial \phi}{\partial t} + A\phi \frac{\partial \Delta x}{\partial t} \qquad\qquad [B.3]$$

The flow rate of liquid is also equal to the rate of reduction in the total volume of the layer:

$$\Delta q = A\frac{\partial \Delta x}{\partial t} \qquad\qquad [B.4]$$

Combining Eq. B.3 and B.4 and taking limits as $\Delta x \rightarrow 0$ gives:

$$\frac{\partial q}{\partial x} = \frac{A}{1-\phi}\frac{\partial \phi}{\partial t} \qquad\qquad [B.5]$$

133

Appendix C

Force balance over fibre column
derivation of Eq. 5.3
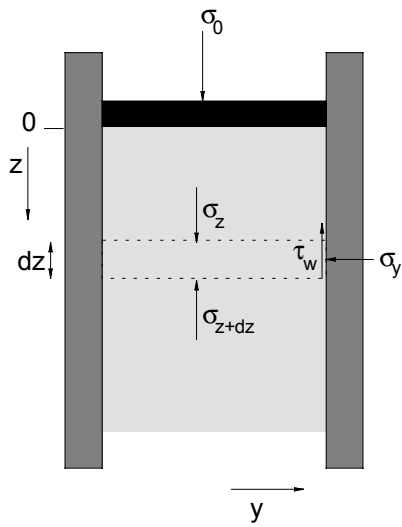
Figure C.1. *Force Balance*

A force balance over volume-element Adz (Fig. C.1) yields:

$$A\sigma_z - A\sigma_{z+dz} - \tau_w O dz + \rho g A dz = 0 \qquad [C.1]$$

The wall friction, τ_w , depends on the pressure perpendicular to the wall (y-direction):

$$\tau_w = c_w + \sigma_y \tan\delta \qquad [C.2]$$

135

The pressure in the y-direction depends on the pressure in the z-direction via the Poisson ratio, ν:

$$\sigma_y = \nu\sigma_z \qquad\qquad [C.3]$$

The density over the column is assumed constant, as the effect of pressure on density in the range of pressures encountered in the column is negligible. Combination of Eq. C.1 to C.3 yields:

$$A(\sigma_z - \sigma_{z+dz}) + (\rho g A - c_w O - \nu\sigma_z \tan\delta O)dz = 0 \qquad\qquad [C.4]$$

which can be written as:

$$\frac{\partial\sigma_z}{\partial z} = C_2 - C_1\sigma_z \qquad \text{with } C_1 = \frac{4\nu\tan\delta}{Z} \quad \text{and} \quad C_2 = \rho g - \frac{4c_w}{Z} \qquad [C.5]$$

Integration of this equation with the boundary condition that $\sigma_z = \sigma_0$ at z=0 yields:

$$\sigma_z = \frac{1}{C_1}\left((C_1\sigma_0 - C_2)\cdot e^{-C_1 z} + C_2\right) \qquad\qquad [C.6]$$

Appendix D

Internal shear surface area
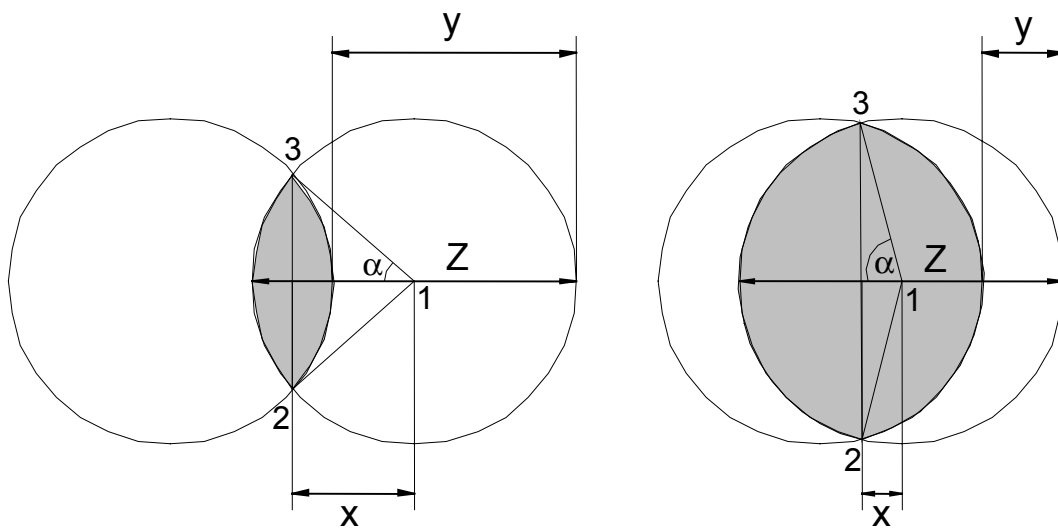
Figure D.1. *Internal shear surface area*

In the C-C cross-section of the fibre rheometer in Figure 5.1 it can be seen that the internal shear surface has a shape like the shaded parts in Figure D.1. In this appendix a formula is derived for the area of this surface related to the distance that the shear block is pushed out of the apparatus, displacement y.

The height, x, of the triangle 123 in figure D.1, is related to the shear block displacement, y:

$$x = \frac{Z}{2} - \left(\frac{Z-y}{2} \right) = \frac{y}{2} \qquad \text{[D.1]}$$

The angle α is given by:

$$\alpha = \arccos\left(\frac{x}{Z/2} \right) = \arccos\left(\frac{y}{Z} \right) \qquad \text{[D.2]}$$

137

The surface area of the wedge 123 of the circle, W, is therefor:

$$W = \frac{2\alpha}{2\pi} \frac{1}{4} \pi Z^2 = \frac{Z^2}{4} \arccos\left(\frac{y}{Z}\right)$$

[D.3]

The surface area of triangle 123, R, is:

$$R = x\sqrt{\frac{Z^2}{4} - x^2} = \frac{y}{4}\sqrt{Z^2 - y^2}$$

[D.4]

The overlapping surface area of the two circles is twice the difference between the surface area of the wedge and the surface area of the triangle:

$$S = \frac{Z^2}{2} \arccos\left(\frac{y}{Z}\right) - \frac{y}{2}\sqrt{Z^2 - y^2}$$

[D.5]

As there are two internal shear planes, the total internal shear surface area becomes:

$$S_i = Z^2 \arccos\left(\frac{y}{Z}\right) - y\sqrt{Z^2 - y^2}$$

[D.6]

Summary

Extrusion pulping is a (chemi-)mechanical pulping method in which fibres are processed by means of compression and shear forces. Fibres are shortened, fibre bundles, consisting of elementary fibres are defibrated and elementary fibres are fibrillated. The extrusion fibre products can be used directly or after a specific post-processing step for bulk applications or as reinforcement in paper, board or textile applications.

Different applications require different fibre qualities, which can be obtained by operating at different process conditions or screw configurations. However, relatively little is known about the mechanisms of extrusion pulping and the relations between product properties and extruder conditions. Knowledge about the mechanisms is necessary for proper control of product quality and development of scale-up rules. The research described in this thesis focused on elucidating the mechanism behind processing, and determining the constitutive equations necessary for mathematical modelling of the pulping.

The pulping extruder is a co-rotating twin-screw extruder, which consists of transport screws followed by reversed screw elements (RSE), which are elements with threads, whose pitch is opposite to the transport screws. Fibres in the transport screws are transported towards the RSE section. Fibres in the channels of the RSE are transported backwards in the direction of the inlet of the extruder. These fibres accumulate in the space between the transport screw and the RSE, which is locked by the flights of the intermeshing screws. The volume of this space reduces when the screws turn, thus causing compression of the fibres. During compression the impregnation liquid is drained from the fibres through a filter placed in the barrel of the extruder. Interaction between the fibres cause the fibres to move in plugs and prevents them for flowing through the slots machined in the flights of the RSE or through the small spaces between the intermeshing screws or between the screws and the barrel. When the screws turn further, the compression of the fibres increases. At a certain instance compression forces become that high that the fibre mass starts shearing and breaks into plugs of fibres, which can flow through the slots in the flights of the RSE or through the smaller slits. Subsequently a new compression chamber is formed and filled with new fibres from the transport screws and yet processed fibres from the RSE, and compression starts again. From experiments it became clear that cutting, defibration and fibrillation of the fibres during extrusion pulping is totally confined to the space between the transport screws and the RSE's. The extent of cutting, defibration and fibrillation during extrusion pulping is assumed to depend on the distribution of compressive and shear forces in this space. Therefore, the model to be developed should calculate compressive and shear forces on the fibres in the extruder influenced by process conditions and extruder geometry.

The complicated geometry of the compression space was simplified by modelling it as a cylinder, which may contain several holes of different geometry and position to simulate the effect of the slots in the RSE. The volume decrease versus time of the piston acting on the fibres in the cylinder is an S-shaped curve that depends on the screw speed and the screw geometry (Appendix A). The amount of fibres during each compression in the compression

chamber depends on the filling degree of the extruder, which is defined as the ratio between throughput and screw speed.

Calculation of the compressive and shear forces in the compression chamber of the extruder requires relations describing the rheology of the fibres. During extrusion fibres often have a consistency higher than 40 %. According to the concentration regimes valid for suspensions of fibres, it appeared that fibre masses at these consistencies should be regarded as a solid. Therefore, models developed for extrusion of polymer melts or food, which use liquid rheology are not to be applied to extrusion pulping. Models developed for low and medium consistency suspensions are based on the pure liquid viscosity, which is corrected for the presence of fibres. High consistencies encountered during extrusion are beyond their validity range. Most models are empirical, and models based on fundamental interactions are based on severe simplifications, like rigid rods and no interfibre friction. Extension of those models to flexible fibres and high concentrations makes them far too complicated to be applicable to describe extruder flows. In order to obtain the right model to describe the flow of high consistency fibre masses, the fundamentals behind solid flow have been studied for its applicability to fibres at high consistency. Granular materials showed to have resemblance with the fibre properties important in extrusion processing, like compressibility, inter-particle friction, and drainage. The constitutive equations for those properties have been determined for hemp bast fibres in this study.

Volume decrease of the 'chamber' between the RSE and the transport screw causes compression of the fibre network. Modelling of this compression process requires a relation between the stress on the solid matrix and the volumetric strain. During compression the liquid phase is expressed from the solid matrix by hydraulic forces. The permeability of the matrix and the hydraulic pressure gradient determine the speed of liquid expression. The permeability of the matrix is a function of the micro-structural properties of the fibre network and the swelling of the fibres. Modelling of the drainage process requires the relation between stress and volumetric strain, relations for the volumetric swelling as function of the pressure applied on the fibre mass and relations that describe the dependence of permeability on fibre swelling and micro-structural properties of the fibre network. Local stress forces in the solid matrix can be calculated using the stress-strain relationship and Poisson's ratio for the fibre network for the transfer of stresses. To be able to determine at which compression and shear stresses the fibre network would break, the shear strength of the fibre network should be known. The model to be developed should be extended and optimised with information obtained from simulation of the performed extrusion experiments.

The relation between the stress on the solid matrix and the volumetric strain was determined for hemp bast fibres (Chapter 2). Untreated, water soaked and NaOH-soaked hemp bast fibres were subjected to varying loads and loading rates and the resulting stress-density and relaxation curves were studied. The stress-density relationship of hemp bast fibres can be described with the compressibility equation. Fibres become more flexible and fibre bending becomes more important in the mechanism of fibre compression at higher temperature and moisture content, resulting in a lower stress over the whole density range. This is shown in a decreased coefficient of the compressibility equation. During compression of soaked fibres at low densities the compressibility equation also applies to the stress-density curve. However, at higher densities a high flow resistance, caused by the dense fibre mat, causes the stress to increase faster. The flow limitation was advanced at higher strain rates and enhanced at higher sodium hydroxide concentrations. This phenomenon is further advanced during repeated compression as the fibre mass shows a plastic strain and forms compact fibre mats. During

repeated compression both maximum stress and the extent of relaxation decreases with the number of repetitions and the total plastic strain increases until a point was reached at which no further changes were observed. Relaxation of the fibre network was described with a generalised Maxwell model. The extent of relaxation slightly decreases with increasing maximum stress, increases with strain rate and increases with moisture content.

The relation between the volumetric swelling of hemp bast fibres and pressure applied on the fibre mass has been studied for both water and sodium hydroxide impregnation (Chapter 3). The measured total volume of the hemp-liquid system appeared to be lower than the solid volume plus the volume of absorbed liquid. The observed volume contraction is attributed to a pressure-dependent decrease in specific volume of the liquid in the fibre. Pressure forces water molecules to migrate to places between the molecules of the cell wall components, which are not accessible under atmospheric pressure. It is shown that removal of cell wall material (lignin and hemicellulose) by NaOH-treatment results in more places per gram of dry fibre becoming available at higher pressures. The swollen cell wall becomes more flexible by the removal of lignin, which results in a higher volumetric swelling under pressure compared to untreated fibres.

The permeability of a hemp bast fibre network is related to the porosity of the network and the swelling of the individual fibres (Chapter 4). The drainage of water and sodium hydroxide solutions through a column of hemp fibres has been studied in order to predict the conditions at which mechanical pulping processes become restricted by flow resistance. In order to find the best model to describe drainage through hemp bast fibres within the desired pressure and time range, the results have been analysed for different models. The drainage process becomes significantly slower at higher sodium hydroxide concentrations, while a higher pressure only slightly enhances the drainage process. Swelling appeared to be a very important parameter in the drainage process. Neglecting fibre swelling results in predictions of drainage processes that are about 50,000 times faster than experimentally observed. The Kozeny-Carman model for flow through porous media has been extended with a proper swelling model. The swelling curve related to pressure appeared to be an S-shaped curve, showing that a certain critical pressure needs to be overcome to compress swollen fibres. The S-shaped curve starts at higher swelling values for higher sodium hydroxide concentrations. These fibres however appeared to be easier collapsible at higher pressures, and volumetric swelling at higher pressures is lower for higher sodium hydroxide concentrations. The degree of volumetric swelling becomes negligible at high pressure.

In Chapter 5 equations are developed for the shear strength of hemp bast fibres in order to be able to determine at which compression and shear stresses the fibre mass would break. The shear strength of dry and high consistency hemp bast fibres (50-90% d.m.) has been studied using an apparatus specially developed for measuring the shear strength of fibres at pressures up to 30 MPa. Coulombs Law, originally developed to describe the shear strength of soil, appeared to be well applicable to describe the shear strength and wall friction of hemp bast fibres. The shear strength appeared to be proportional to normal pressure. The tangent of the angle of internal friction increases with dry matter content. The internal friction coefficient for dry fibres is 0.46, with a permanent structural strength of 1.3 MPa. The wall friction coefficient for dry fibres with stainless steel is 0.05 with an adhesional stress of 0.20 MPa. For wet fibres the shear strength increases linearly with dry matter content with a proportionality constant of 0.29 MPa/% dry matter for the range of dry matter contents studied. In contrast to dry fibres, wall friction for wet fibres with stainless steel appears negligible.

Chapter 6 describes extrusion experiments performed to determine the empirical relations between product properties and extruder conditions. The effect of screw speed, throughput, temperature and pre-treatment on the energy consumption and quality of the product has been studied. The extruded pulps have been analysed for several strength and optical properties in order to obtain qualitative predictions. Defibration, shortening and fibrillation appear not to be controllable independently. Therefore, in some cases post-processing by beating, refining or extrusion at different conditions, might be necessary. The filling degree, defined as the ratio between throughput and screw speed, appeared to be an important parameter in relating pulp properties to extruder conditions. When the filling degree is decreased (by either decreasing the throughput or increasing the screw speed), fibres remain in the extruder during a higher number of screw revolutions and therefore obtain a higher number of impacts. This causes higher specific energy consumption, breaking length and beating degree and a reduced tear index. The specific energy consumption also appeared to increase with decreasing throughput (at constant filling degree), which mainly results in lower tear strength.

Pre-treatment with sodium hydroxide instead of water or changing the process temperature has no influence on the specific energy consumption. However, pretreatment with sodium hydroxide appears to increase breaking length, burst index and tear strength, because of improved bonding and higher fibre length. Decreasing the process temperature increases breaking length and beating degree of the product.

Samenvatting

Tijdens extrusie worden vezels door middel van compressie- en afschuifkrachten op (chemi)mechanische wijze gepulpt: vezels worden verkort, vezelbundels worden gedefibreerd tot elementaire vezels, en deze elementaire vezels worden gefibrilleerd. De geëxtrudeerde vezels kunnen direct of na een bepaalde nabewerking worden gebruikt voor bulktoepassingen of voor het versterken van papier, karton of textiele toepassingen.

Voor de diverse toepassingen zijn verschillende specifieke vezeleigenschappen nodig, welke kunnen worden verkregen door te extruderen onder verschillende procescondities of met verschillende schroefconfiguraties. Er is echter weinig bekend over het mechanisme achter vezelextrusie en de relaties tussen producteigenschappen en extrusiecondities. Kennis van dit mechanisme is noodzakelijk voor een goede beheersing van de productkwaliteit en voor het kunnen opstellen van opschalingsregels. Het onderzoek dat in dit proefschrift wordt beschreven, was gericht op het ophelderen van het extrusiemechanisme en het bepalen van de constitutieve vergelijkingen die nodig zijn voor het modelleren van het pulpproces.

De vezelextruder is een coroterende dubbelschroefsextruder, opgebouwd uit transport-schroeven, die gevolgd worden door schroefelementen met een tegengestelde schroefdraad, de zogenaamde 'reversed screw elements' (RSE's). Vezels die zich in de transportschroeven bevinden worden in de richting van de RSE-sectie getransporteerd en vezels die zich in de kanalen van de RSE's bevinden worden in tegenovergestelde richting getransporteerd. De vezels hopen zich op deze manier op in de ruimte tussen de transportschroef en de RSE. Deze ruimte is afgesloten door het schroefdraad van de erop ingrijpende schroeven. Het volume van de ruimte neemt af tijdens het draaien van de schroeven, waardoor de vezels worden gecomprimeerd. Tijdens het comprimeren wordt vloeistof uit de vezels geperst en afgevoerd door een filter die zich in de barrel van de extruder bevindt. Door interactie en frictie tussen de vezels vormen de vezels zich tot proppen, die niet door de gaten in het schroefdraad van de RSE of door de smalle spleten, tussen de schroeven of tussen de schroeven en de barrel, kunnen stromen. Tijdens het draaien van de schroeven neemt de compressie van de vezels toe, welke op een gegeven moment zo hoog wordt dat de vezelmassa begint af te schuiven en in kleine vezelproppen opbreekt. Deze kleinere vezelproppen kunnen wel door de gaten in het schroefdraad van de RSE of door de smalle spleten stromen. Vervolgens wordt een nieuwe 'compressiekamer' gevormd, die gevuld wordt met nieuwe vezels uit de transportschroeven en reeds verwerkte vezels uit de RSE, waarna de compressie opnieuw begint. Uit experimenten is gebleken dat het verkorten, de defibratie en de fibrillatie van de vezels alleen plaatsvindt in de beschreven ruimte tussen de transportschroeven en de RSE's. Er wordt aangenomen dat de mate van verkorten, defibratie en fibrillatie afhangt van de grootte en verhouding van de compressie- en afschuifkrachten in deze ruimte. Het vezelextrusiemodel zal daarom de compressie- en afschuifkrachten op de vezels in de extruder moeten berekenen als functie van de procescondities en geometrie van de extruder.

De gecompliceerde geometrie van de compressiekamer werd vereenvoudigd door het te modelleren als een cilinder, welke verscheidene gaten van verschillende geometrie en positie kan bevatten, waarmee het effect van de gaten in het schroefdraad van de RSE kan worden

gesimuleerd. De afname van het volume van deze cilinder met de tijd is een S-vormige curve die afhankelijk is van de schroefsnelheid en de schroefgeometrie (Appendix A). De vulgraad van de extruder, gedefinieerd als de verhouding tussen de doorzet en de schroefsnelheid, bepaalt de hoeveelheid vezels die per omwenteling wordt samengeperst.

Het kunnen berekenen van de compressie en afschuifkrachten in de 'compressiekamer' van de extruder vereist relaties die de reologie van de vezels beschrijven. Tijdens extrusie hebben vezels meestal een consistentie hoger dan 40%. Volgens de voor vezelsuspensies opgestelde concentratieregimes moet een vezelmassa bij zulke hoge consistenties beschouwd worden als een vaste stof. Modellen, die ontwikkeld zijn voor het beschrijven van polymeerextrusie of extrusie van voedsel, maken gebruik van vloeistofreologie en zijn dus niet toepasbaar voor het beschrijven van vezelextrusie. Reologiemodellen die opgesteld zijn voor laag en matig consistente suspensies zijn gebaseerd op de pure vloeistofreologie, welke wordt gecorrigeerd voor de aanwezigheid van de vezels. De hoge consistenties, zoals deze tijdens vezelextrusie voorkomen, vallen buiten hun geldigheidsbereik. De meeste ontwikkelde modellen zijn empirisch, terwijl modellen die gebaseerd zijn op fundamentele interacties sterk vereenvoudigd zijn, doordat ze gebruik maken van bijvoorbeeld stijve staafjes en frictie tussen de vezels verwaarlozen. Uitbreiding van deze modellen voor flexibele vezels en hoge concentraties maken deze modellen zodanig complex dat ze niet toepasbaar zijn om de gecompliceerde stroming in de extruder mee te beschrijven. De theorie van vastestofstroming werd bestudeerd voor haar toepasbaarheid om de stroming van vezelmassa's met hoge consistentie te beschrijven. Granulaire materialen bleken vergelijkbare eigenschappen te bezitten als de eigenschappen die voor vezels essentieel zijn voor verwerkbaarheid met behulp van extrusie, zoals samendrukbaarheid, frictie tussen de deeltjes en ontwatering. Tijdens de in dit proefschrift beschreven studie zijn de constitutieve vergelijkingen voor deze eigenschappen bepaald voor hennep-bastvezels.

Door volume-afname van de ruimte tussen de transportschroeven en de RSE's wordt het vezelnetwerk gecomprimeerd. Deze compressie kan gemodelleerd worden met behulp van een relatie tussen de spanning in de vaste stofmatrix en de dichtheid van het vezelnetwerk. Tijdens compressie wordt de vloeistof uit de vezelmassa geperst door het ontstaan van een hydraulisch drukverschil. De snelheid van ontwatering wordt bepaald door de permeabiliteit van de matrix en de grootte van de hydraulische drukgradiënt. De permeabiliteit van de matrix is een functie van de microstructurele eigenschappen van het vezelnetwerk en de mate van zwelling van de vezels. Het ontwaterproces kan gemodelleerd worden met behulp van relaties tussen de spanning en de dichtheid van het netwerk, relaties voor de volumetrische zwelling als functie van de druk op de vezelmassa en relaties tussen de permeabiliteit, vezelzwelling en microstructurele eigenschappen van het vezelnetwerk. Locale spanningen in de vaste stofmatrix kunnen worden berekend met behulp van spanning-dichtheid-relaties en met behulp van de Poisson-ratio van het vezelnetwerk voor de overdracht van spanningen. Voor het bepalen van de grootte van de compressie- en afschuifkrachten waarbij het vezelnetwerk zal breken, moet de afschuifsterkte van het vezelnetwerk bekend zijn. Met informatie verkregen uit simulatie van uitgevoerde extrusie-experimenten zal het model moeten worden uitgebreid en geoptimaliseerd.

De relatie tussen de spanning in de vaste stofmatrix en de dichtheid is bepaald voor hennep-bastvezels (Hoofdstuk 2). Onbehandelde, in water gedrenkte en in natronloog gedrenkte hennep-bastvezels werden onderworpen aan variërende belasting onder verschillende snelheden. De resulterende spanning-dichtheid- en relaxatiecurven werden bestudeerd. De spanning-dichtheid-relatie van hennep-bastvezels kan worden beschreven met de

compressibiliteitsvergelijking. Bij hogere temperatuur of een hoger vochtgehalte worden vezels flexibeler en in het mechanisme van compressie van de vezelmassa wordt het buigen van de vezels belangrijker, hetgeen resulteert in een lagere spanning over de gehele dichtheidsrange. Dit blijkt uit een afname van de coëfficiënt van de compressibiliteitsvergelijking. De compressibiliteitsvergelijking is bij lage dichtheden ook toepasbaar op de spanning-dichtheidscurve van gedrenkte vezels. Bij hogere dichtheden neemt de spanning echter sneller toe door een sterk toegenomen stromingsweerstand door de dichte vezelmassa. Deze stromingslimitering wordt bevorderd bij hogere compressiesnelheden en versterkt door hogere natronloogconcentraties. Dit verschijnsel wordt verder bevorderd door herhaalde compressie, doordat de vezelmassa een permanente vervorming verkrijgt en een compacte massa gaat vormen. Tijdens herhaalde compressie neemt zowel de maximale spanning als de mate van relaxatie af met het aantal herhalingen. De totale permanente vervorming neemt toe, maar bereikte een maximum na een aantal herhalingen. Relaxatie van het vezelnetwerk werd beschreven met een gegeneraliseerd Maxwell model. De mate van relaxatie neemt licht af met toenemende maximumspanning en neemt toe met toenemend vochtgehalte.

De relatie tussen volumetrische zwelling van hennep-bastvezels en de druk die op de vezelmassa wordt uitgeoefend is bestudeerd voor zowel water- als natronlooggedrenkte vezels (Hoofdstuk 3). Het gemeten totale volume van de vochtige vezels bleek lager dan het volume van de vaste stof en het volume van de geabsorbeerde vloeistof samen. De waargenomen volumecontractie is toegeschreven aan een drukafhankelijke afname van het specifieke volume van de vloeistof in de vezel. De druk dwingt de watermoleculen naar plaatsen tussen de moleculen van de celwand, welke onder atmosferische druk niet toegankelijk zijn. Door verwijdering van celwandmateriaal (lignine en hemicellulose) door middel van drenking in natronloog komen meer plaatsen per gram droge vezel beschikbaar bij hogere druk in vergelijking met drenking in water. Door het verwijderen van lignine wordt de gezwollen celwand flexibeler, hetgeen resulteert in een hogere volumetrische zwelling onder druk in vergelijking met vezels in water.

De permeabiliteit van een hennep-bastvezel-netwerk is gerelateerd aan de porositeit van het netwerk en de zwelling van de individuele vezels (Hoofdstuk 4). De ontwatering van hennep-bastvezels gedrenkt in water en natronloog is onderzocht om zo de condities, waaronder het mechanische pulpproces door stromingsweerstand gelimiteerd wordt, te kunnen voorspellen. Het model waarmee de ontwatering door hennep-bastvezels het best kan worden beschreven is bepaald door de resultaten te analyseren met verschillende modellen. De ontwatering wordt duidelijk langzamer bij hogere natronloogconcentraties, terwijl een hogere druk het ontwaterproces slechts licht bevordert. Zwelling blijkt een zeer belangrijke parameter in het ontwaterproces. Het negeren van zwelling resulteert in voorspellingen van ontwaterprocessen die 50.000 maal sneller zijn dan experimenteel is waargenomen. Het Kozeny-Carman model voor stroming door poreuze media is uitgebreid met een passend zwellingsmodel. De zwellingscurve als functie van de druk blijkt een S-vormige curve, die laat zien dat een zekere kritische druk moet worden bereikt om gezwollen vezels te kunnen comprimeren. Voor hogere natronloog-concentraties begint de S-vormige curve bij hogere zwellingswaarden. Doordat deze vezels makkelijker in blijken te klappen bij hogere drukken is de volumetrische zwelling bij hogere drukken lager voor hogere natronloogconcentraties. Bij hoge druk wordt de volumetrische zwelling van zowel water- als natronlooggedrenkte vezels verwaarloosbaar.

In Hoofdstuk 5 zijn relaties opgesteld voor het beschrijven van de afschuifsterkte van hennep-bastvezels. Deze afschuifsterkte is nodig voor de bepaling van de compressie en

afschuifspanningen waarbij de vezelmassa zal breken. De afschuifsterkte van droge en hoog-consistente hennep-bastvezels (50-90% d.m.) is onderzocht door middel van een apparaat, dat speciaal is ontwikkeld voor het meten van afschuifsterktes van vezelmassa's bij drukken tot 30 MPa. De wet van Coulomb, welke oorspronkelijk is ontwikkeld om de afschuifsterkte van aarde te beschrijven, bleek goed toepasbaar voor het beschrijven van de afschuifsterkte van hennep-bastvezels en de wandfrictie met hennep-bastvezels. De afschuifsterkte bleek evenredig met de normaaldruk. De tangens van de interne frictiehoek is 0.46 voor droge vezels met een permanente structurele sterkte van 1.3 MPa. De wandfrictiecoëfficiënt voor droge vezel met roestvrij staal is 0.05 met een adhesiespanning van 0.20 MPa. Voor natte vezels neemt de afschuifsterkte lineair toe met een evenredigheidsconstante van 0.29 MPa/% droge stof voor de onderzochte range van droge stofgehaltes. In tegenstelling tot droge vezels is de wandfrictie met roestvrij staal voor natte vezels verwaarloosbaar.

Hoofdstuk 6 beschrijft de extrusie-experimenten, die zijn uitgevoerd om de empirische relaties tussen producteigenschappen en extrusiecondities te bepalen. Het effect van schroefsnelheid, doorzet, temperatuur en voorbehandeling op de energieopname en de kwaliteit van het eindproduct is onderzocht. Om kwalitatieve voorspellingen te kunnen doen zijn de geëxtrudeerde pulpen geanalyseerd op verschillende sterkte en optische eigenschappen. Verkorting, defibratie en fibrillatie blijken niet onafhankelijk van elkaar te kunnen worden geregeld. Daarom zal in sommige gevallen een nabehandeling door maling, refining of een tweede extrusiestap noodzakelijk zijn. De vulgraad, gedefinieerd als de verhouding tussen doorzet en schroefsnelheid, blijkt een belangrijke parameter in het relateren van producteigenschappen met extrusiecondities. Als de vulgraad wordt verlaagd (door het verlagen van de doorzet of het verhogen van de schroefsnelheid), verblijven de vezels gedurende een groter aantal omwentelingen in de extruder en ondervinden ze een groter aantal compressies. Dit veroorzaakt een hogere specifieke energie-opname, treksterkte en maalgraad en een verlaagde scheursterkte. De specifieke energie-opname blijkt ook toe te nemen met een afnemende doorzet (bij een constante vulgraad). Dit resulteert voornamelijk in een lagere scheursterkte.

Het voorbehandelen van vezels met natronloog in plaats van water of het wijzigen van de procestemperatuur heeft geen invloed op de specifieke energieopname. Het drenken van vezels in natronloog blijkt echter te resulteren in een hogere treksterkte, berststerkte en scheursterkte door verbeterde binding tussen de vezels en een grotere vezellengte. Het verlagen van de procestemperatuur verhoogt de treksterkte en de maalgraad van het product.

Dankwoord

Met het afronden van dit boekje kan ik terugkijken op een interessante en leerzame periode. Ik ben dankbaar dat ATO-DLO mij de gelegenheid heeft gegeven dit onderzoek uit te voeren en met een promotie af te ronden. Vierenhalf jaar geleden begon ik bij ATO-DLO aan het onderzoek met als doel het verpulpen van vezels met behulp van extrusie te beschrijven in een model. Hoewel al snel bleek dat er weinig bekend was over het vezelextrusie-mechanisme, heb ik veel gehad aan de inzichten van Gertjan van Roekel. Hoewel ik altijd graag meer wilde dan alleen het fundamentele onderzoek, ben ik Gertjan dankbaar dat hij mij 'gedwongen' heeft de eerste 2 jaar mijn tijd fulltime te besteden aan dit onderzoek. Zonder zijn dwang had ik het onderzoek niet op dit tijdstip af kunnen ronden. Gedurende de laatste tweeënhalf jaar heeft Ed de Jong mij gestimuleerd om de in de eerste twee jaar verkregen inzichten om te zetten naar gericht wetenschappelijk onderzoek naar de voor vezelextrusie-modellering belangrijke mechanismen, hetgeen nu in dit proefschrift beschreven staat. Ook voor goede begeleiding, de vele talrijke interessante discussies en zijn kritische blik op de resultaten ben ik Ed zeer dankbaar. Ik ben professor Westerterp zeer erkentelijk voor zijn voortdurende enthousiasme en interesse in het onderzoek en voor de tijd en energie die hij in mijn begeleiding heeft gestoken. Ook professor Weickert wil ik bedanken voor zijn bereidheid mij te begeleiden in het onderzoek en zijn kritische blik op de verwerking van de resultaten.

Een aantal stagiaires hebben mij tijdens het onderzoek ondersteuning geboden in het experimentele werk. Liesbeth Baudoin wil ik bedanken voor het optimaliseren van de vezelreometer. Hoewel ze zelf nauwelijks aan meten is toegekomen, heeft ze ervoor gezorgd dat Frank Waayer en Maarten Verhoeven mij hebben voorzien van een enorme hoeveelheid data waarmee uiteindelijk de modellen voor ontwatering en afschuifsterkte zijn gebouwd.
Jan Stroomer en Didi Wong-Lun-Hing wil ik bedanken voor de uitvoering van de grote hoeveelheid extrusieproeven en met name Didi voor haar grote bijdrage aan de verwerking van de resultaten. Verder wil ik Mariëlle Ramaekers en Josh Ang bedanken voor het opstarten van de experimenten voor zwelling en ontwatering.

Uiteraard wil ik al mijn ATO-collega's bedanken voor hun aanwezigheid, gezelligheid en interesse in het onderzoek. Een onbeschrijfelijke hoeveelheid dank gaat hierbij uit naar Kees Melis, die gedurende de gehele onderzoeksperiode zowel mij als de stagiaires veel ondersteuning heeft gegeven bij de uitvoering van de extruderproeven, zoals het opbouwen van de extruder, het constant voeden van de extruder, het openbreken van de extruder bij de vele vastlopers, en het schoonmaken en opruimen, soms tot in de late uurtjes. Richard Op den Kamp wil ik bedanken voor zijn hulp bij het inwerken van de stagiaires en voor zijn hulp bij de extrusie-experimenten, waar ik ook Martijn Wevers voor wil bedanken. Jocco Dekker wil ik bedanken voor het schrijven van de data-acquisitieprogramma's, die nodig waren voor het op de juiste manier verwerken van de meetresultaten. Steef Lips wil ik bedanken voor de interessante discussies. John Senger, thank you for improving and correcting my English, for your critical questions on all my articles and for our fruitful discussions.

Verder gaat dank uit naar onze familie en vrienden voor hun begrip. We zullen alle gemiste bezoekjes de komende jaren inhalen! Patrick van Gerner wil ik hierbij met name bedanken voor de prachtige omslag van dit proefschrift. En niet te vergeten, wil ik mijn ouders enorm bedanken voor hun steun tijdens de gehele onderzoeksperiode en het opvangen van de huishoudelijke taken en klusjes gedurende de afgelopen maanden. Op deze wijze hebben jullie een grote bijdrage geleverd aan dit prachtige resultaat. Tenslotte Mark; bedankt voor het lay-outen van dit proefschrift en natuurlijk voor je onverdeelde steun en begrip. Zonder jou was het zeker minder leuk geweest!

Curriculum Vitae

Annita Westenbroek werd op 6 mei 1972 geboren te Steggerda. Haar Gymnasium β diploma behaalde ze aan de Rijksscholengemeenschap Jan Hendrik Tromp Meesters te Steenwijk in 1990, waarna ze begon aan haar studie Chemische Technologie aan de Universiteit Twente te Enschede. Tijdens haar stage in 1994 bij ICI Katalco in Billingham, Engeland, verrichtte zij onderzoek aan het gekatalyseerde afbraakproces van Natriumhypochloriet. In september 1995 sloot zij haar studie (cum laude) af met haar afstudeeropdracht bij de vakgroep Industriële Processen en Producten onder de titel "Modellering van warmte- en stoftransport in een enkel polymeriserend deeltje met behulp van het MultiGrain Model".

Op 15 juli 1995 was Annita reeds aangesteld bij het instituut voor Agrotechnologisch Onderzoek (ATO-DLO) in Wageningen als Onderzoeker In Opleiding voor een periode van vier jaar. Binnen de hoofdafdeling Agrovezels en Cellulose verrichtte zij haar promotie-onderzoek naar het mechanisme achter vezelextrusie onder leiding van dr. ir. E. de Jong, met als promotor prof. dr. ir. K.R. Westerterp.

Momenteel is Annita werkzaam in de groep Vezel- en Papiertechnologie van ATO in Wageningen en bij het Kenniscentrum Papier en Karton in Arnhem als projectleider voor onderzoeksprojecten ter optimalisatie van de stofvoorbereiding en de grondstofbenutting van de Papier- en Kartonindustrie.